**Title**
Structural and biochemical studies of ring-shaped DNA translocases



**Author**
Strycharska, Melania Slawa

**Publication Date**
2013

Peer reviewed|Thesis/dissertation

"Structural and biochemical studies of ring-shaped DNA translocases"

by

Melania Sława Strycharska

A dissertation submitted in partial satisfaction of the
requirements for the degree of

Doctor of Philosophy
in
Biophysics
in the
Graduate Division
of the
University of California, Berkeley

Committee in charge:

Professor James M. Berger, Co-Chair
Professor Carlos J. Bustamante, Co-Chair
Professor Michael Botchan
Professor David E. Wemmer

Fall 2013

Abstract

"Structural and biochemical studies of ring-shaped DNA translocases"

by

Melania Sława Strycharska

Doctor of Philosophy in Biophysics

University of California, Berkeley

Professor James M. Berger, Co-Chair
Professor Carlos J. Bustamante, Co-Chair

Cellular replication forks are universally powered by ring-shaped, hexameric helicases that encircle and unwind DNA. To better understand the molecular mechanisms and control of these enzymes, we used an ensemble of methods to investigate the bacterial replicative helicase, DnaB. A 3.3Å crystal structure of *Aquifex aeolicus* DnaB complexed with nucleotide reveals a new conformational state for this family of motor proteins. Electron microscopy and small angle X-ray scattering studies confirm the state seen crystallographically, showing that the DnaB ATPase domains and an associated N-terminal collar transition between two physical states in a nucleotide-dependent manner. Mutant helicases locked into either collar state are active, but display different capacities to support critical activities such as duplex translocation and primase-dependent RNA synthesis. Our findings establish the DnaB collar as a key auto-regulatory hub that controls the ability of the helicase to transition between different functional states in response to nucleotide and both replication initiation and elongation factors.

To my parents for being my original and most important scientific role models and to the red monster for reminding me to enjoy life in between experiments…

# Table of Contents

# Acknowledgments

I would like to thank the incredible community of the Biophysics graduate students, in particular Aathavan Karunakaran, Phillip Elms, Derek Greenfield, Viviana Risca, Ann McEvoy, and Ania Labno for all the support, encouragement, scientific conversations and great California adventures. I could have not asked for better friends and more inspiring science colleagues. This work would also not have been possible without the help from the generations of the Berger and Bustamante Lab co-workers, in particular the mentoring of Jeffrey Moffitt, Ken Dong, Andy Antczak, Karl Duderstadt and the great collaborations with Ernesto Arias-Palomo and Art Lyubimov. I would like to further acknowledge Richard Rymer, Seychelle Vos, Alessandro Costa, Kevin Jude, Iris Hood, Franziska Bleichert, Ninning Liu, Craig Hetherington, Lacra Bintu, Shannon Yan, Michel Dedeo and Tim Wendorff for all the technical assistance, helpful discussions and simply being there when I needed somebody to talk to and brainstorm with. I am grateful to the Nogales laboratory and the staff at beamlines 8.3.1 and 12.3.1 of the Advanced Light Source and beamline BL4-2 of the Stanford Synchrotron Radiation Lightsource for help with data collection and analysis, and Tiago Barros of the Kuriyan lab for the τ domains III and IV construct.

My two advisors, James Berger and Carlos Bustamante, as well as the thesis committee members, Mike Botchan and David Wemmer, provided invaluable support and insights throughout all the stages of this work.

# Chapter 1 – Introduction to ring translocases

(Portions reproduced from: Lyubimov, A.Y., Strycharska, M. and Berger, J.M. (2011), *Curr. Opin. Struct. Biol.*, Apr 21(2), 240-248)

## ASCE MOTOR FAMILY

The processive and forceful movement of extended biopolymers, such as nucleic acids and polypeptides, is vital for a wealth of cellular transactions. Many of these events are catalyzed by multi-subunit, ring-shaped **N**ucleosidyl-**T**ri**P**hosphatases (**NTP**ases) that actively couple NTP turnover to directed substrate movement. A large number of oligomeric translocases belong to a broad grouping of proteins known as the **A**dditional **S**trand **C**atalytic glutamat**E** (**ASCE**) superfamily (Iyer et al., 2004; Leipe et al., 2003). The ASCE group is itself composed of several subfamilies, including RecA-like ATPases and **AAA+** (**A**TPases **A**ssociated with various cellular **A**ctivities) enzymes (**Figure 1.1A**). Ring-translocases typically form homohexameric assemblies, although heterohexamers, homopentamers and homoheptamers also exist.

The core RecA- and AAA+-type folds are related (**Figure 1.1B**), consisting of a conserved five-stranded, parallel β-sheet sandwiched between several α-helices (Iyer et al., 2004; Story and Steitz, 1992; Story et al., 1992). Each protomer contains a pair of conserved sequence motifs – termed Walker A and B – that interact with both the phosphate groups of bound nucleotide and an essential $Mg^{2+}$ cofactor to control catalysis (Abrahams et al., 1994; Story and Steitz, 1992; Walker et al., 1982). The Walker motifs are often accompanied by a conserved glutamate residue (the namesake of the ASCE family), which resides either within the Walker-B sequence or at a spatially proximal position (**Figure 1.1B**) (Subramanya et al., 1996; Thomsen and Berger, 2008). When present, this amino acid helps polarize a water molecule for nucleophilic attack on the bound NTP to elicit hydrolysis.

The NTPase active site lies at the interface between adjoining protomers, such that the catalytic motifs of each motor subunit are complemented by contributions from a partner subunit in the form of an arginine (or lysine), termed the "arginine finger". In addition to contributing functionally to NTP hydrolysis the Arg-finger facilitates intersubunit communication, allowing NTP binding and product release to induce conformational changes between neighboring protomers and consequently around the ring (Iyer et al., 2004; Nadanaciva et al., 1999; Thomsen and Berger, 2008).

RecA and AAA+ NTPases are often described as a single motor family. However, this grouping overlooks significant differences between the two protein

classes. In particular, the core ASCE folds of RecA and AAA+ enzymes are differentially oriented within the context of higher-order oligomers such that their translocation pores run roughly perpendicular to one another (**Figure 1.1C**) (Wang, 2004). Consequently, the primary sequence positions of both the arginine finger and the substrate-interacting elements that form the pore are not conserved between the two families. Other family-specific functional motifs (e.g., the Sensor-II element of AAA+ proteins) similarly are not shared. This fundamental difference in quarternary organization likely underlies some of the disparate functional properties of these evolutionarily related motors.

## COORDINATION OF NTPASE STATUS

In all ring-translocases, cycles of binding and hydrolysis are coupled to conformational rearrangements of the substrate-binding elements. To date, three major types of mechanisms – rotary, concerted and stochastic – have been proposed for the progression of nucleotide turnover within the system (**Figure 1.2**). In the rotary model **(Figure 1.2A,B)**, hydrolysis proceeds from one subunit to the next in sequential fashion similar to the mechanism demonstrated for the $F_1$ ATPase (Abrahams et al., 1994; Adachi et al., 2000), a RecA-type ACSE NTPase that forms a portion of the ATP synthesis machinery of mitochondria, chloroplasts and bacteria. By contrast, the concerted model **(Figure 1.2C)** invokes an "all-or-none" mechanism, in which all NTPase sites in the translocase bind, hydrolyze, and release nucleotide simultaneously. The stochastic or "probabilistic" model **(Figure 1.2D)** posits a mechanism with no set order to hydrolysis events.

Myriad studies on a variety of ring-translocase systems have provided data supporting one model or another. Structures of nucleotide-bound or -free hexameric translocases organized into radial arrangements of discrete nucleotide-binding states (akin to those seen for $F_1$) have been linked to biochemical studies supporting a rotary mechanism (Augustin et al., 2009; Enemark and Joshua-Tor, 2006; Glynn et al., 2009; Massey et al., 2006; Sanders et al., 2007; Singleton et al., 2000; Thomsen and Berger, 2009; Yoshimoto et al., 2010). The visualization of fully symmetrized-particles in which all subunits occupy similar conformations and undergo uniform, *en bloc* transitions between nucleotide binding events has at times been taken as evidence for the concerted model (Gai et al., 2004; Wang et al., 2001). Other analyses, particularly of some protein unfoldases, have shown that individual NTPase subunits can in certain circumstances bind nucleotide and function independently of each other, suggesting a lack of enforced firing order (Martin et al., 2005; Yakamavich et al., 2008).

To date, few hexameric motors have been imaged with a translocation substrate. The three exceptions – the papilloma virus E1 replicative helicase, the Rho transcription termination factor and the bacterial replicative helicase DnaB – act on single-stranded (ss) nucleic acid chains (Enemark and Joshua-Tor, 2006; Itsathitphaisarn et al., 2012; Thomsen and Berger, 2009). Recent

structures of these proteins, bound to either ssDNA (E1, DnaB) or ssRNA (Rho), reveal a radially asymmetric arrangement of NTPase states (interestingly, E1 adopts a similar conformation even in the absence of DNA and nucleotide (Enemark and Joshua-Tor, 2006)). In these cases, NTPase states are distributed around the ring in a sequence that appears to recapitulate a full hydrolysis cycle (**Figure 1.2B**). These structures provide some of the strongest visual evidence yet supporting a rotary firing model (discussed below).

How generalizable are the observations for E1, Rho and DnaB to ring-translocases as a whole? The asymmetric "dimer-of-trimers" and "trimer-of-dimers" states visualized for many hexameric motors are consistent with a rotary mechanism. Whether these symmetrized ring-forms represent a functional difference with the asymmetric E1, DnaB and Rho models, or whether they convert into an asymmetric conformation upon binding substrate is not known. Computational studies on the SV40 large T-antigen (LTag) indicate that concerted, all-or-none NTP turnover may be incapable of inducing directional movement (Yoshimoto et al., 2010). Furthermore, despite some debate as to whether LTag translocates along one or two DNA strands, the structure of the closely related E1 helicase suggests that LTag may also employ a rotary mechanism. Finally, more recent studies of the ClpX protein unfoldase, proposed initially to function by a stochastic mechanism, have shown that certain combinations of functional and inactive protomers can cooperatively influence the activity of the entire ring (Martin et al., 2005). This finding, together with a recent structure of ClpX captured in a dimer-of-trimers configuration (Glynn et al., 2009), suggest that ClpX may typically employ a rotary NTPase mechanism, but retain sufficient flexibility to allow alternative subunits to hydrolyze NTP if one or more partner protomers is inactivated. Thus, it appears that the most prevalent mechanism of NTP turnover in ring-shaped translocases relies on the sequential, radial progression of hydrolysis around the translocase ring.

The peculiar properties of ClpX, mirrored to some extent by other ring-translocases, raise intriguing questions about the plasticity of the NTPase mechanism. Here, plasticity refers to the degree to which neighboring NTPase sites are constrained to turn over nucleotide in a fixed sequence. As most ring-translocases are homo-oligomers, this issue has been difficult to address due to the inherent difficulty of inactivating specific subunits. Nonetheless, titration experiments with different ratios of defective and wild-type subunits have shown that certain motors cannot tolerate even a single defective protomer without losing function (Adelman et al., 2006; Crampton et al., 2006; Massey et al., 2006), whereas others (including ClpX) are more permissive (Bochman and Schwacha, 2008; Ilves et al., 2010; Martin et al., 2005; Moreau et al., 2007).

We propose that these differences imply the existence of a continuum with respect to the plasticity of ring NTPase firing order. In this spectrum, the behavior of many RecA-type proteins (e.g., the T7 gp4 helicase and Rho) can be considered "strictly" sequential (Adelman et al., 2006; Crampton et al., 2006), whereas several AAA+ motors (the MCM helicases, possibly ClpX) fall into a

"loosely" sequential category (Martin et al., 2005; Moreau et al., 2007). Given that every subunit in a ring translocase is sandwiched between two others, it is clear that a circular assembly affords ample opportunity for catalytic events to be sensed at a distance through allosteric mechanisms. What is less clear is how such networks have adapted at the physical level to be more or less permissive of subunits that do not fire properly.

Another aspect of the firing-order models that has not been (and indeed cannot be) addressed by structure is whether hydrolysis proceeds at constant monotonic rate between subunits. Interestingly, single-molecule analyses of the bacteriophage ϕ29 packaging protein – a pentameric, RecA-type ring NTPase that translocates along double-stranded DNA – provide compelling evidence for a rotary firing mechanism (Chemla et al., 2005; Moffitt et al., 2009); however, these efforts also indicate that packaging occurs in well-defined 10-base pair "bursts" composed of four rapid and successive substeps. Each packaging cycle may consist of a loading phase in which four (or five) ATPase sites engage ATP, followed by a second phase in which four consecutive hydrolysis events propel the motor along DNA. Similarly, presteady-state studies on RNA substrates containing single, phased deoxyribonucleotides indicate that Rho requires a 2'-OH on every seventh base for efficient translocation (Schwartz et al., 2009). Available structural data are not necessarily inconsistent with these observations. For instance, the sequential order of ATPase states seen in Rho or E1 could reflect an intermediate in which a hydrolysis burst has only partly occurred. Alternatively, it may prove that different motor systems have significantly distinct properties with respect to the relative timing of hydrolysis. At present, no one system exists in which complementary structural and solution data are available to resolve this issue.

## SUBSTRATE INTERACTIONS AND NTPASE/TRANSLOCATION COUPLING

A particularly fundamental question in ring translocases is how substrate movement in the pore is effected by catalytic events at distal NTPase sites. Although the polymer-binding regions of different motor families are divergent in their primary sequence, they typically adopt either loop or β-hairpin structures. In all cases, except where a six-fold symmetric ring is observed, these elements wrap around the central axis of the translocation pore in a helical or semi-helical array (Enemark and Joshua-Tor, 2006; Glynn et al., 2009; Itsathitphaisarn et al., 2012; Singleton et al., 2000; Thomsen and Berger, 2009; Wang et al., 2001). When nucleotide-bound and -free states are compared for a given translocase (including fully-symmetrized forms), the vertical position of a given loop or hairpin in the pore is seen coupled to the nucleotide status of its associated NTPase center. Thus, the subunit "rocking" events so frequently seen to accompany NTP binding, hydrolysis, and release, also help cause the loops to lever up and down the ring axis (Enemark and Joshua-Tor, 2006; Gai et al., 2004; Glynn et al., 2009; Itsathitphaisarn et al., 2012; Mancini et al., 2004;

Singleton et al., 2000; Thomsen and Berger, 2009; Wang et al., 2001), walking the motor along substrate.

Whether substrates are passed from one subunit to the next in a "bucket-brigade" fashion, or whether each subunit escorts a single portion of the substrate through the entirely of the central channel, has been addressed by substrate-bound structures of E1, Rho and most recently DnaB (Enemark and Joshua-Tor, 2006; Itsathitphaisarn et al., 2012; Thomsen and Berger, 2009). These enzymes manifest a right-handed, spiral staircase of pore loops, upon which the translocation substrate sits curled into a matching helical configuration **(Figure 1.3)**. Both E1 and Rho proteins overwind the substrate, compressing it in the core, DnaB however appears to interact with an extended piece of single-stranded DNA spanning roughly 32Å in comparison to 10.9Å for Rho and 12.8Å for E1. As one follows the progression of NTPase states around the ring (from E→T→DP), the loops of E1 and Rho helicase wrap around the ring axis in a smoothly graded manner (**Figure 1.3**). The transition between states at the beginning or end of the NTPase cycle is marked by a single subunit positioned midway between the top and bottom of the ring. The loops curl around either the 5' or 3' face of the phosphodiester backbone, appearing to "tug" on substrate in a direction consistent with the translocation polarity of E1 and Rho, respectively. In the case of DnaB replicative helicase translocation of DNA appears to be achieved through the motions of the entire ATPase subunits rather than just the nucleic acid binding elements. When bound to ssDNA DnaB adopts a helical conformation, where the ATPase domains create a spiral staircase with a 5.6Å rise per protomer. Upon nucleotide hydrolysis the topmost ATPase domain is thought to dissociate from the two nucleotides at the 5′ end of the ssDNA and when γ-phosphate is released the domain drops to the bottom-most position tugging onto the DNA. Therefore whereas E1 and Rho have been proposed to act via an escort model in which a pore loop or hairpin contacts a nucleobase at the start of the NTPase cycle and chaperones it continuously through the translocation pore, the mechanism of DnaB is described as hand-over-hand or rope climber scenario, where DnaB has to let go of one basepair to translocate and grab onto another ~30Å away. The 3-fold longer pitch of bound ssDNA furthermore results in a larger stepsize of 2nucleotides per subunit in contrast with a single nucleotide per subunit in the case of E1 and Rho.

The translocation substrate may not be a passive participant during motor movement. In the case of Rho, each change in nucleotide state appears to be accompanied by significant flexing and rearrangement of a conserved salt bridge network that runs from the substrate-binding pore to the NTPase active site. The degree to which all available salt bridges in the network are fully formed depends on the interactions with RNA and the nucleotide state. The network becomes fully interconnected exactly where the Rho subunit making the greatest number of contacts to RNA also adopts a hydrolysis-competent (T*) state. The fully formed network appears necessary to properly position the catalytic glutamate and its associated nucleophilic water next to the γ-$PO_4$ moiety of the bound nucleotide. Thus, the RNA seems to act as a "timing belt", whereby its relative

position in the translocation pore controls the firing order of the subunits and establishes the observed RNA dependence or the Rho NTPase activity. The critical nature of this network is supported by its invariance among Rho homologs across all bacteria. Altering these amino acids has been shown have deleterious effects on both RNA binding and hydrolysis activity, even though they do not contact either substrate or ATP directly (Dombroski et al., 1988; Miwa et al., 1995; Thomsen and Berger, 2009; Wei and Richardson, 2001; Xu et al., 2002).

Whether AAA+ enzymes employ a similar network is unclear. The mitochondrial m-AAA unfoldase appears to retain several amino acids that sense the nucleotide state of each ATPase site at a distance; they couple this status to substrate translocation by controlling intersubunit conformational changes (Augustin et al., 2009). Less clear is the existence of conserved and flexible cross-protomer interactions (outside the active site) in E1 that might also correlate with substrate contacts. Whether this distinction is due to the presence of only 1-2 ATP-bound states in E1, while Rho contains at least four (consistent with a biochemically-observed delay between the timing of ATP binding and hydrolysis (Adelman et al., 2006), is also unknown. To date, there has been relatively little study of residues that do not directly contact substrate molecules or participate in NTPase chemistry.

## GENERALITY OF THE ASCE TRANSLOCATION MECHANISMS

A detailed picture of ring-shaped translocase mechanism has been slowly coming into focus. Progress on these systems has been hindered in part by their conformational dynamism, multistep reaction cycle, and complex structural organization. Although diverse models have been proposed to explain how NTP turnover is transduced into physical movement, a growing number of findings implicates a rotary firing order in coordinating hydrolysis among subunits.

Nonetheless, functional differences between various classes of ring-shaped translocases imply that likely mechanistic divergences also exist. For Rho and E1, one such difference (translocation direction) appears to arise from an inverted order by which waves of NTP hydrolysis progress around their respective rings. Whether this approach is generalizable to other motors is uncertain: as already seen with distantly-related Superfamily-1 and -2 helicases, there exists a myriad of divergent chemo-mechanical means for altering directional polarity (see (Singleton et al., 2007) and references therein). Other significant issues, such as how hydrolysis is timed, whether NTP turnover events are uniform or clustered, how NTPase cycles and translocation elements have adapted to different (and sometime non-uniform) substrates, which NTPase step constitutes the “power-stroke” for translocation, or why certain motors are more or less tolerant of subunit “misfiring”, also remain to be determined. Many more surprises undoubtedly await investigators as they continue to dig deeper into this essential and complex class of molecular machines.

## DnaB as a model system for a RecA motor

When the work described here was initiated, structures of E1 and Rho helicases were the only available examples of ring-shaped translocases imaged in the presence of their substrates. To investigate whether the mechanism proposed for Rho helicase was generalizable across other members of the RecA-type subfamily of ASCE motors we chose to study bacterial helicase DnaB.

Out of a myriad of helicases found in bacteria, DnaB is the only essential one since it acts as the engine propelling replisome during DNA replication. It's basic biochemical properties have been thoroughly characterized with various biochemical approaches and there are a number of available substrate-free structures making it a great candidate for a more in-depth mechanistic study. Furthermore, since DnaB lies at the heart of the replisome (**Figure 1.4**) and interacts with multiple replication factors, it is likely subjected to complex regulation mechanisms and thus presents an even more challenging and interesting motor to study.

Before a structure of *Bst*DnaB in complex with nucleotide and single-stranded DNA was published, we attempted to address questions surrounding the interplay between the structure and function of DnaB by seeking a nucleotide bound structure of the helicase from *Aquifex aeolicus*. We determined a 3.3 Å resolution X-ray crystal structure of the helicase in complex with ADP with architecture distinct from other previously-observed ring states of this motor. In particular, the N-terminal domains have undergone a large conformational rearrangement from that seen in substrate-free helicase structures, transitioning from a widened, or "dilated," configuration (which encircles a broad central channel), into a highly-constricted form with a narrow pore. Concomitant with this action, the ATP- and nucleic acid-binding elements of DnaB have re-aligned into a new configuration that appears poised to support nucleotide turnover. Using electron microscopy (EM) and small-angle X-ray scattering (SAXS), we confirmed that in both *A. aeolicus* and other bacteria, DnaB can adopt the constricted state observed in the crystal structure, and further demonstrate that this transition is promoted by nucleotide in both the presence and absence of DNA. Structure-derived mutants of *Escherichia coli* DnaB that preferentially form one collar state or the other can unwind DNA, but have markedly altered properties with respect to double-stranded DNA translocation and their ability to support either priming by DnaG or helicase activation by the clamp-loader tau subunit. Together, our data show that, like their eukaryotic counterparts, bacterial replicative helicases are complex, multistate machines whose properties can both modulate and be modulated by other replication factors.

## McrB as a model system for a AAA+ motor

Although multimeric ring ATPases have been extensively studied with bulk biochemistry and structural biology methods, the precise mechanism by which hydrolysis drives inter-subunit conformational rearrangements that result in

substrate translocation is unknown. As discussed earlier in this Chapter, all examples of ASCE motors imaged to date with their translocation substrates interact with single-stranded nucleic acids. Experiments testing whether mechanisms proposed for these single-stranded translocases can be generalized across the whole RecA-type and AAA+ subfamilies need to be carried out in order to fully understand these complex ring-shaped NTPases. We chose to study a AAA+ protein that is predicted to act as a motor domain of an McrBC restriction enzyme thought to translocate dsDNA in order to bring two distant recognition sites together before cleavage can occur. Obtaining crystal structures of dsDNA complexed with McrB motor ring in combination with biochemical and single molecule characterization could provide us with important insights into the mechanism of McrB translocation and would eventually lead to better understanding of other dsDNA translocases.

**Figure 1.1**

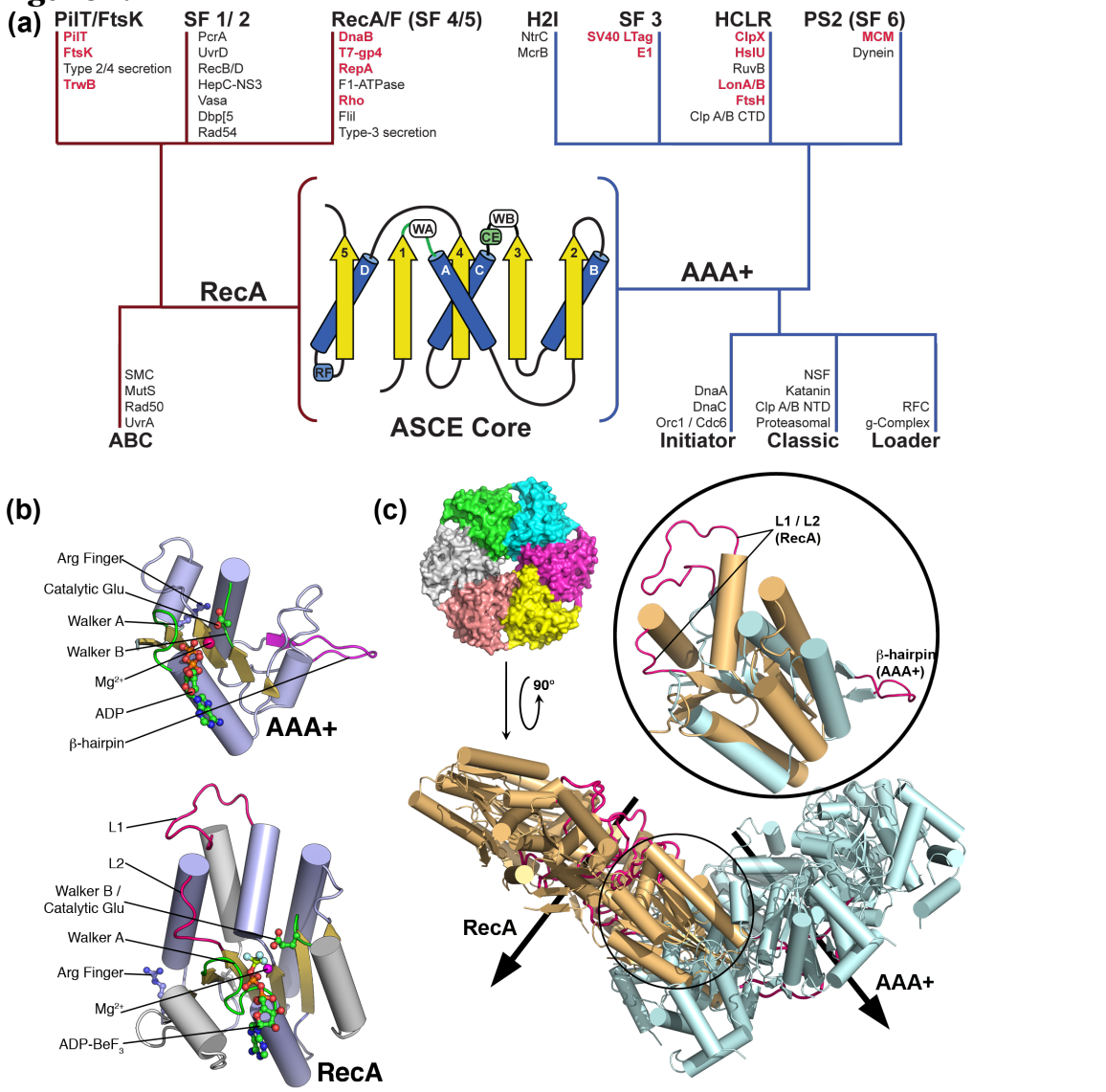


**Figure 1.1. Conservation and divergence of RecA and AAA+ ring translocases**. A) A phylogenetic tree showing the main clades of the RecA-type (red) and AAA+ (blue) subgroups of the ASCE superfamily. Representative examples of NTPases are listed above each clade, with translocases highlighted in bold red. The base of the tree shows a diagram of the conserved ASCE fold with the main elements of the NTPase active site indicated. Abbreviations: SF1-6 – helicase superfamilies one through six, H2I – helix 2 insert, HCLR – (HslU, ClpABC-CTD, LonAB, RuvB), ABC – ATP Binding Cassette, AAA+ - ATPases Associated with diverse cellular Activities, ASCE – Additional Strand, Catalytic glutamate. B) Cartoon representation of NTPase and substrate-binding elements of an AAA+ (E1) and RecA-type (Rho) ring-translocase. Nucleotide molecules and Arg are shown as ball and stick. C) Perpendicular orientation of RecA (Rho, beige) and AAA+ (E1, cyan) rings and translocation pores results when the core folds are aligned (inset). Pore loops are shown in magenta

## Figure 1.2

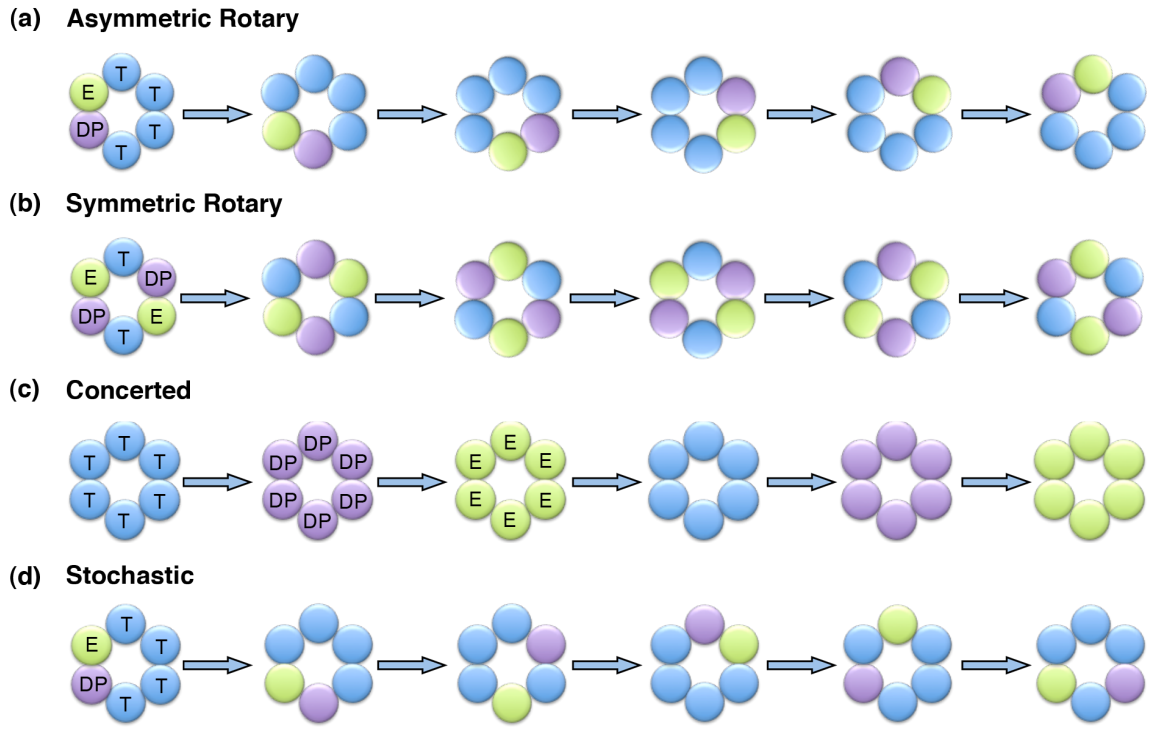


**Figure 1.2. NTP hydrolysis models in ring-translocases.** A) Symmetric rotary mechanism: NTPase events proceed sequentially along three consecutive subunits and are repeated by the opposing three subunits. B) Asymmetric rotary mechanism: NTPase events (nucleotide binding, hydrolysis and product release) proceed sequentially around the ring. C) Concerted mechanism: NTPase events occur simultaneously in all six subunits. D) Stochastic mechanism: NTPase events occur without a set order. T (blue) – NTP state, DP (purple) – NDP + Pi state, E (green) – nucleotide exchange state.

**Figure 1.3**

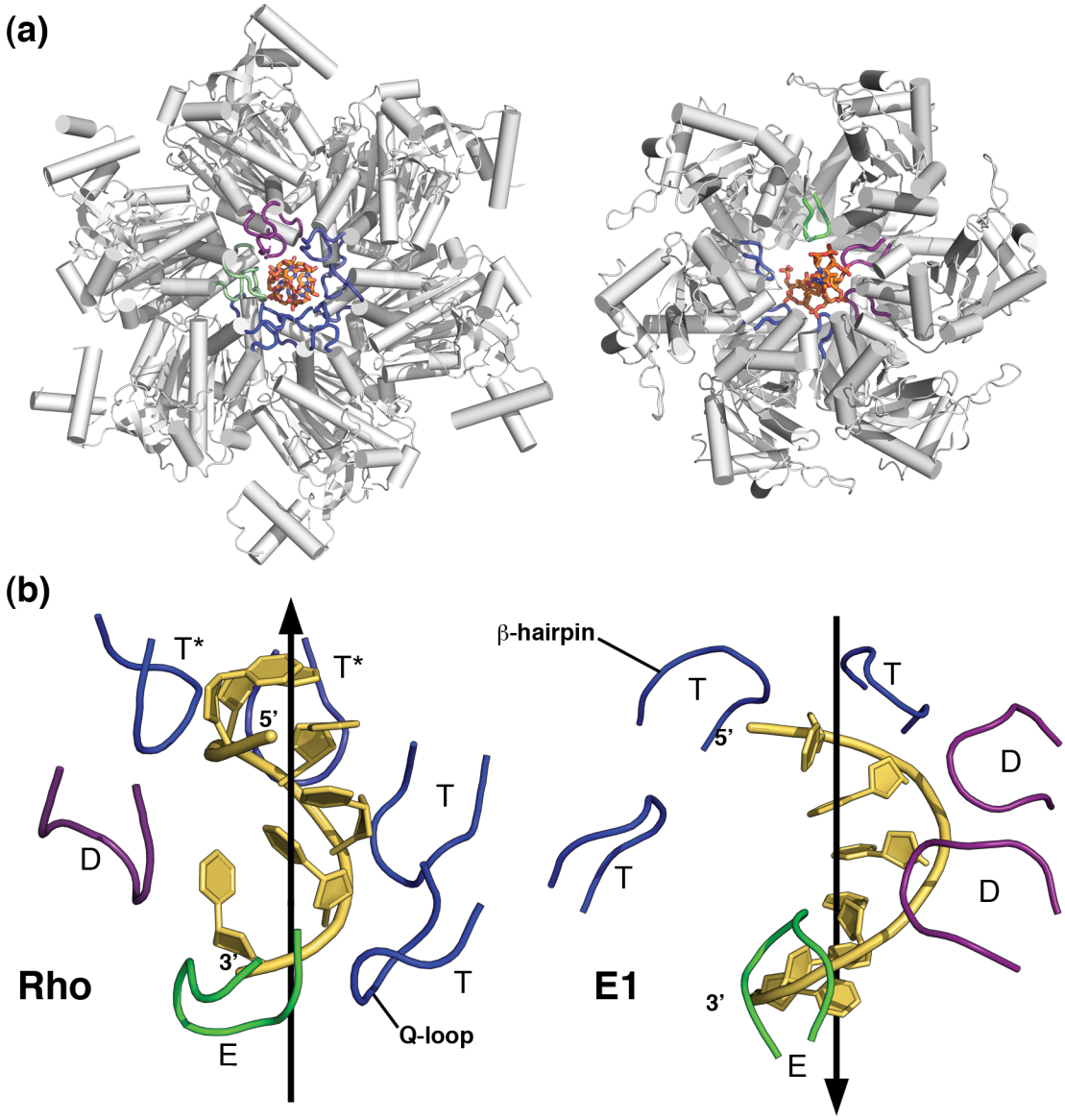


**Figure 1.3. Substrate binding and translocation by single-stranded nucleic acid translocases.** A) A top-down view of Rho (PDB ID: 3ICE) and E1 (PDB ID: 2GXA) in complex with their single-stranded nucleic acid substrates. B) Pore loops of Rho and E1 engaged with ssRNA and ssDNA, respectively. Nucleic acid is oriented such that the 5' end is on top. In the case of Rho, the transitioning loop is associated with the NDP + Pi (D) state, while in E1 it is associated with the NTP-bound (T) state. Loops are colored by subunit nucleotide state, according to the same scheme as in Figure 2.

## Figure 1.4

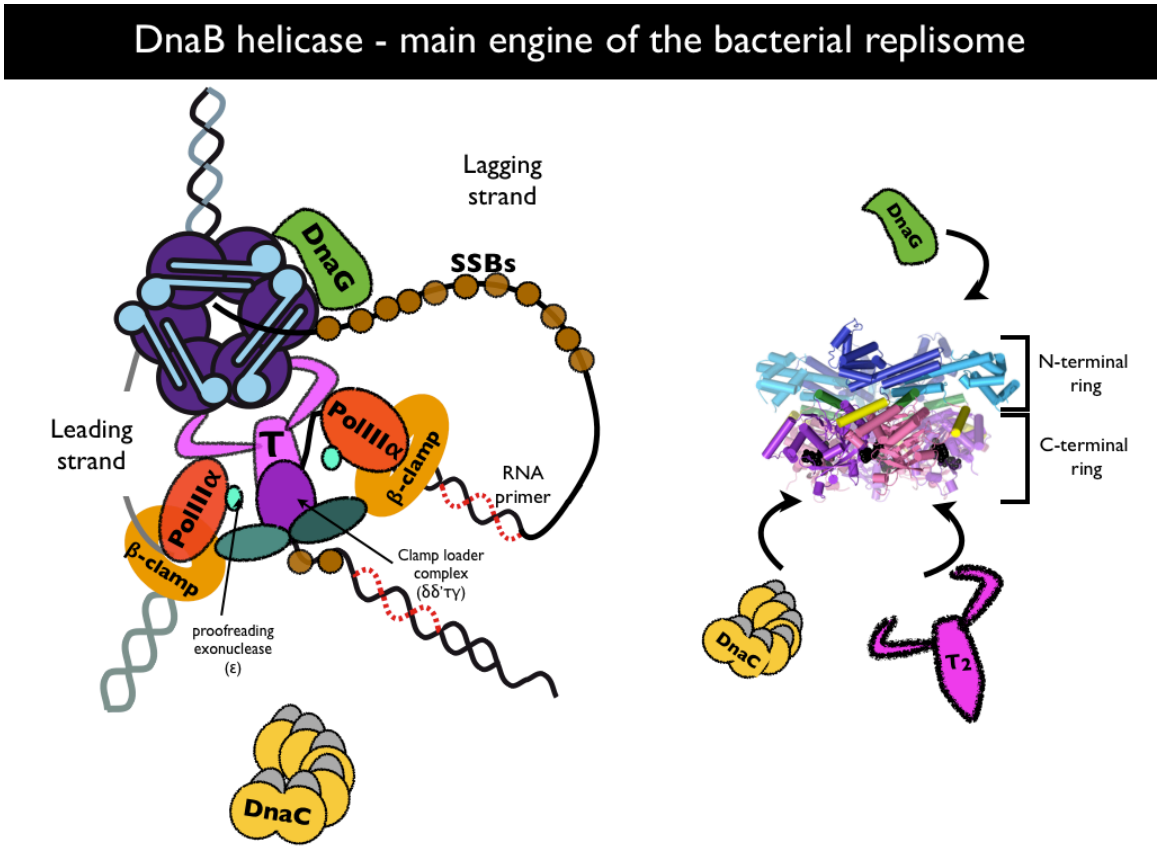


**Figure 1.4. DnaB helicase is the main motor of the bacterial replisome.** Cartoon representation of the bacterial replisome with DnaB helicase drawn in purple (C-terminal RecA-type ATPase domains) and blue (N-terminal domains). On the right is a side view of the crystal structure of DnaB, color coded like the cartoon representation, highlighting interactions with the replication factors investigated in this study.

# Chapter 2 – New conformation of the bacterial replicative helicase - DnaB

## INTRODUCTION

The accurate and timely replication of DNA is essential for the proliferation of all cells (Costa et al., 2013; Fuller et al., 1981; Kaguni et al., 1982). Dedicated enzymes known as helicases are key drivers of replication fork progression, unwinding parental DNA duplexes to provide single-stranded template to DNA polymerases for strand synthesis (Pomerantz and O'Donnell, 2007). Cellular replicative helicases universally form either homohexameric or heterohexameric rings, which encircle DNA and use ATP hydrolysis to drive the processive separation of paired duplex substrates (Singleton et al., 2007). Despite extensive study, the mechanisms by which hexameric helicases couple ATP turnover to DNA unwinding remain poorly defined. How helicase activity is coordinated with specific replication initiation and progression factors is likewise unclear.

Replicative hexameric helicases fall into two evolutionarily distinct classes – **M**ini**C**hromosome **M**aintanence (MCM) proteins and DnaB-family enzymes – that share a conserved ATPase fold but that differ in their quaternary organization and accessory domains (Iyer et al., 2004; Leipe et al., 2003; Lyubimov et al., 2011; Wang, 2004). DnaB helicases, which are found in all bacteria, as well as certain bacteriophage (Leipe et al., 2000), assemble into two-tiered homohexameric rings, in which a C-terminal, RecA-type ATPase domain from each of the six subunits comprises one tier and an N-terminal structural domain forms the other (Bailey et al., 2007b; Itsathitphaisarn et al., 2012; Lo et al., 2009; Wang et al., 2008). In each DnaB protomer, the N-terminal domain is connected to the C-terminal region by a **L**inker **H**elix (LH) that anchors adjoining subunits together through a domain-swapping event. Interestingly, DnaB-family enzymes all display a natural symmetry mismatch between their two tiers (San Martin et al., 1998; San Martin et al., 1995): the C-terminal domains exhibit variable, but roughly cyclic, quasi-six-fold symmetry (Bailey et al., 2007b; Lo et al., 2009; Wang et al., 2008), whereas the N-terminal domains form homodimers that self-associate into a trimeric collar (Bailey et al., 2007b; Biswas and Tsodikov, 2008; Itsathitphaisarn et al., 2012; Lo et al., 2009; Wang et al., 2008). The C-terminal RecA domains encircle single-stranded DNA substrate and harness energy of ATP hydrolysis to effect translocation of the helicase in a 5'→3' direction with the C-terminal domains facing towards the 3' end of DNA (Baker et al., 1987; LeBowitz and McMacken, 1986; Mok and Marians, 1987). The N-terminal collar also appears to be essential for DNA unwinding in bacterial orthologs of DnaB (Bird et al., 2000; Biswas and Biswas, 1999b; Biswas et al., 1994; Nakayama et al., 1984) and has been proposed to act as a structural scaffold that holds the hexameric DnaB ring together (Biswas et al., 1994). Nonetheless, the specific structural and functional role of the N-terminal

domains has remained elusive.

In the absence of substrate, DnaB-family helicases display a high degree of positional variation and separation in the relative conformations of their C-terminal domains (Bailey et al., 2007b; Lo et al., 2009; Wang et al., 2008). Upon binding of single-stranded DNA and nucleotide, however, the active sites of DnaB have recently been shown to condense into a more uniform, compact conformation that resembles related nucleotide-bound, hexameric helicases such as the Rho transcription termination factor and T7 bacteriophage gp4 (Itsathitphaisarn et al., 2012; Singleton et al., 2000; Thomsen and Berger, 2009). Interestingly, EM experiments have indicated that conformational heterogeneity persists within DnaB even when nucleotide is present, implying that the fully-liganded helicase still exhibits significant plasticity (Yang et al., 2002; Yu et al., 1996).

## DETERMINATION OF THE AQUIFEX AEOLICUS DNAB CRYSTAL STRUCTURE

To better define the physical consequences of nucleotide binding to DnaB, we determined the crystal structure of the full-length helicase from *A. aeolicus*. The primary sequence of *Aa*DnaB is 40% identical to other enzymes of the family (**Figure 2.1**). To obtain crystals, full-length *Aa*DnaB was overexpressed and purified from *E. coli*. Gel-filtration analysis indicated that the purified material migrated as a stable hexamer, with no monomeric species evident in sample preparations. Crystals from the protein diffracted to 3.3Å and belonged to the cubic spacegroup, I23. Solution of the structure by molecular replacement revealed one DnaB homodimer per asymmetric unit, with the operation of a crystallographic three-fold symmetry recapitulating a two-tiered, hexameric particle formed by a set of N-terminal scaffolding elements (tier 1) and a set of C-terminal ATPase domains (tier 2) (**Figure 2.2**). Electron density maps showed clear evidence for ADP•$Mg^{2+}$ bound at each interface between the adjacent monomers (**Figure 2.3A**). The final model was refined to an $R_{work}/R_{free}$ of 22.1%/25.9%, with excellent stereochemistry as judged by MolProbity (Chen et al., 2010) (**Table 2.1**).

## NUCLEOTIDE BINDING CORRELATES WITH ATPASE DOMAIN ENGAGEMENT

DnaB-family helicases, like all oligomeric RecA-like ATPases, rely on a bipartite ATPase active site for function, in which residues from neighboring subunits collaborate to carry out ATP turnover (Leipe et al., 2000; Thomsen and Berger, 2008). Two highly-conserved elements in one protomer, the Walker A (WA) and B (WB) motifs, interact with the triphosphate moiety of ATP and an essential $Mg^{2+}$ cofactor, while a neighboring subunit provides a conserved basic amino acid (typically arginine, termed an “arginine finger” (RF)) to coordinate

the γ-$PO_4$ group *in trans*. This arrangement not only allows each subunit to facilitate ATP hydrolysis in a partner protomer, but also provides a means to elicit and coordinate nucleotide-dependent conformational changes around the helicase ring. In available apo structures of bacterial DnaB-type proteins, the RecA folds of adjoining subunits are positioned too far apart to form a functional ATPase site (Bailey et al., 2007b; Lo et al., 2009) (**Figure 2.3**). As a consequence, the arginine finger residue on each of these subunits fails to engage the active site of its neighboring protomer, uncoupling adjoining ATPase domains from one another and giving rise to a wide pore in the center of the DnaB toroid.

The *Aa*DnaB structure determined here markedly differs from these prior models. A conserved "linker" helix (LH), which anchors neighboring ATPase domains to one another, maintains the same set of contacts in *Aa*DnaB as in more loosely-associated structures (e.g., *Bacillus stearothermophilus* DnaB (Bailey et al., 2007b)); however, all six ATPase domains interact with each other much more extensively (~1000Å$^2$ per protomer, **Figure 2.3**). As a consequence, although the ATPase regions of *Aa*DnaB still form a pseudo-6-fold symmetric ring reminiscent of that found in orthologous proteins, the central pore of the *A. aeolicus* helicase is much more constricted compared to its counterparts (**Figure 2.4**). Moreover, even though the bound ADP molecule lacks the γ-$PO_4$ usually coordinated by the RF, the arginine residue of each subunit is pulled into the active site of its partner (**Figure 2.3**).

Closer inspection of both ATPase centers in *Aa*DnaB reveals that the active site configurations between alternating pairs of subunits are slightly different. Nearly all of the conserved functional motifs of monomer A fully engage the bound ADP, whereas in monomer B, the catalytic glutamate (CE) normally responsible for positioning a water molecule for nucleophilic attack on a γ-phosphate group is oriented away from the nucleotide (**Figure 2.3**). In addition, although the α- and β-phosphates of ADP are coordinated by the WA elements in an arrangement canonical to RecA (and AAA+) ATPases, the base position varies between the two protomers.

A curious feature shared by both classes of active sites is the environment of the adenine moiety. Generally, in RecA-family proteins the nucleotide base is stacked between a pair of amino acids (often one aromatic and one basic side chain) (Abrahams et al., 1994; Sawaya et al., 1999; Singleton et al., 2000; Thomsen and Berger, 2009) (**Figure 2.5**). In *Aa*DnaB, however, the two residues expected to perform this task (Arg393 and Phe428) associate with each other, occluding the adenine-binding pocket. Interestingly, the collapsed pocket and the Arg/Phe interaction are preserved in the existing nucleotide-free structures of DnaB (Bailey et al., 2007a, b; Lo et al., 2009; Wang et al., 2008). Given the canonical contacts made to the $Mg^{2+}$•diphosphate group and the co-localization of catalytic amino acids seen in the *Aa*DnaB structure, the basis for the noncanonical base configuration is not clear. Inspection of a recent GDP•AlF4-associated DnaB structure reveals a similar binding mechanism to

that seen for *Aa*DnaB (Itsathitphaisarn et al., 2012), suggesting that bacterial replicative helicases have evolved a divergent means for coordinating substrate nucleotides within the RecA ATPase superfamily.

## NUCLEOTIDE BINDING PROMOTES A NOVEL CONFORMATION OF THE N-TERMINAL COLLAR

A distinguishing feature of all bacterial (and certain phage) DnaB-family helicases from other RecA-family ring ATPases is the presence of a conserved N-terminal domain consisting of a globular helical bundle appended to an extended α-helical hairpin (Bailey et al., 2007a, b; Fass et al., 1999; Kashav et al., 2009; Weigelt et al., 1999). The helical hairpins of two neighboring N-terminal domains form homodimers, giving rise to a twin-lobed, dumbbell-shaped element. Both on their own and in the context of a DnaB hexamer, neighboring N-terminal domain dimers have been seen to self-organize into a triangular, trimeric structure that circumscribes a wide inner channel (~50Å in diameter) (**Figure 2.6**) (Bailey et al., 2007b; Biswas and Tsodikov, 2008; Itsathitphaisarn et al., 2012; Lo et al., 2009; Wang et al., 2008). The sides of the triangle are formed by helical hairpin dimers of the N-terminal domains, whereas the apices are created by globular helical bundles from different dimers that abut one another. Thus far, only one type of trimer configuration has been observed for the N-terminal collar in the context of DnaB alone, indicating it is a favored quaternary state of the region.

The conformation seen for the *Aa*DnaB N-terminal domains differs markedly in comparison to other DnaB structures (**Figure 2.6**). Although the N-terminal domains of the helicase maintain the hairpin interfaces within each homodimer, the globular domains of adjoining dimers manifest a completely different set of interactions between each other (**Figure 2.7**). In attaining this state, each N-terminal homodimer has undergone an ~40˚ rotation within the plane of the ring, projecting three globular lobes outward from the ring and clustering three others in the interior. The resultant rearrangement leads to a distinctive triskelion that constricts the diameter of the channel formed between the N-terminal domains by ~30 Å from that seen in the other, more dilated state. The new interactions between the globular subdomains and the distal ends of the helical hairpins are modest, reducing the buried surface area per globular subdomain by ~40% compared to the widened, triangular form (from 370Å$^2$ to 230 Å$^2$) (**Figure 2.7**).

At first glance, constriction of the N-terminal domains would appear to help promote the observed tightening of the C-terminal domains and formation of productive ATPase centers. However, close engagement of neighboring motor domains is also seen in the structure of *B. stearothermophilus* DnaB bound to ssDNA and nucleotide, which exhibits a dilated collar (Itsathitphaisarn et al., 2012). A significant structural difference between these two states is that the

*Bst*DnaB hexamer forms a lockwasher, or cracked-spiral configuration, whereas the *Aa*DnaB ring is closed-planar. However, in both instances, ATPase domain clustering is coincident with an inward tilt toward the pore of the ring compared to that seen in apo DnaB models (**Figure 2.6**). Tilting appears to be coordinated by both a linker α-helix that connects the N- and C-terminal domains together and by an additional α-helix in the motor domains. This latter α-helix in particular makes extensive contacts with the N-terminal domain of a neighboring protomer when the collar is dilated, but with its own N-terminal domain upon entry into the constricted state, suggesting that it helps to transduce conformational signals between the two domains. Consistent with this notion, mutations in the transducer helix have pronounced effects on properties such as single-stranded DNA binding, the DNA-dependence of ATP hydrolysis, and DNA unwinding (Biswas and Biswas, 1999a, b; Nitharwal et al., 2012)**.**

## CONCLUSION

Taken together, these observations suggest that upon engaging nucleotide, the N-terminal collar and RecA domains of DnaB can convert from a dilated apo state, in which the helicase exhibits a large central pore, into a constricted form that displays a reordered collar and tightened ATPase ring. Curiously a recently published structure of a *Bacillus stearothermophilus* DnaB (*Bst*DnaB) bound to ssDNA and GDP•$AlF_4$ and a nucleotide-free crystal structure of the *Bacillus subtilis* bacteriophage SPP1 G40P, a viral DnaB-like helicase, both exhibit a blend of both states (Itsathitphaisarn et al., 2012; Wang et al., 2008) (**Figure 2.6**): the C-terminal domain rings of these helicases are constricted, yet their N-terminal collars remain dilated as in all nucleotide-free DnaB structures. In the DNA-bound structure both tiers of the hexamer are additionally slightly cracked and helical. It is very likely that these two structures represent additional conformations of the bacterial replicative helicase utilized during different stages of replication, further emphasizing the great versatility and modularity of the DnaB helicase architecture.

## MATERIALS AND METHODS

*Protein expression and purification*

The full length *Aquifex aeolicus dnaB* gene (residues 1-468) was amplified from genomic DNA and cloned into an *Escherichia coli* expression vector pET24A. The plasmid was transformed into BL21 RIL cells, and the protein was overexpressed in 2xYT media by induction at an $OD_{600}$ of 0.3 with 0.25 mM IPTG at 37°C for 3-5 hours. Cells were resuspended in 50 mM HEPES-KOH pH 7.5, 1 M KCl, 10% Glycerol, 5 mM $MgCl_2$, 1 mM ATP, 1 μM Pepstatin-A, 1 μM leupeptin and 1 mM PMSF, and lysed by sonication. The crude lysate was heat-treated for 15 minutes at 65°C, left on ice for 30 minutes, and recentrifuged. After re-adjusting the salt concentration to 200mM KCl by dilution, the supernatant was applied to a POROS HQ anion exchange column (Perseptive Biosystems). Protein

was then further purified with two sizing runs using a Sephacryl S-300 gel-filtration column (Amersham) pre-equilibrated in a high-pH buffer (100mM Tris pH 8.5, 800mM KCl, 5mM $MgCl_2$, 1mM ATP, 10% Glycerol) to separate contaminating DNA. Peak fractions were pooled and concentrated by ultrafiltration (Amicon-Ultra, Millipore) to 15-20 mg/ml and stored at 4°C.

*Crystallization and Data Collection*

For crystallization, *Aa*DnaB was dialyzed overnight into 10 mM HEPES-KOH pH 7.5, 50 mM KCl, 5 mM $MgCl_2$, 1 mM ADP, and 0.1 mM AMPPNP. Hanging-drop crystals were grown by mixing 1µl of protein solution with 1µL of well solution containing 100mM Hepes pH 7.5, 200-300mM KSCN or NaSCN and 18-22% PEG 3350. Cubic crystals grew between 2-14 days. Crystals were cryoprotected, looped and flash frozen in liquid nitrogen. Diffraction data were collected on Beamline 8.3.1 at the Advanced Light Source (MacDowell et al., 2004).

*Structure Solution and Refinement*

XDS was used to process diffraction data (Kabsch, 2010). Phases were obtained by molecular replacement using PHASER (McCoy et al., 2007), with ensembles of individual domains from all available DnaB structures utilized as a search model. Initial rigid body and grouped B factor refinement were performed using PHENIX (Adams et al., 2002). At this stage Fo-Fc electron density maps showed clear density for the nucleotide. In subsequent steps, we performed iterative steps of multidomain refinement with torsional NCS averaging and simulated annealing in PHENIX, followed by manual building in COOT (Emsley and Cowtan, 2004). Model bias was removed using composite-omit maps calculated in CNS (Brunger et al., 1998). The final model was validated using MolProbity (Chen et al., 2010). Molecular models were rendered using PyMOL (DeLano, 2009).

## Figure 2.1

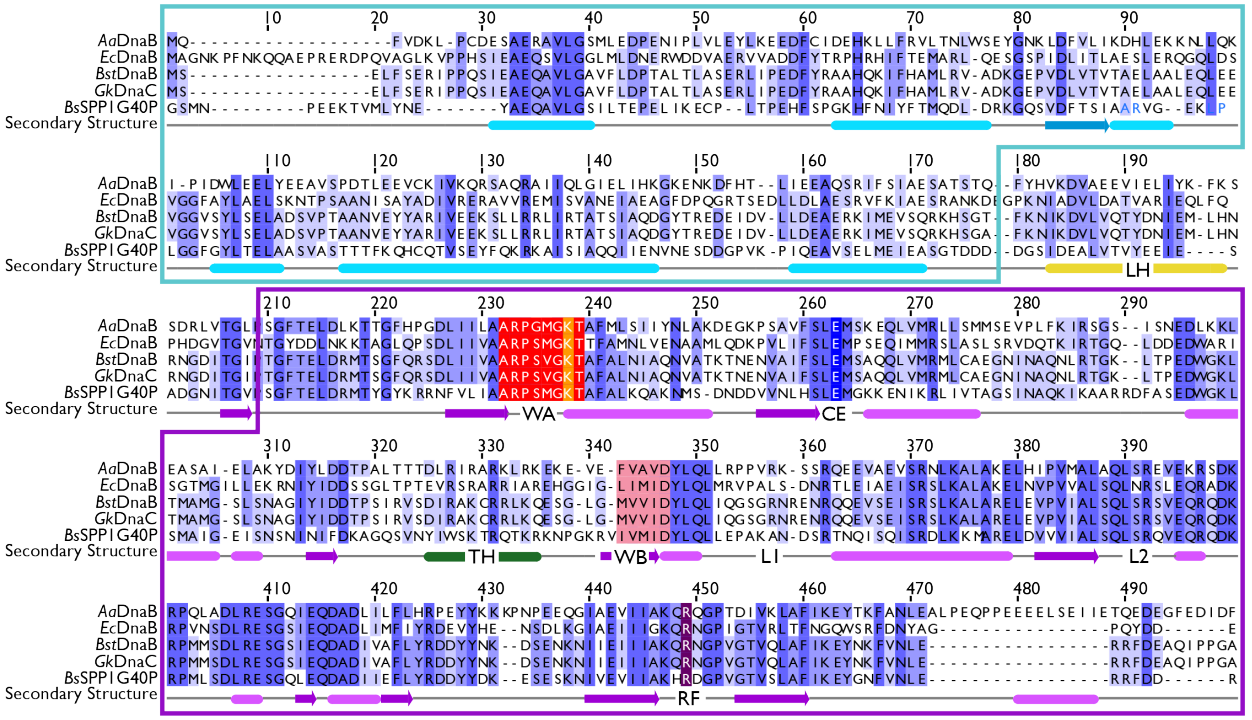


**Figure 2.1. Multiple sequence alignment of *Aa*DnaB with other bacterial and viral DnaB-type helicases with known structures.** Secondary structure and key functional elements are indicated (LH – linker helix; TH – transducer helix; CE – catalytic glutamate; RF – arginine finger; WA – Walker A; WB – Walker B). N- and C-terminal domains are boxed. Alignment generated using MAFFT and visualized in JalView ((Katoh et al., 2009; Waterhouse et al., 2009)).

**Figure 2.2**

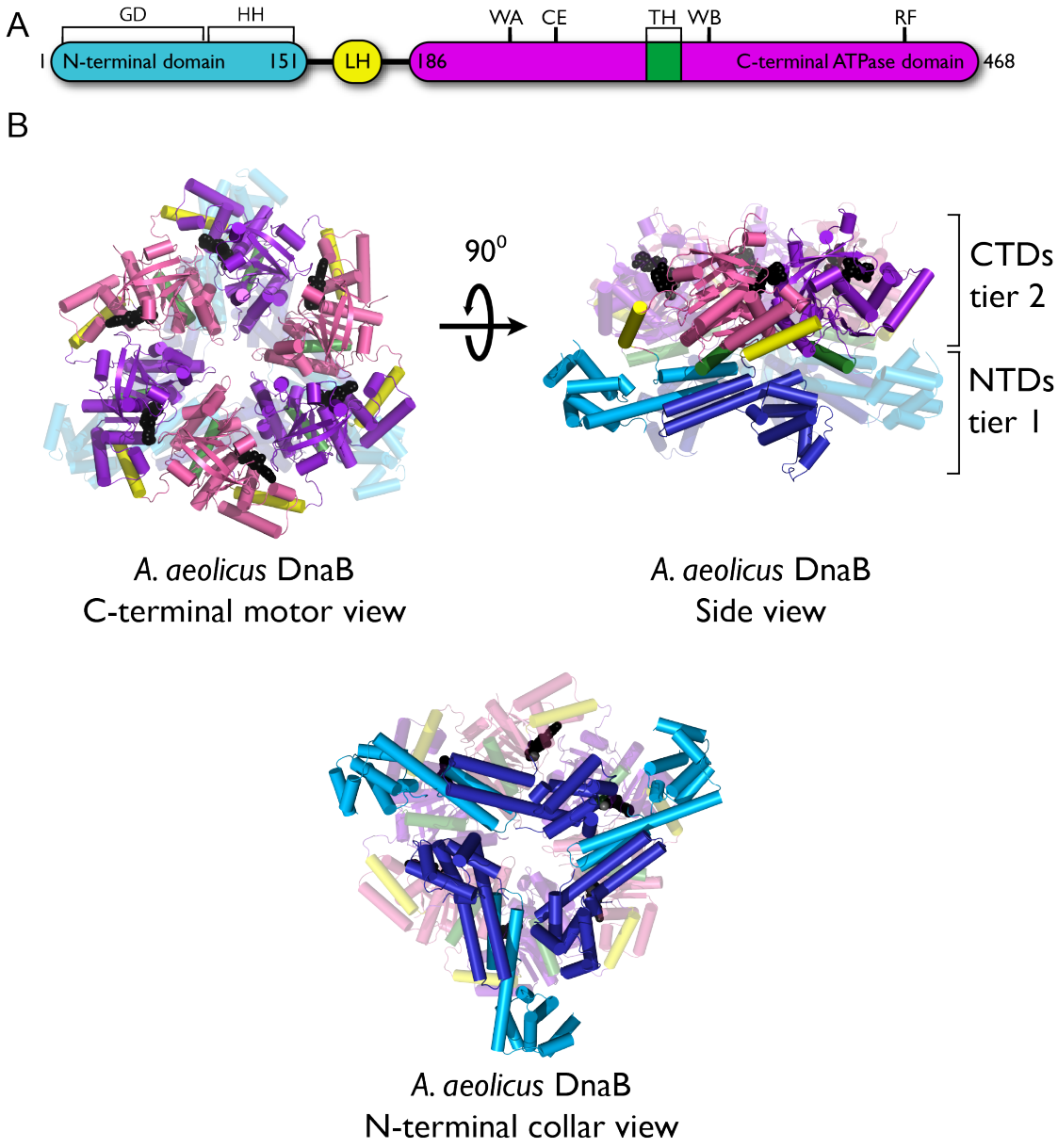


**Figure 2.2. Overview of *Aa*DnaB structure.** A) Domain organization of *Aa*DnaB. Specific regions discussed in the text are labeled: GD – globular domain, HH – helical hairpin, LH – linker helix, WA – Walker A motif, CE – catalytic glutamate, TH – transducer helix, WB – Walker B motif, RF – arginine finger. B) Cartoon representation of the structure for hexameric *Aa*DnaB, shown in three views. Coloring of structural elements follows that of panel A.

## TABLE 2.1 SUMMARY OF X-RAY PARAMETERS

| | |
|---|---|
| **Data Collection** | |
| Wavelength (Å) | 1.1 |
| Resolution range (Å) | 69.2 - 3.3 (3.5 - 3.3) |
| Space group | $I2_13$ |
| Unit cell (a, b, c) | 195.7 195.7 195.7 |
| (α, β, γ) | 90.0° 90.0° 90.0° |
| Total reflections | 101479 (12875) |
| Unique reflections | 18616 (2457) |
| Multiplicity | 5.5 (5.2) |
| Completeness (%) | 98.4 (85.1) |
| Mean I/σ (I) | 8.9 (2.5) |
| Wilson B-factor | 92.7 |
| $R_{merge}$ [a] | 0.116 (0.554) |
| $R_{pim}$ [b] | 0.053 (0.256) |
| **Refinement** | |
| $R_{work}$ [c] | 0.221 (0.316) |
| $R_{free}$ [d] | 0.259 (0.350) |
| Number of atoms | 6901 |
| macromolecules | 6813 |
| ligands | 63 |
| water | 9 |
| Protein residues | 854 |
| RMS(bonds) | 0.004 |
| RMS(angles) | 1.21 |
| Ramachandran favored (%) | 97.7 |
| Ramachandran allowed (%) | 1.9 |
| Ramachandran outliers (%) | 0.4 |
| Average B-factor | 112.30 |
| macromolecules | 112.40 |
| solvent | 69.90 |

[a] $$R_{merge} = \sum_{hkl}\sum_{i}\left|I_i(hkl) - \overline{I(hkl)}\right| \Big/ \sum_{hkl}\sum_{i} I_i(hkl)$$

[b] $$R_{pim} = \sum_{hkl}\left(\frac{1}{N-1}\right)^{1/2}\sum_{i}\left|I_i(hkl) - \overline{I(hkl)}\right| \Big/ \sum_{hkl}\sum_{i} I_i(hkl)$$

[c] $$R_{work} = \sum \left|\left|F_o\right| - \left|F_c\right|\right| \Big/ \sum \left|F_o\right|$$

[d] $R_{free}$ was calculated using 5% of data omitted from refinement

**Figure 2.3**

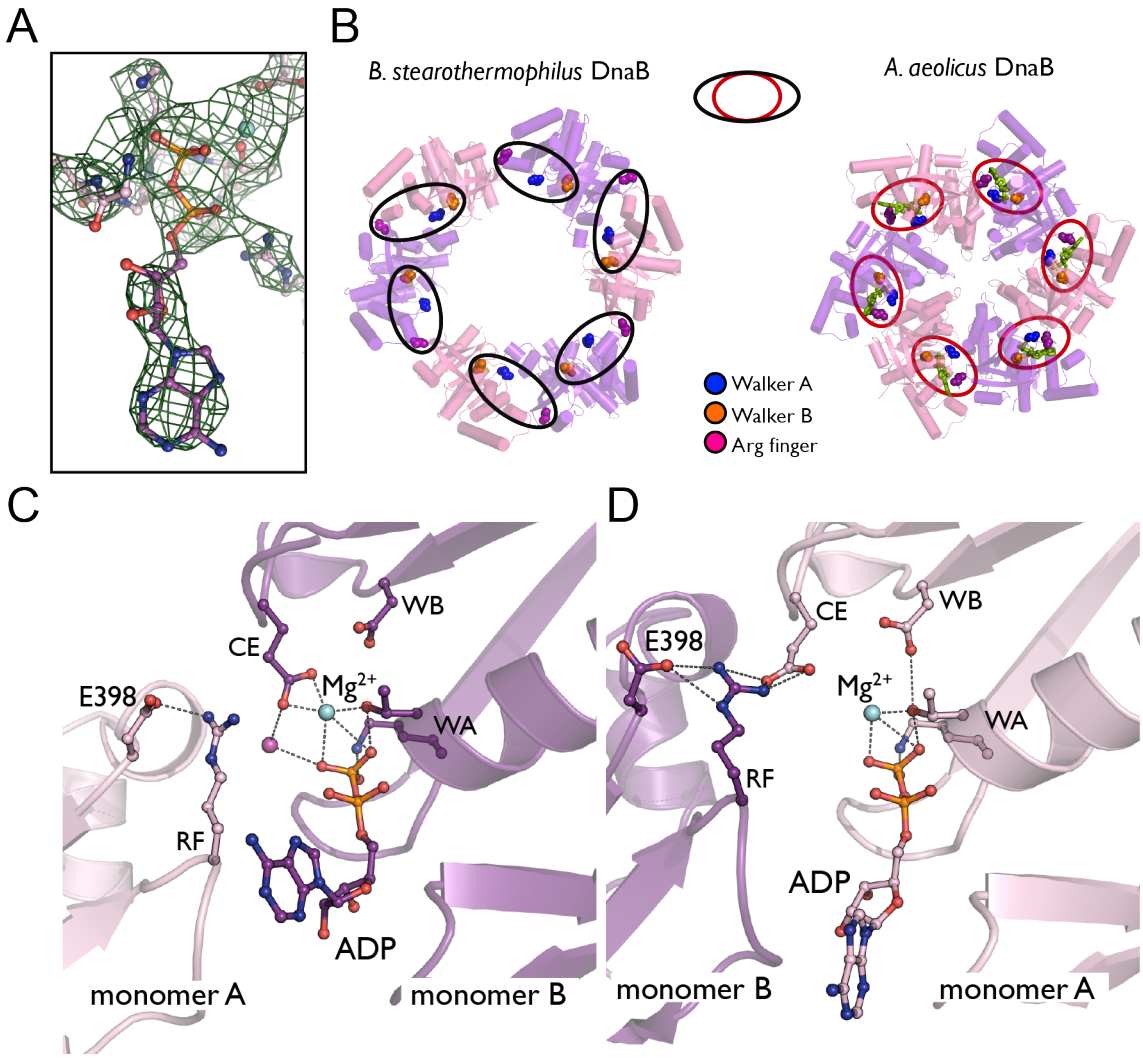


**Figure 2.3. Active site status of *Aa*DnaB.** A) Representative composite-omit electron density (at 4σ) of ADP•$Mg^{2+}$ and nearby residues. B) ATPase site alignment in constricted *vs.* dilated ring (PDB ID 2R6A) conformations; active sites indicated by oval enclosure. C, D) Views of the ATPase sites in each of the two protomers in the crystal asymmetric unit, colored by subunit as in **Figure 2.2**

**Figure 2.4**

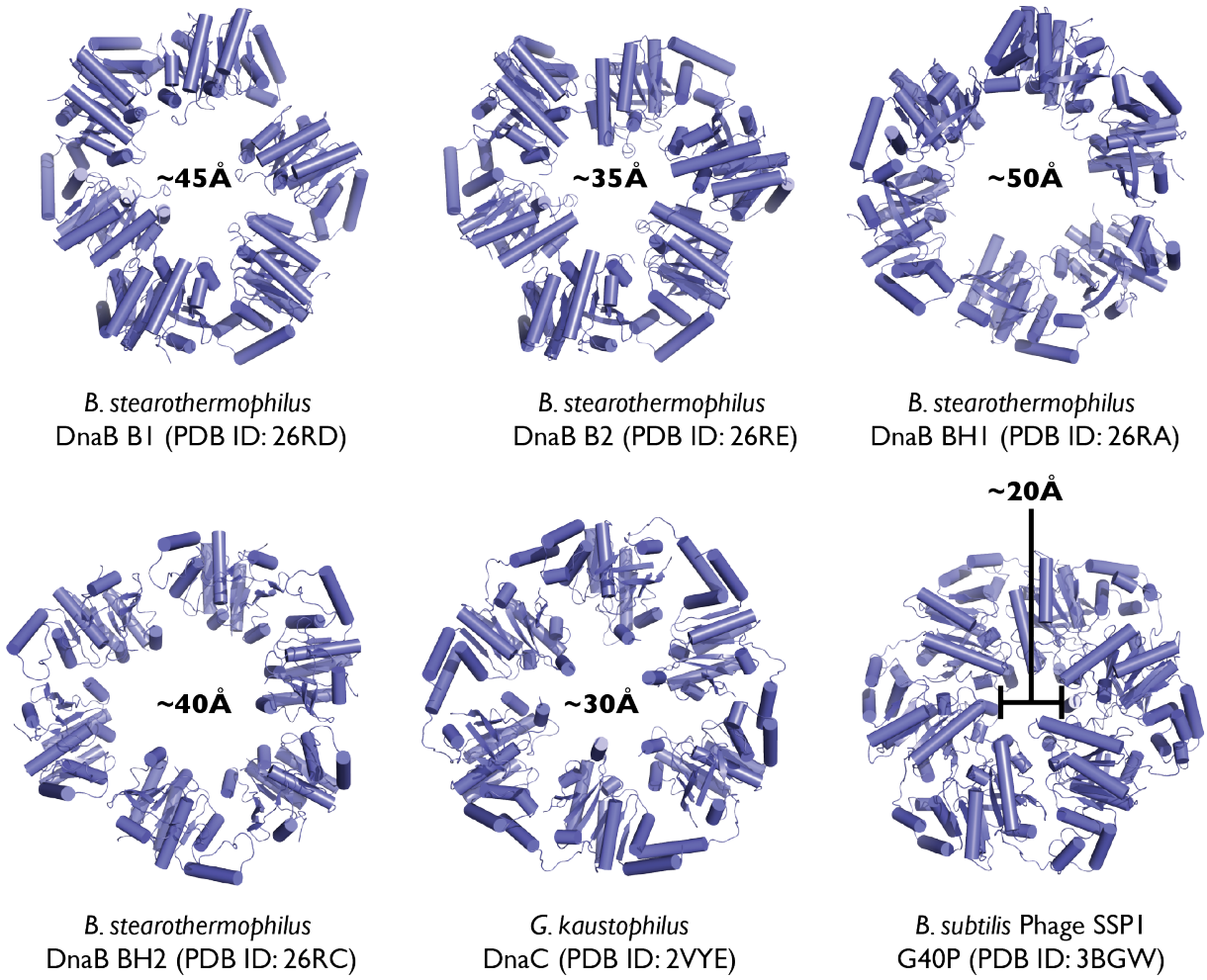


*B. stearothermophilus* DnaB B1 (PDB ID: 26RD)

*B. stearothermophilus* DnaB B2 (PDB ID: 26RE)

*B. stearothermophilus* DnaB BH1 (PDB ID: 26RA)

*B. stearothermophilus* DnaB BH2 (PDB ID: 26RC)

*G. kaustophilus* DnaC (PDB ID: 2VYE)

*B. subtilis* Phage SSP1 G40P (PDB ID: 3BGW)

**Figure 2.4. Crystal structures of the C-terminal ATPase motor rings from bacterial and viral DnaB-type helicases.** N-terminal collars are omitted for clarity. Approximate diameter of the central pore is indicated for each structure.

**Figure 2.5**

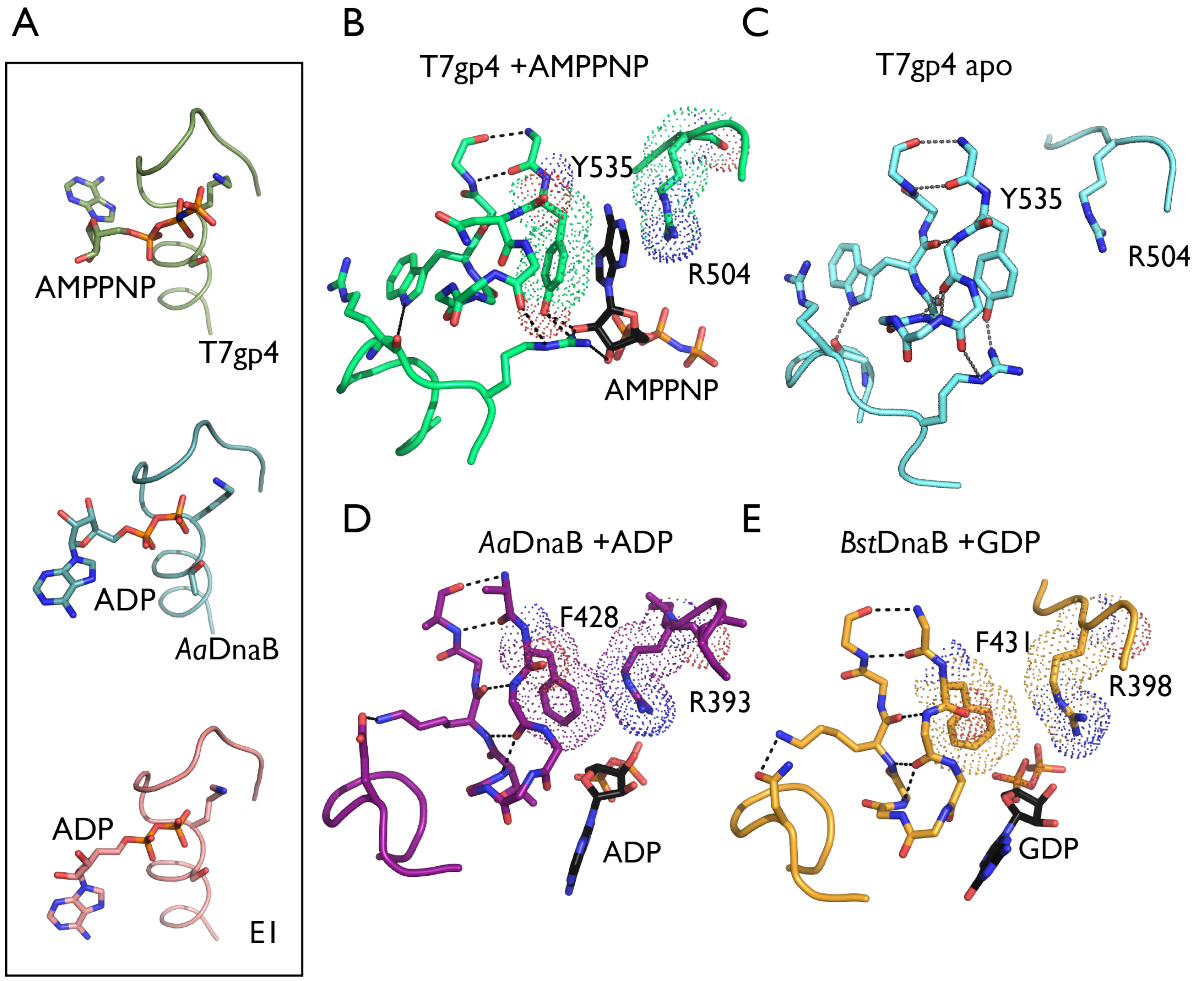


**Figure 2.5. ADP binds the DnaB active site in an unusual orientation.** A) Nucleotide binding orientations in RecA-type and AAA+ helicases, shown with respect to the Walker A motif. The base orientation of *Aa*DnaB, a RecA enzyme, differ from that of another RecA-family protein T7 gp4 ((Singleton et al., 2000)), and is instead similar to that of the AAA+ E1 helicase (Enemark and Joshua-Tor, 2006). B-E) The base-binding region of several known helicases (T7 gp4, *Aa*DnaB, *Bst*DnaB) (Bailey et al., 2007b; Itsathitphaisarn et al., 2012; Singleton et al., 2000) is shown in the presence (B,D,E) and absence (C) of nucleotide. Thus far all DnaB orthologs exhibit a collapsed base-binding pocket. PDB ID: 1E0J (T7gp4), 2GXA (E1), 4ESV (*Bst*DnaB)

**Figure 2.6**

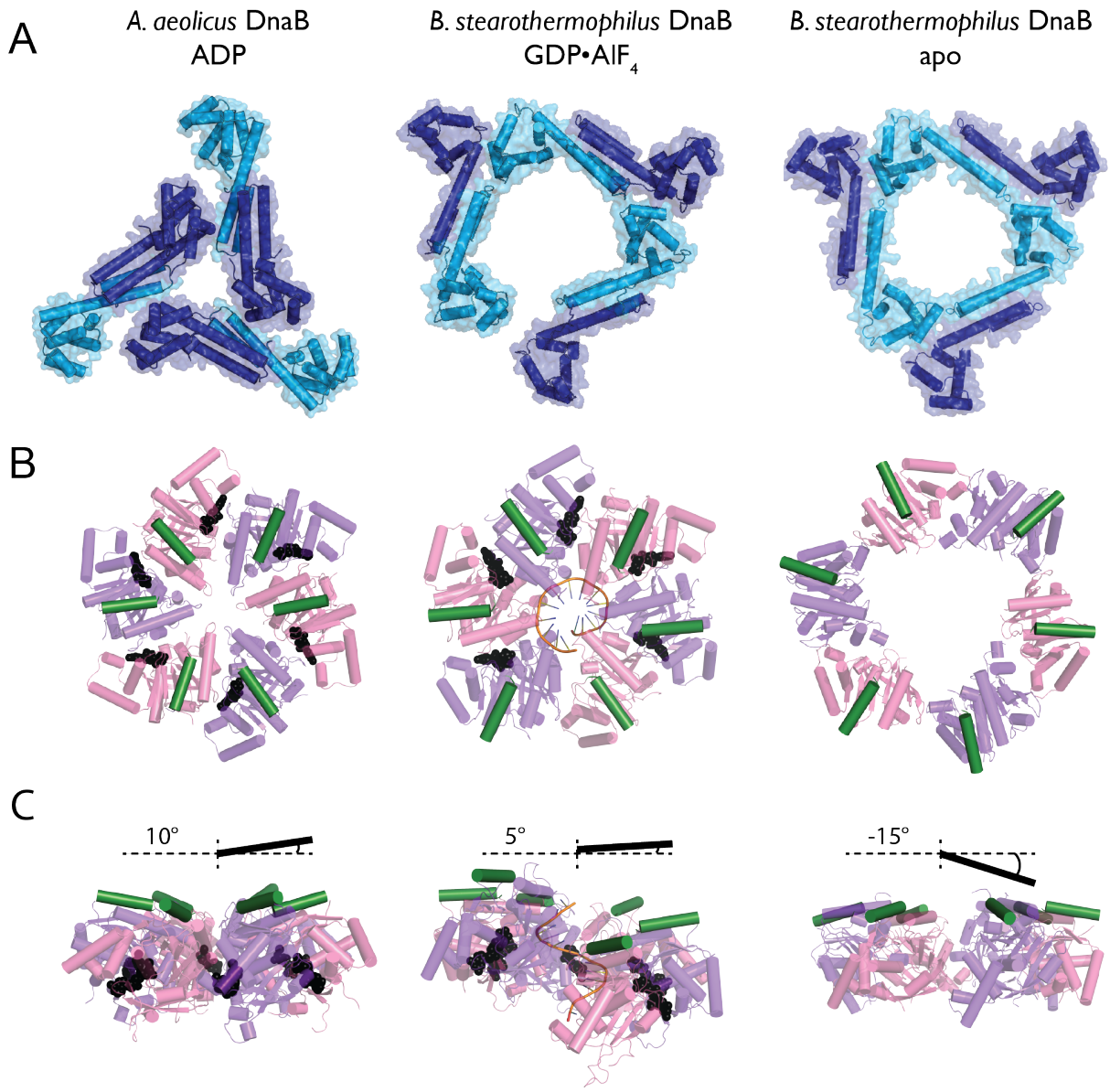


**Figure 2.6. The DnaB N-terminal collar is a conformational switch.** N-terminal collar (A), and top (B) and side (C) views of the C-terminal motor ring for ADP-bound *Aa*DnaB (left), DNA- and GDP•$AlF_x$-bound *Bst*DnaB (middle, PDB ID 4ESV), and apo *Bst*DnaB (right, PDB ID 2R6A). Subunits are alternatingly shaded light and dark to emphasize the transitions between N-terminal domain homodimers. The angle of the transducer helix (green) orientation relative to the plane of the ring is shown above the side views of the motor domain (C).

**Figure 2.7**

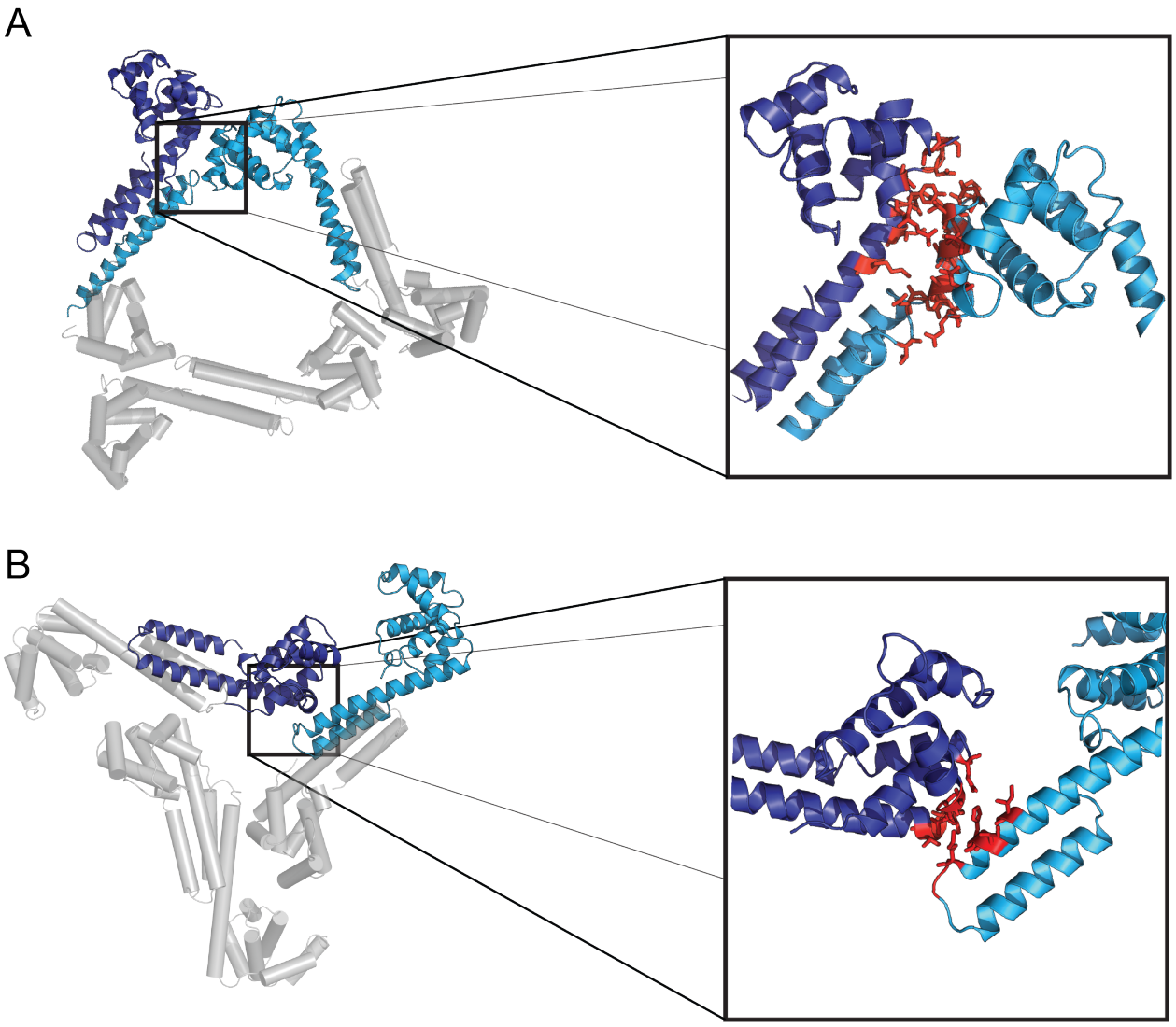


**Figure 2.7. Interactions between N-terminal domains in the dilated and constricted state.** Close-up view of the interactions between the globular domain of one N-terminal domain and the helical hairpin of its neighbor, shown in the context of the dilated (A) and constricted (B) N-terminal collar. Interacting residues are highlighted in red.

# Chapter 3 - Structural studies of DnaB helicase

## INTRODUCTION

Although the structures of DnaB-family proteins have been extensively studied by both crystallography and electron microscopy (Bailey et al., 2007; Barcena et al., 1998; Donate et al., 2000; Lo et al., 2009; Nunez-Ramirez et al., 2006; San Martin et al., 1995; Stelter et al., 2012; Wang et al., 2008; Yang et al., 2002; Yu et al., 1996), the *Aa*DnaB conformation seen here did not fully resemble any previously described state. We therefore set out to investigate whether the constricted particle corresponded to a native state of *Aa*DnaB and also whether it could be adopted by DnaB helicase from other bacterial species that live under less extreme conditions.

## 3D ELECTRON MICROSCOPY RECONSTRUCTION OF *A. AEOLICUS* DNAB

We first turned to negative stain EM to characterize the *Aa*DnaB and verify the constricted state observed crystallographically (**Figure 3.1**). The similarity between the 2D reference-free class averages and re-projections of our atomic structure was clearly evident, confirming that most or all of the molecules in the sample were constricted ring-shaped hexamers similar to that observed in the crystal structure.

Although 3-fold symmetry is readily apparent in the *Aa*DnaB crystal structure, we processed the data using 6-fold, 3-fold, or no symmetry to avoid biasing the outcome of the reconstructions. 3D models generated either in the absence of symmetry or with 3-fold symmetry clearly recapitulated the trimer-of-dimers architecture seen in our *Aa*DnaB crystal structure (**Figure 3.2**). By contrast, many structural features were lost when 6-fold symmetry was enforced. The consistency of the EM reconstructions was supported by the close resemblance between reprojections of the 3D model and reference-free 2D class averages (**Figures 3.1**). The similarity of the filtered atomic structure to the EM model (**Figure 3.1**), together with the fitting of the atomic coordinates into the 3D reconstruction (**Figure 3.1**), demonstrates that the conformation of *Aa*DnaB found in the crystal corresponds to a dominant population state of the protein.

## NUCLEOTIDE ALTERS THE CONFORMATIONAL EQUILIBRIUM BETWEEN DILATED AND CONSTRICTED STATES

Because the constricted *Aa*DnaB state had not been observed previously, we set out to determine whether it was specific to the thermophilic protein, and whether nucleotide might help promote constriction. Using the well-studied *E.*

*coli* DnaB helicase as a model system, we prepared samples both in the presence and absence of ATP and the ATP analogs AMPPNP, ADP•$BeF_3$ and ATPγS, and analyzed these complexes by EM. 2D classification of apo *Ec*DnaB failed to reveal any evidence for a constricted particle state, showing only dilated forms of the enzyme (**Figure 3.3**). By contrast, two kinds of 2D class averages were observed for *Ec*DnaB in the presence of ATPγS, ATP and AMPPNP (**Figure 3.3, Figure 3.4**), approximately half of which adopted a dilated configuration and the other half a constricted state. These findings demonstrate that while a dilated ring conformation is the default state for *Ec*DnaB, nucleotide can trigger the enzyme to switch into a constricted form. Curiously addition of ADP•$BeF_3$ did not effect any conformational rearrangements in *Ec*DnaB sample (**Figure 3.5**).

To better define the factors controlling the dilated/constricted transition, we next used EM to look at the distribution of the two *Ec*DnaB states under different substrate-binding conditions. Interestingly, even at nucleotide concentrations as high as 5mM, 2D class averages showed that *Ec*DnaB did not fully shift to the constricted state. The inclusion of ssDNA (ranging from 10 to 35 bases in length) and nucleotide in the sample likewise did not appear to have any additional effect on the distribution of the two populations (although the classes did show extra density inside the helicase pore, consistent with DNA binding **Figure 3.4**). Single-stranded DNA alone was unable to induce any apparent ring constriction. As an additional comparison, we examined the nucleotide-dependent response of *Bst*DnaB, whose crystal structures have thus far exhibited only dilated forms of the protein (Bailey et al., 2007; Itsathitphaisarn et al., 2012); 2D EM analysis again revealed evidence for a constricted species in the presence of ATP (**Figure 3.4**).

## STUDIES OF CONFORMATIONAL REARRANGEMENTS OF *A. AEOLICUS* DNAB

In addition to the experiments with *Ec*DnaB we attempted to capture a dilated conformation of *Aa*DnaB. We looked at apo samples, prepared according to the same protocol as apo *Ec*DnaB, where the protein was dialyzed out of the nucleotide following a sizing column; we also tried to purify protein in the absence of the nucleotide. While the purified apo DnaB hexamers remained intact, we could still observe only constricted 2D class averages (**Figure 3.6**). This result prompted us to test different steps of the *Aa*DnaB purification protocol and their possible effects on the conformation of the protein. In particular we hypothesized that heating DnaB lysate to 65°C during purification might provide enough energy to cause the conformational rearrangement of the N-terminal collar and permanently lock the helicase ring in a constricted conformation. Unfortunately, eliminating the heat step or performing it in the absence of nucleotide and with additional EDTA to further chelate magnesium ions also did not produce dilated particles (**Figure 3.6**). However negative stain 3D EM reconstruction of *Aa*DnaB in complex with *Aa*DnaC in the presence of ADP•$BeF_3$ solved by Ernesto Arias-Palomo (unpublished) revealed a planar DnaB

particle with a dilated N-terminal collar. Curiously this complex differed markedly from the *E. coli* Dna$(BC)_6$ reconstruction where DnaB was found in a slightly cracked, helical and constricted lock-washer state (Arias-Palomo et al., 2013); however now it appeared more similar to a recently published reconstruction of *Bst*Dna$(BC)_6$ (Liu et al., 2013) (**Figure 3.7**). It is possible that all these structures are intermediate states along a single pathway, where the helicase loader DnaC binds a dilated state of DnaB and then drives the conformational rearrangement to constrict and crack the helicase to load it onto the melted origin of replication. However, discrepancies between *A. aeolicus* and *E. coli* DnaB structures might also underline the general difference between thermophilic and mesophilic helicases, where thermophilic DnaBs (such as *Aa*DnaB and *Bst*DnaB) are harder to open at mesophilic temperatures and thus more predisposed to be captured in the more stable ground state of a dilated N-terminal collar.

## CONCLUSION

Together, these findings show that the nucleotide-dependent constriction seen for *Aa*DnaB is conserved across different DnaB homologs and that intact DnaB rings can adopt one of two dominant conformational states in solution. The nucleotide can toggle a switch from one state to the other but it does not appear capable of completely transforming an entire population of DnaB particles from one state to another.

## MATERIALS AND METHODS

*Protein preparation*

*Ec*DnaB was expressed in C41 strain (Lucigen) by induction with 1mM IPTG at 37°C for 3-4hours. Cells were harvested by centrifugation and resuspended in 20mM Hepes-KOH pH 7.5, 500mM NaCl, 10% Glycerol, 10mM $MgCl_2$, 0.1mM ATP, 1mM β-mercaptoethanol, 1mM PMSF, 1μg/mL PepstatinA and 1μg/mL Leupeptin. Fresh (or thawed pellets that were previously flash frozen in liquid nitrogen) were lysed by sonication. Protein was purified by ammonium sulfate precipitation (10% initial cut to remove contaminating proteins and 30% cut to isolate DnaB). Resuspended pellets from the ammonium sulfate cut were applied to a HiTrap Q HP column (GE Healthcare) in 100mM NaCl buffer, washed with 300mM NaCl buffer and eluted with 400mM NaCl buffer. Anion exchange chromatography was followed by gel-filtration on a HiPrep 16/60 Sephacryl S-300 column (GE Healthcare) in a buffer containing 20mM Tris-HCl pH 8.5, 800mM NaCl, 10% Glycerol, 5mM $MgCl_2$, 0.1mM ATP, 1mM β-mercaptoethanol, 1mM PMSF, 1μg/mL PepstatinA and 1μg/mL Leupeptin. To prepare apo samples *Ec*DnaB was dialyzed overnight into a buffer containing 100mM NaCl, 20mM Hepes-KOH pH 7.5, 5% glycerol, 10mM EDTA, no nucleotide and no magnesium, followed by a second 8-hour dialysis into 100mM NaCl , 20mM Hepes-KOH pH 7.5, 5% glycerol and 5mM $MgCl_2$. *Ec*DnaB samples

with non-hydrolysable ATP-analogues were prepared through overnight dialysis of protein purified in 0.1mM ATP into a buffer containing 100mM NaCl, 5mM $MgCl_2$, 5% glycerol, 20mM Hepes-KOH pH 7.5 and a desired amount of AMPPNP, ATPγS or $ADPBeF_3$ in the presence or absence of ssDNA.

*Aa*DnaB was purified as described in Chapter 2. Apo samples were treated like apo *Ec*DnaB and first dialyzed into a buffer containing EDTA but no magnesium or nucleotide, followed by dialysis out of EDTA and into 5mM $MgCl_2$. Additionally protein was also purified in the absence of any nucleotide or omitting the heat step to test whether the high temperature during purification had any effect on the N-terminal collar arrangement.

*Bst*DnaB was expressed with an N-terminal $His_6$MBP affinity tag and purified by $Ni^{2+}$ column chromatography followed by overnight TEV digest and ion exchange chromatography on a HiTrap Q HP column (GE Healthcare) with a final gel filtration step on a HiPrep 16/60 Sephacryl S-300 column (GE Healthcare).

*Negative staining*

Freshly purified *Aa*DnaB was directly applied from an analytic sizing column (Superex 200 5/150 GL, GE, run in 50mM HEPES pH 7.5, 200mM KCl, 5% Glycerol, 5mM $MgCl_2$, 1mM $ADPBeF_3$) to glow-discharged continuous carbon grids and stained using a 2% (w/v) uranyl formate solution. In some cases, to obtain different orientations of the particles, the glow-discharged grids were first floated on 40 µl drops of a 0.1% (w/v) aqueous solution of polylysine hydrobromide (Mw 40–120 kDa; Polysciences, Inc.) for two minutes, blotted, and briefly rinsed with distilled water prior to application of specimen. Analysis of *E. coli* and *Bst*DnaB was conducted similarly to that of the *A. aeolicus* protein; for *Ec*DnaB, samples were dialyzed over-night into the desired nucleotide or nucleotide-DNA combination.

*Electron microscopy*

All specimens were examined under an FEI Tecnai-12 Bio-Twin electron microscope equipped with a LaB6 filament and operated at 120 kV. Data were acquired using a dose of ~20 e-/$Å^2$ at a nominal magnification of 49,000x and then binned to 4.36 Å per pixel. All images were recorded on a TemCam-F416 (TVIPS, Gauting, Germany) 4k x 4k pixel camera utilizing the Leginon data collection software (Suloway et al., 2005).

*Image processing*

In the case of *Aa*DnaB, 23702 particles were initially picked using DoG picker (Voss et al., 2009), as available in Appion (Lander et al., 2009). The contrast transfer function of the microscope for each micrograph was estimated using CTFFIND3 and phase flipped using SPIDER (Mindell and Grigorieff, 2003; Shaikh et al., 2008). Reference-free 2D methods implemented in EMAN (Ludtke et al., 1999), and 2D maximum-likelihood classification (Scheres et al., 2005) as

implemented in XMIPP (Scheres et al., 2008), were used to analyze these datasets. *Ec*DnaB and *Bst*DnaB particles were processed as for *Aa*DnaB. Over one million DnaB particles were processed with an average of 20000 particles for each condition.

*Aa*DnaB molecules adsorbed to grids with a strong preferential observation (top view), initially preventing efforts to obtain a 3D reconstruction. To overcome this problem, we additionally collect 15000 *Aa*DnaB particles from grids pre-treated with polylysine. In addition to the previously observed top views, new side views of the molecule could now be observed (**Figure 3.4B and C**). To avoid model bias, atomic structures were never used as an initial model. We used instead the dilated *Ec*DnaB EM structure filtered at 100 Å obtained from in a parallel study of the *Ec*DnaBC complex (Arias-Palomo et al.). To explore the symmetry of the molecule, the *Aa*DnaB dataset was processed using either no symmetry, or using 3-fold or six-fold symmetry with SPARX (**Figure 3.4E**) (Hohn et al., 2007). The unsymmstrized and 3-fold rotationally average models gave the best results, allowing determination of the final structure to a resolution of 23 Å as estimated by the 0.5 Fourier shell correlation coefficient cutoff (**Figure 3.4D**). Despite starting with a filtered dilated DnaB model for *Ec*DnaB, the EM volumes for *Aa*DnaB clearly displayed a constricted state, allowing for the straightforward computational docking of the *Aa*DnaB crystal structure into the density using UCSF Chimera (Pettersen et al., 2004).

**Figure 3.1**

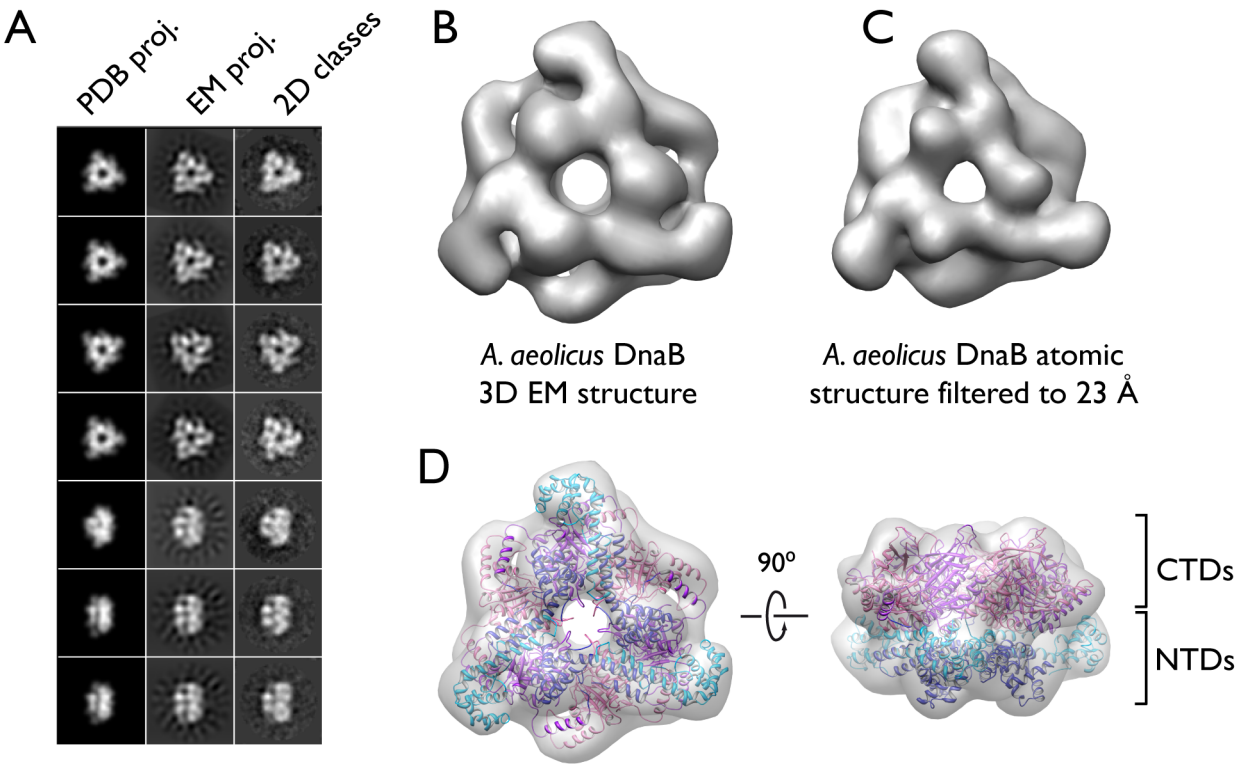


**Figure 3.1. 3D EM reconstitution of *Aa*DnaB.** A) Reference-free 2D class averages of *Aa*DnaB compared to forward re-projections of the 3D EM model and the crystal structure. B) Single-particle 3D EM reconstruction of *Aa*DnaB. C) Filtered model (23 Å resolution) of the *Aa*DnaB crystal structure. D) Fitting of the *Aa*DnaB crystal structure into the 3D EM volume.

**Figure 3.2**

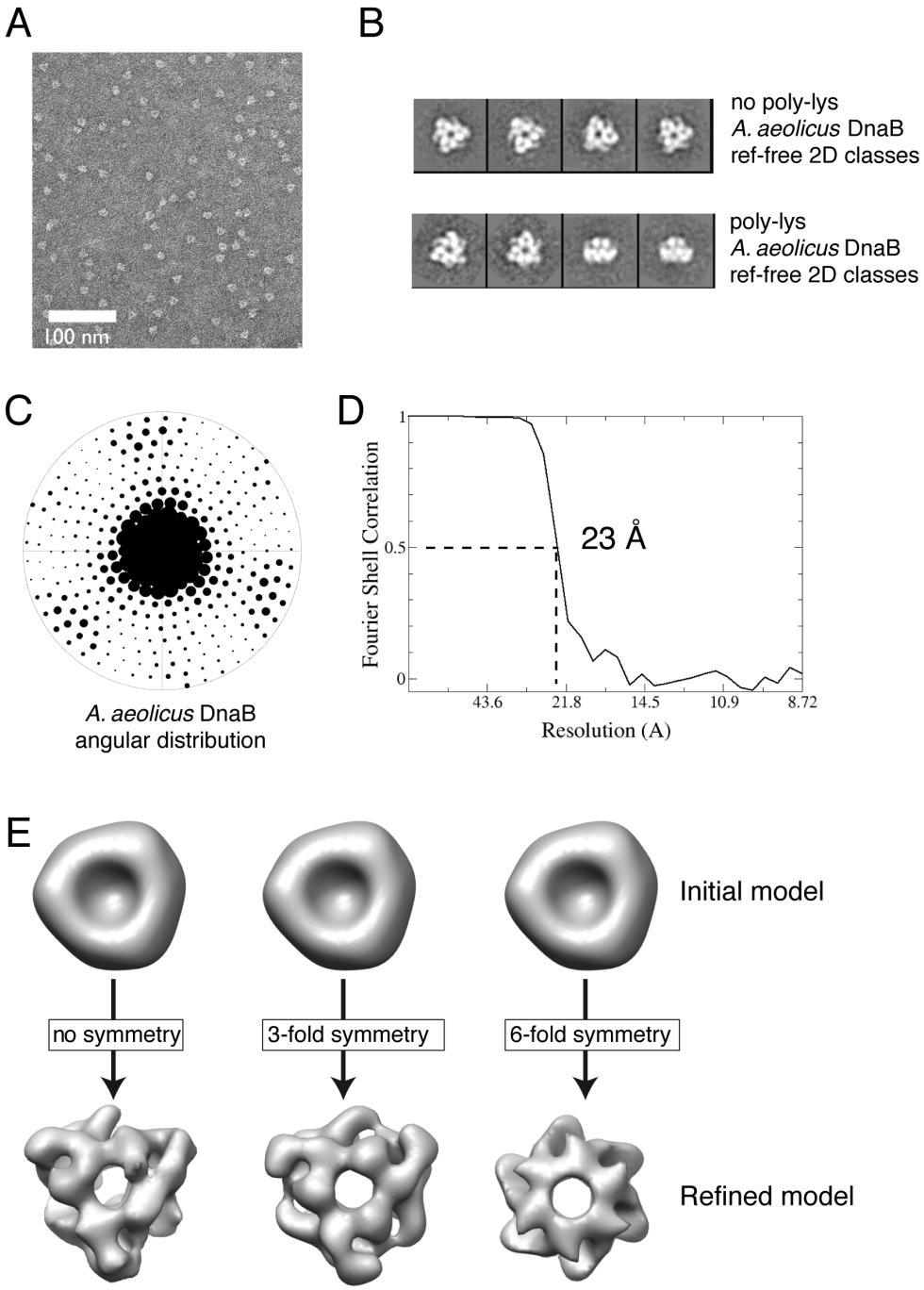


**Figure 3.2. Analysis of *Aa*DnaB structure by electron microscopy.** A) Electron micrograph of *Aa*DnaB in the presence of nucleotide. B) Representative reference - free 2D class averages of *Aa*DnaB (obtained from un-treated grids as well as grids treated with poly-lysine). C) Euler angle distribution diagram. D) Fourier shell correlation analysisfor projection-matching refinement. E) Results ofprojection-matching refinement using no symmetry, 3-fold symmetryand 6-fold symmetry.

**Figure 3.3**

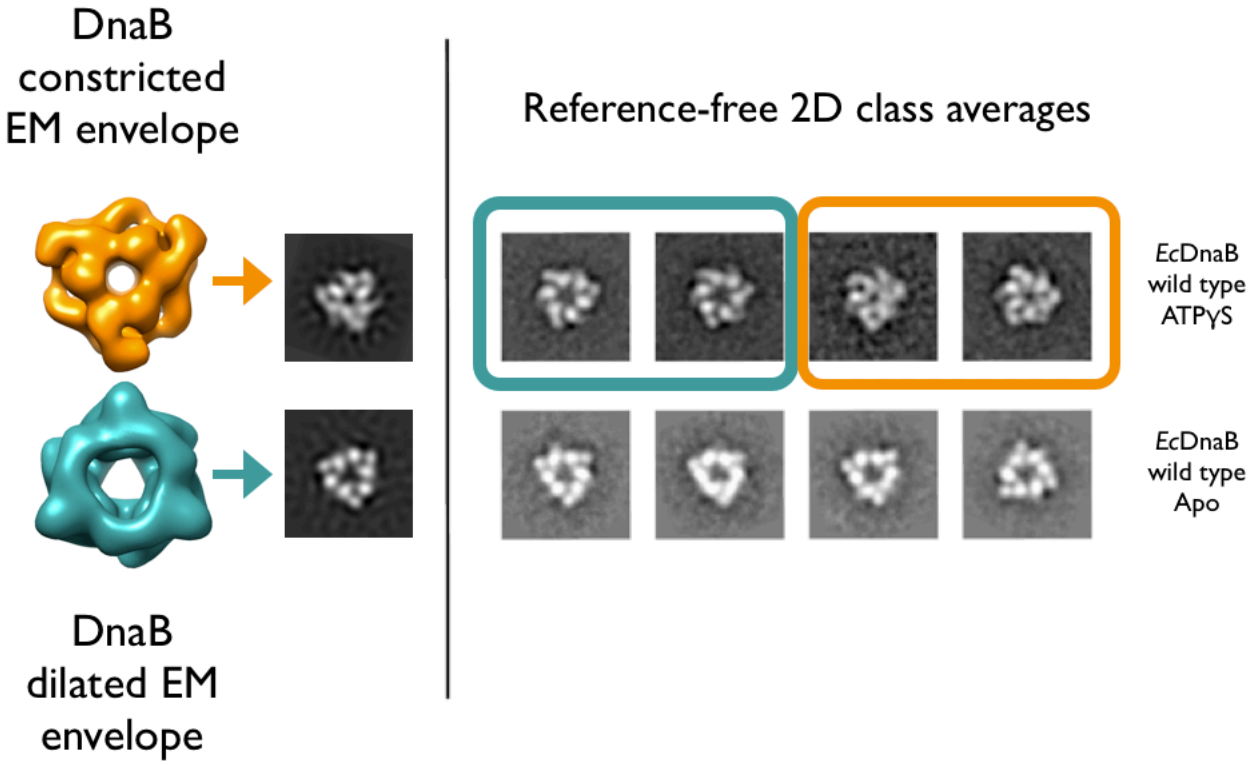


**Figure 3.3. Nucleotide promotes DnaB constriction.** Reference-free 2D class averages of wild type *Ec*DnaB in the presence and absence of nucleotide. Dilated *Ec*DnaB and constricted *Aa*DnaB EM models and their re-projections are shown on the left for comparison.

**Figure 3.4**

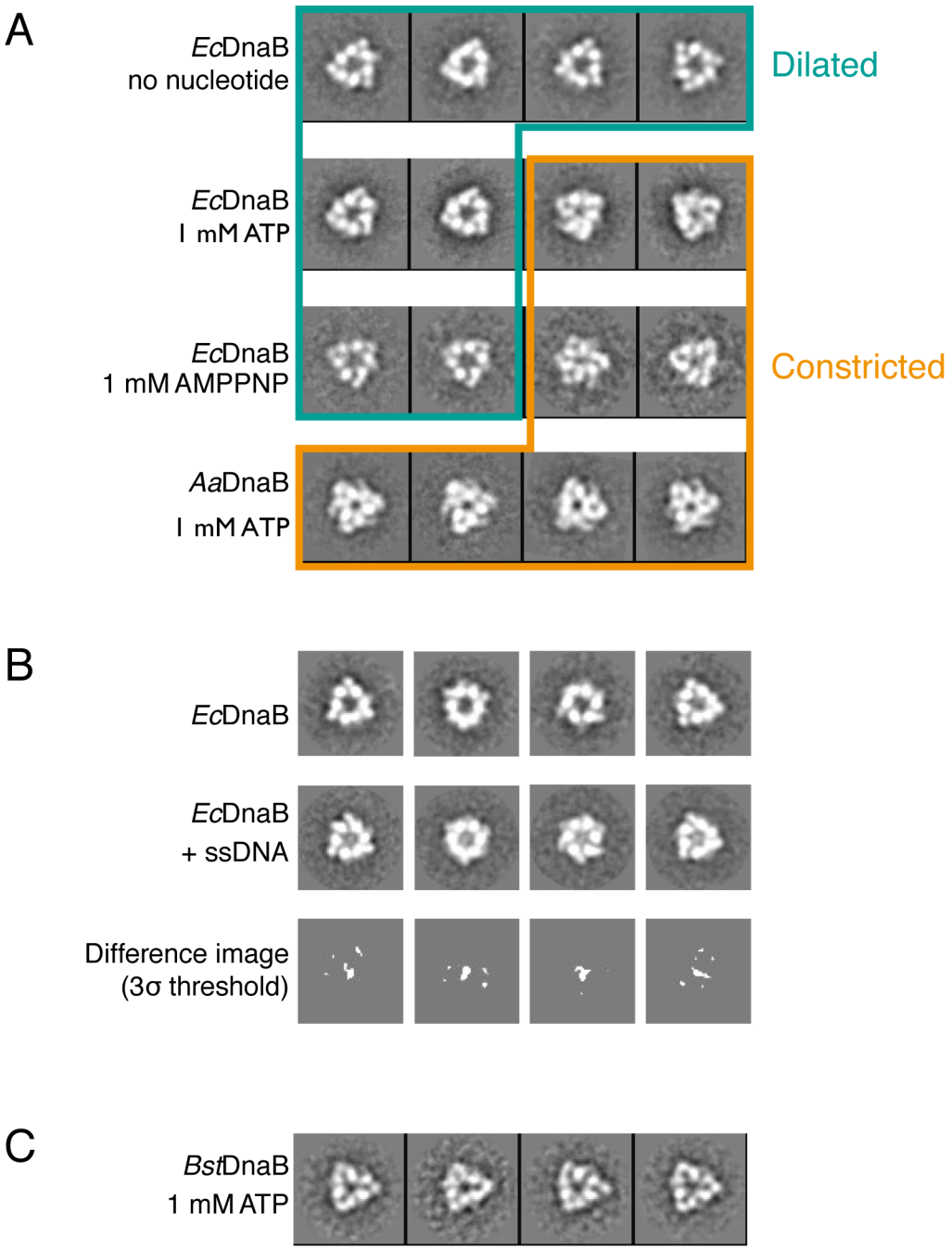


**Figure 3.4. Effect of nucleotide and ssDNA binding in *Ec*DnaB and *Bst*DnaB.** A) *Ec*DnaB reference-free 2D classes in the absence and presence of ATP and AMPPNP (note the mixture of constricted and dilated forms). B) ssDNA binding does not affect the equilibrium. The difference images show density in *Ec*DnaB channel that could correspond to ssDNA C) Reference-free 2D classes of *Bst*DnaB in the presence of 1mM ATP.

**Figure 3.5**

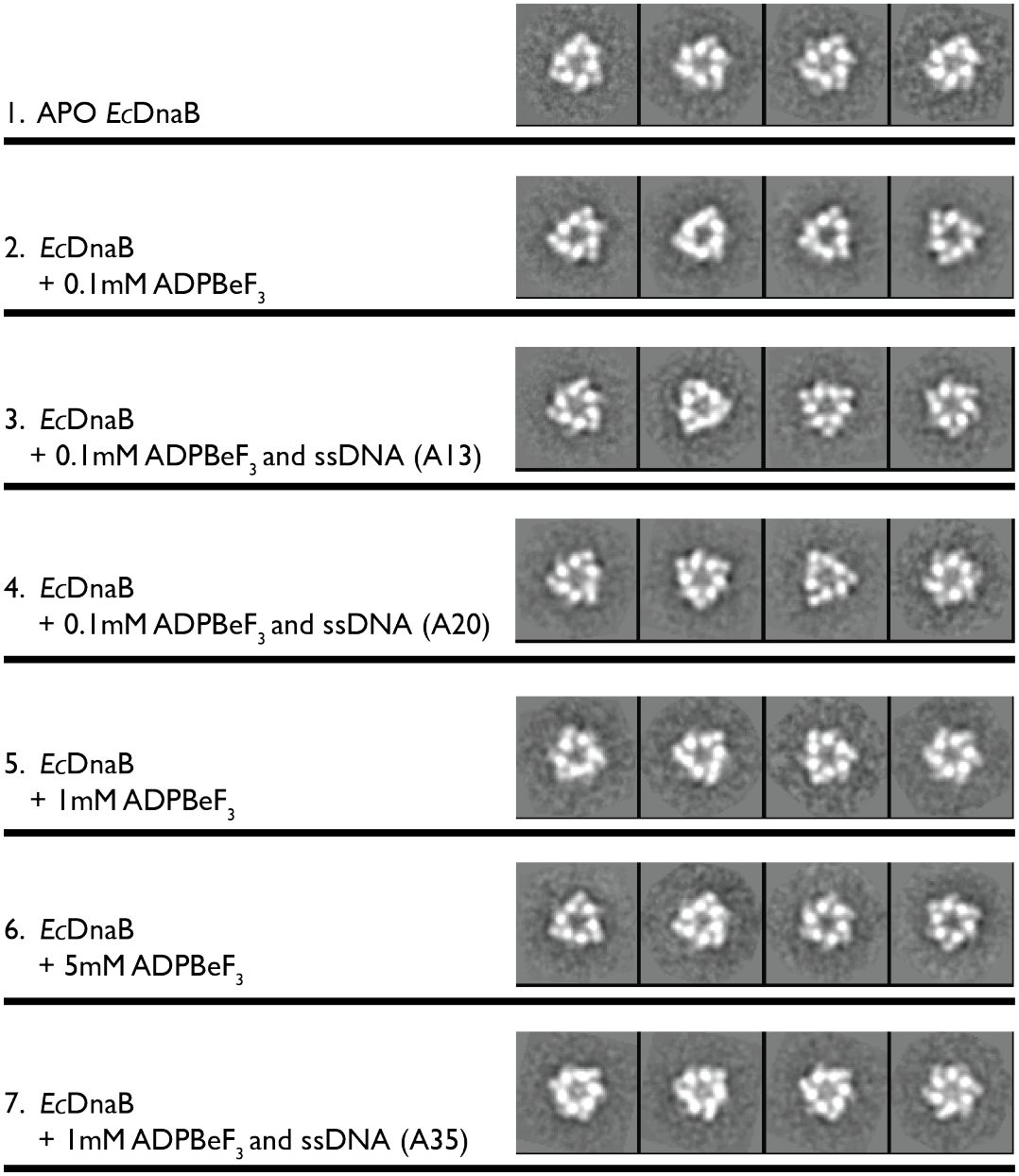


**Figure 3.5. ADP•$BeF_3$ does not promote constriction of *Ec*DnaB N-terminal collar.** A summary of initial experimental approaches to visual a constricted *Ec*DnaB ring.

**Figure 3.6**

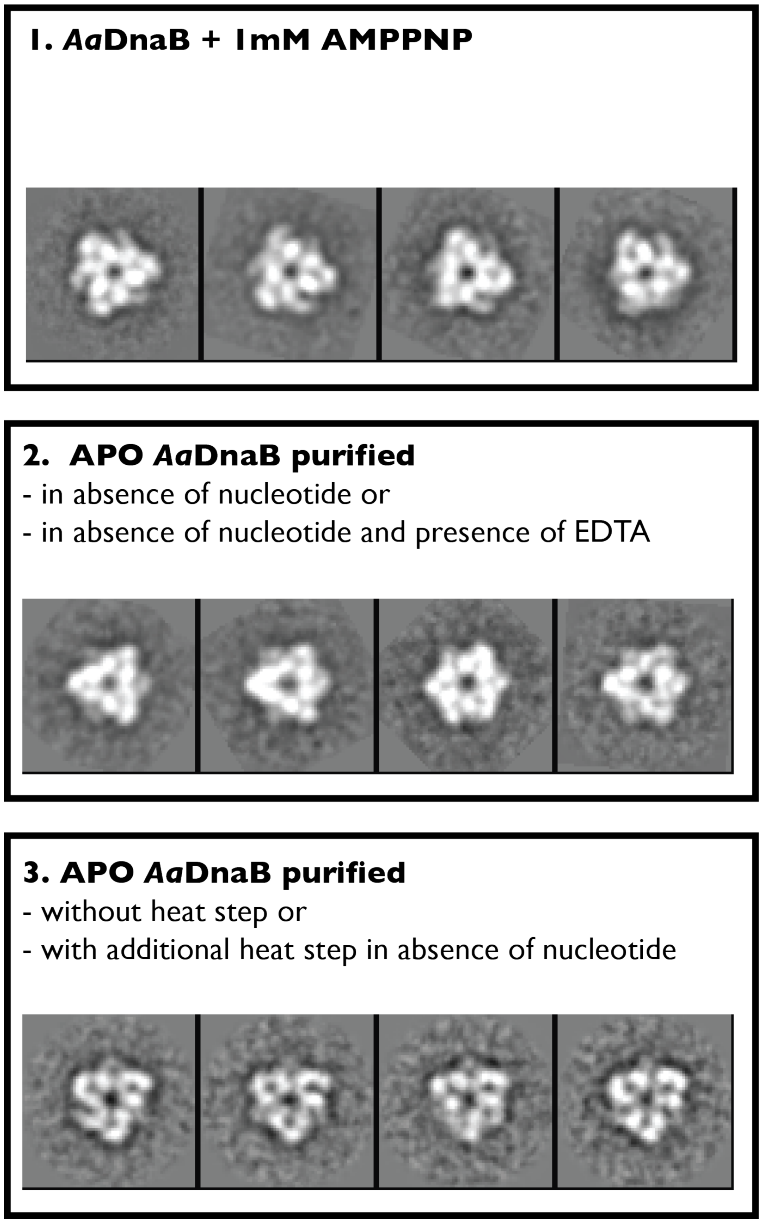


**Figure 3.6. *Aa*DnaB is always constricted.** A summary of experimental attempts designed to capture a dilated conformation of the *Aa*DnaB ring.

**Figure 3.7**

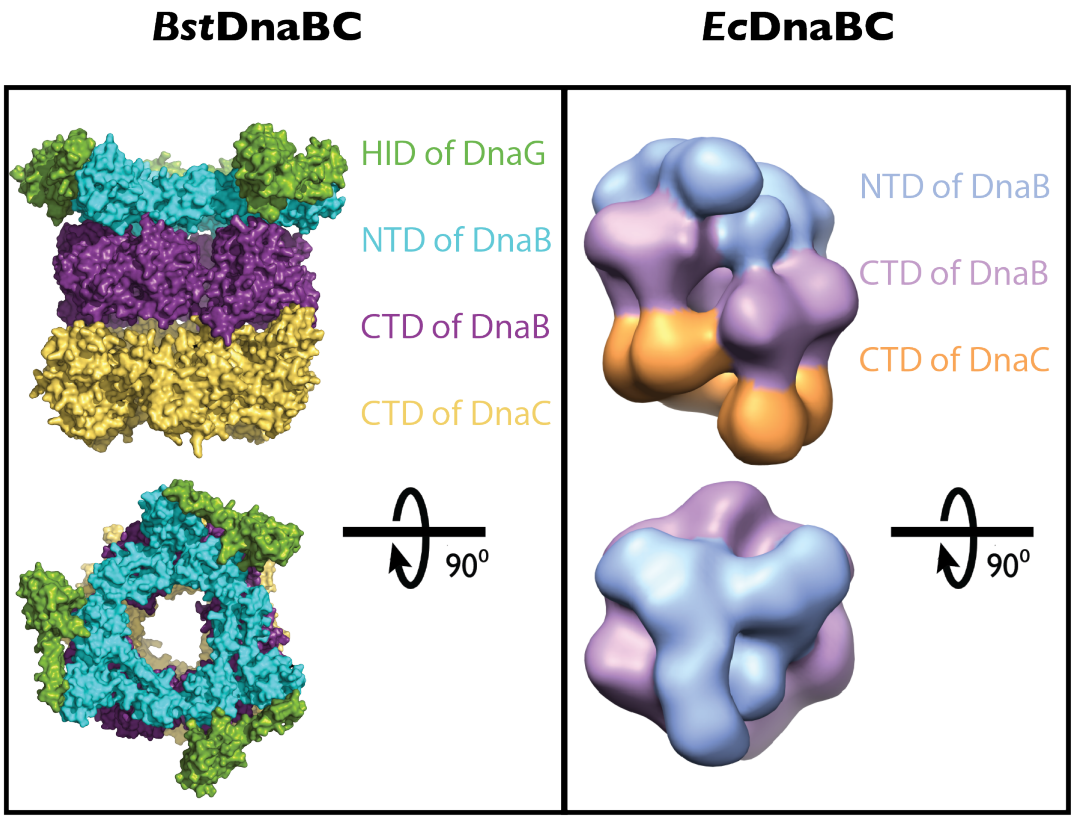


**Figure 3.7. Reconstructions of a complex between DnaB helicase and its loader from different bacterial species.** Left panel shows the recently published low resolution crystal structure of a primosome containing helicase-binding domain of DnaG and DnaB helicase from *B. stearothermophilus* found in complex with the loader protein from *B. subtilis* (PDB ID: 4M4W) (Liu et al., 2013). As seen in the bottom panel the N-terminal domains of DnaB adopt a dilated conformation. Right panel represents a 3D negative-stain reconstruction of a DnaBC complex from *E. coli* (Arias-Palomo et al., 2013), where the N-terminal domains of DnaB are seen in a constricted conformation.

# Chapter 4 - Specific intersubunit interactions mediate the stability of the N-terminal DnaB collar

## INTRODUCTION

The inability of closed-ring *Ec*DnaB hexamers to fully transition from a dilated to constricted state upon binding nucleotide was somewhat unexpected. On the one hand, this behavior could reflect the existence of inactive particles in our sample preparations, which might have failed to interconvert because of a local assembly defect or due to an inability to properly bind ATP. Alternatively, the interactions between N-terminal domain homodimers might be sufficiently strong that nucleotide binding can only provide a portion of energy necessary to overcome the free energy barrier of their association in the dilated state, thereby predisposing DnaB to oscillate between the two forms in solution.

To distinguish between these possibilities, we created point mutations in *Ec*DnaB that would be expected to disrupt or stabilize interfaces present in the dilated form of the N-terminal collar ring, and used 2D EM and SAXS to observe the conformations accessible to our mutants.

## MUTANT DESIGN

Since no crystal structures of full-length *Ec*DnaB are currently available, we created homology models for the *E. coli* helicase using *Bst*DnaB and *Aa*DnaB as templates. We tested two approaches; in one we selected residues that were closely apposed in one conformation but solvent exposed in the other and mutated them to cysteine residues that would cross-link the collar in one conformation by forming stabilizing disulfide bonds (**Figure 4.1**, **Table 4.1**). Alternatively the apposed residues were mutated to create electrostatic repulsion or steric clashes that would disrupt one collar state and thus drive the whole population to adopt the more favored conformation (**Figure 4.2**, **Table 4.1**). Designed cysteine mutants were cloned into the regular tagless DnaB vector and could be easily expressed and purified following the *Ec*DnaB purification protocol described in Chapter 3. In contrast, the mutants designed to disrupt either dilated or constricted interfaces in *Ec*DnaB could not be expressed from a standard pET vector in a C41 (Lucigen) strain (apparently due to toxicity). We therefore cloned the mutant genes into a periplasmic expression vector with an N-terminal $His_6$MBP tag. N-terminally tagged native *Ec*DnaB expressed by the periplasmic system behaved identically to the intracellularly expressed wild-type protein (data not shown). Purified DnaB collar mutants were then characterized using 2D EM and SAXS.

## CHARACTERIZATION OF THE CONSTRICTED AND DILATED E. COLI DNAB MUTANTS

Ultimately the constricted mutant was formed by replacing two side chains, Ser36 and Ile85, which are closely apposed in the dilated collar interface of DnaB but solvent-exposed in the constricted form (**Figure 4.2**) with arginines to generate electrostatic repulsion between the globular heads in the dilated ring state and favor ring constriction. For the dilated mutant, we replaced Thr86 and Ala121, which lie ~5 Å apart in the dilated state, with cysteines, thereby preventing the N-terminal collar from assuming a constricted conformation via disulfide bonds (**Figure 4.1**). When the dilated mutant was run on an SDS Page gel, we could clearly see dimerization of about 30% of the DnaB particles in the absence of reducing reagent, a value that corresponds to approximately one cross-linked dimer per hexamer. Consistent with our predictions, 2D class averages revealed that the S36R/I85R mutant exclusively adopted a constricted conformation (**Figure 4.3**), whereas the oxidized T86C/A121C construct formed only dilated species even in the presence of 1mM ATP (**Figure 4.3**).

## SMALL ANGLE X-RAY SCATTERING (SAXS) OF E. COLI DNAB HELICASE

To provide a more quantitative assessment of the distribution between dilated and constricted forms in solution in the presence of nucleotide, we turned to small-angle X-ray scattering (SAXS). Theoretical calculation of scattering curves using homology models of the *E. coli* helicase threaded onto either the ADP-bound (constricted) *Aa*DnaB structure, or the fully-liganded (dilated) *Bst*DnaB coordinates, revealed distinct SAXS signatures for the two conformations; in particular, a distinguishing dip and hump, visible from q=0.07-0.1 for the dilated state, flattened out in the constricted form (**Figure 4.4**). Unfortunately, while experimental scattering curves of *Ec*DnaB displayed similar features to the theoretical predictions, they did not overlay perfectly, likely due to differences between homology models and actual *E. coli* specific DnaB features. However once we obtained experimental scattering profiles of our dilated and constricted mutants, which revealed features respectively similar to the two theoretical extremes, we were able to fit data obtained for wild-type *Ec*DnaB in the presence of nucleotide and show a predicted mixture of the two states to further verify our EM findings discussed in Chapter 3 (**Figure 4.5**). Furthermore the scattering behaviors of the constricted and dilated mutants were not sensitive to the nucleotide titration, while wild type *Ec*DnaB scattering curves showed a gradual shift from a population where dilated particles were more prevalent towards a more constricted ratio when more nucleotide was added.

## CONCLUSIONS

Collectively, the EM and SAXS observations indicate that DnaB collar can adopt at least two highly-distinct conformations, and that nucleotide can toggle a

switch from one form to the other. The interactions between the globular subdomains and the distal ends of the helical hairpins in the constricted conformation are modest, reducing the buried surface area per globular subdomain by ~40% when compared to the dilated state (from 370Å$^2$ to 230 Å$^2$). The more extensive interactions within the dilated collar appear to restrain the helicase ring and partially counter effects of nucleotide binding. Overall our findings show that specific interactions between N-terminal domains not only help to control the conformational state of the DnaB ring, but these elements further predispose the native helicase toward a dilated collar conformation.

## MATERIALS AND METHODS

*Protein expression and purification*

*Ec*DnaB mutants designed to form disulfide bonds were purified as per wild-type DnaB, except that following the first gel filtration column, the samples were dialyzed out of nucleotide and reducing agent and then run over the second gel filtration column in the absence of nucleotide and DTT to ensure robust cross-linking.

*Ec*DnaB mutants based on electrostatic or steric clashes were purified from a periplasmic expression vector with an N-terminal tag. Transformed C41 cells were grown in the presence of 2% glucose and induced at 16°C for 20-22hours. Harvested cells were resuspended in 500mM NaCl, 20mM Hepes-KOH pH 7.5, 10% Glycerol, 10mM $MgCl_2$, 30mM Imidazole, 0.1mM ATP, 1mM β-mercaptoethanol, 1mM PMSF, 1μg/mL PepstatinA and 1μg/mL Leupeptin. Fresh (or thawed pellets that were previously flash frozen in liquid nitrogen) were lysed in the presence of DnaseI by sonication in 3-4 short 3s pulses to not overheat and denature the proteins. Proteins were purified by a combination of $Ni^{2+}$ and anion exchange chromatography (HiPrep Q column was used and mutants were eluted with a continuous gradient of NaCl, different mutants eluted at different salt concentrations); the N-terminal $His_6$MBP tag was cleaved with TEV protease in an overnight step. Final step of the purification was gel-filtration on a HiPrep 16/60 Sephacryl S-300 column (GE Healthcare) in a buffer containing 20mM Tris-HCl pH 8.5, 800mM NaCl, 10% Glycerol, 5mM $MgCl_2$, 0.1mM ATP, 1mM β-mercaptoethanol, 1mM PMSF, 1μg/mL PepstatinA and 1μg/mL Leupeptin. Proteins were then dilazyed overnight into 20mM Hepes-KOH pH 7.5, 100mM NaCl, 5% Glycerol, 5mM $MgCl_2$ and 0.1mM ATP, aliquoted and flash frozen in liquid nitrogen for storage.

*Electron Microscopy*

Negative staining, microscopy and image processing was done according to the procedures discussed in Chapter 3.

*Small Angle X-ray Scattering (SAXS) Experiments*

SAXS data were collected at beamline BL4-2 of the Stanford Synchrotron Radiation Lightsource. The samples contained 1 mg/mL wild type *Ec*DnaB

(dialyzed out of nucleotide over night and run over an analytical sizing column) with a nucleotide titration in 3-fold dilution steps from 1mM to 0mM AMPPNP. Data were processed and analyzed using Primus (Konarev et al., 2003). Theoretical scattering curves for *E. coli* homology models were generated by FoxS (Schneidman-Duhovny et al., 2010).

**Table 4.1**

| Name | Mutated Residues | Cloning | EM |
|---|---|---|---|
| wild type | none | IPTG tagless (EcB)<br>Arabinose tagless (Ara_EcB)<br>Periplasmic with $H_6$MBP (PPL EcB) | Equilibrium of constricted and dilated conformations |
| **CONSTRICTED** | | | |
| **SRIR (IRSR)** | **Ser36Arg, Ile85Arg** | **Periplasmic vector only (could not clone into tagless IPTG vector or Arabinose vector)** | **Constricted 2D class averages with ATP Constricted SAXS profile** |
| SDID | Ser36Asp, Ile85Asp | IPTG tagless and Periplasmic with $H_6$MBP tag | Never characterized (had interestingly enhanced ATPase activity, did not rescue ts strain E107) |
| SWIW | Ser36Trp, Ile85Trp | IPTG tagless and Periplasmic with $H_6$MBP tag | Not enough yield to characterize (did not rescue ts strain E107) |
| ND | Asn118Asp | Periplasmic vector only (could not clone into IPTG tagless vector or Arabinose vector) | Constricted 2D class averages |
| x-linked SE | Ser115Cys, Glu144Cys | IPTG tagless | Never characterized |
| **DILATED** | | | |
| SRER | Ser115Arg, Glu144Arg | Periplasmic with $H_6$MBP tag | Equilibrium of constricted and dilated conformations (partially rescued ts strain E107) |
| SDED | Ser115Asp, Glu144Asp | Periplasmic with $H_6$MBP tag | Equilibrium of constricted and dilated conformations |
| SWEW | Ser115Trp, Glu144Trp | IPTG tagless and Periplasmic with $H_6$MBP tag | Never characterized (partially rescued ts strain E107) |
| SE | Ser115Glu | Periplasmic with $H_6$MBP tag | Never characterized |
| **x-linked TA** | **Thr86Cys Ala121Cys** | **IPTG tagless** | **Dilated 2D class averages** |

**Figure 4.1**

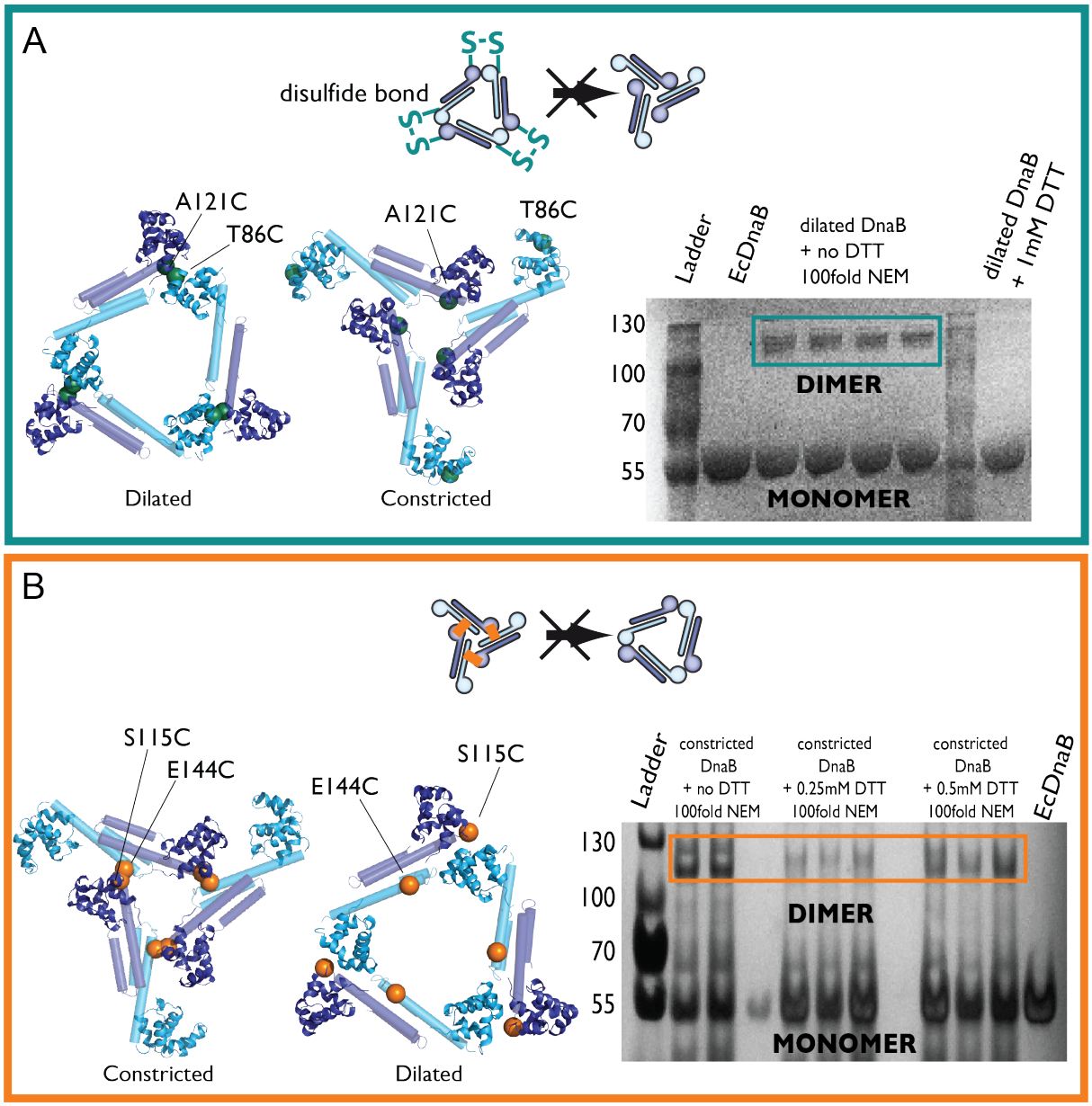


**Figure 4.1. Interactions between N-terminal domains in the dilated and constricted state: cross-linking** A) Amino acids buried between dimers in the dilated N-terminal collar do not associate in a constricted state. Cysteine residues engineered to form disulfide bonds and cross-link dilated collar state are shown as teal spheres. Gel showing disulfide bond formation and dimerization of the dilated DnaB mutant. B) Amino acids buried between dimers in the constricted N-terminal collar do not associate in a dilated state. Cysteine residues engineered to form disulfide bonds and cross-link constricted collar state are shown as orange spheres. Gel showing disulfide bond formation and dimerization of the constricted DnaB mutant.

**Figure 4.2**

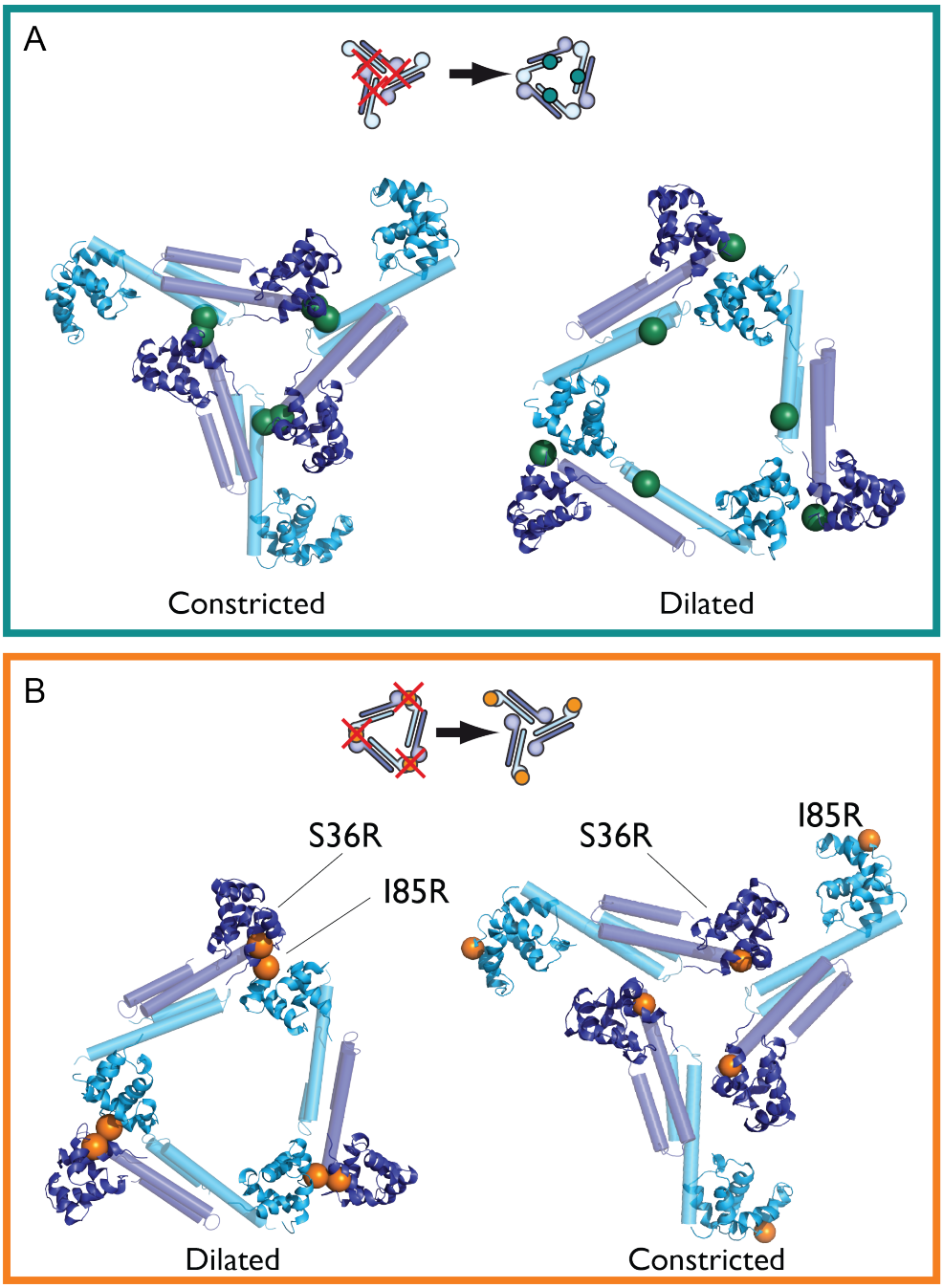


**Figure 4.2. Interactions between N-terminal domains in the dilated and constricted state: electrostatic repulsion.** A) Teal spheres (or red "X's" on the cartoon) correspond to two amino acids in *Ec*DnaB that, when mutated, prevent formation of the constricted state. B) Orange spheres (or red "X's" on the cartoon) correspond to two amino acids in *Ec*DnaB that, when mutated, prevent formation of the dilated state.

**Figure 4.3**

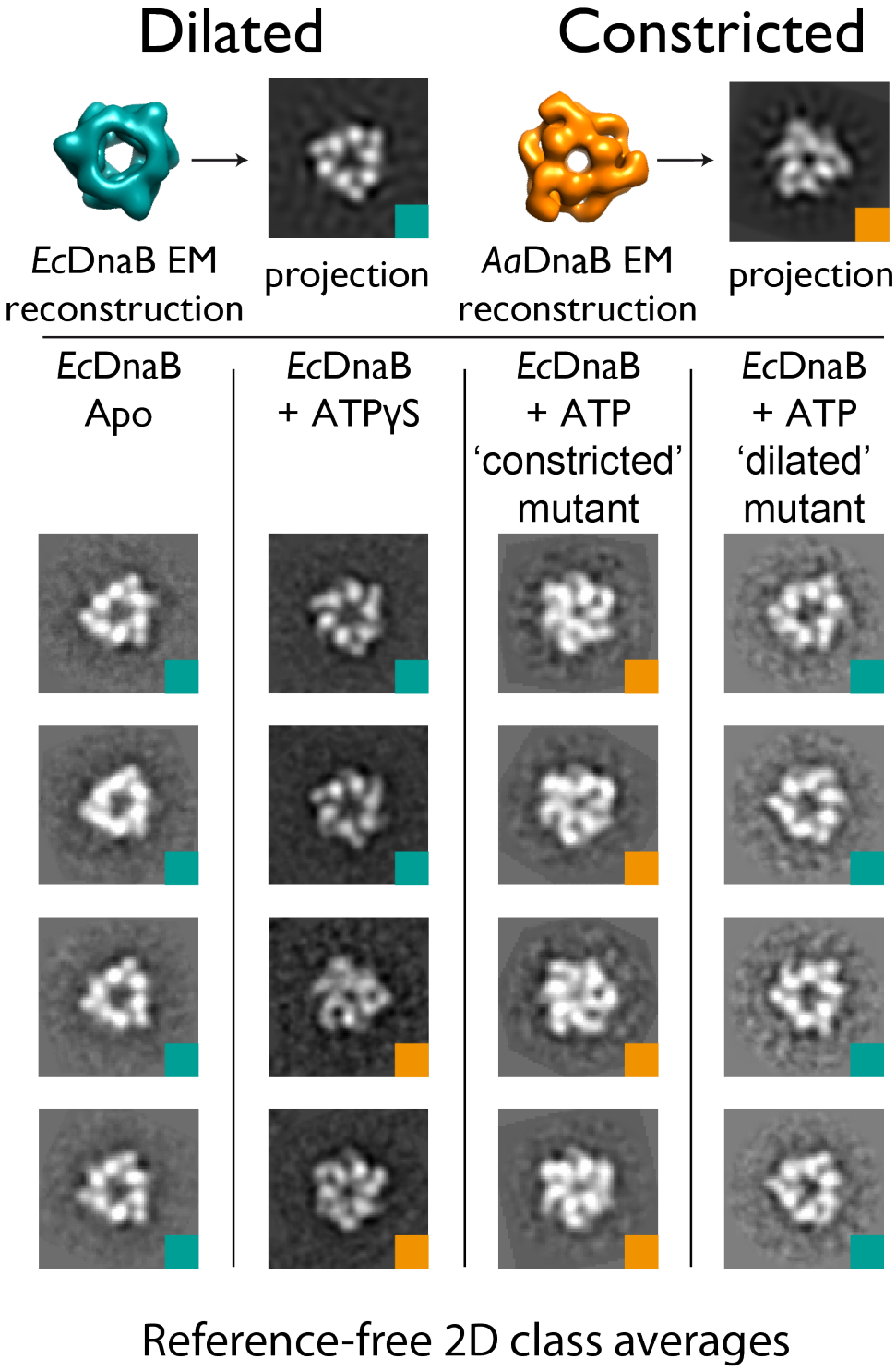


**Figure 4.3 Nucleotide promotes DnaB constriction.** A) Reference-free 2D class averages of wild type *Ec*DnaB and two *Ec*DnaB mutants with different nucleotides. Dilated (teal) *Ec*DnaB and constricted (orange) *Aa*DnaB EM models are shown at top for comparison.

**Figure 4.4**

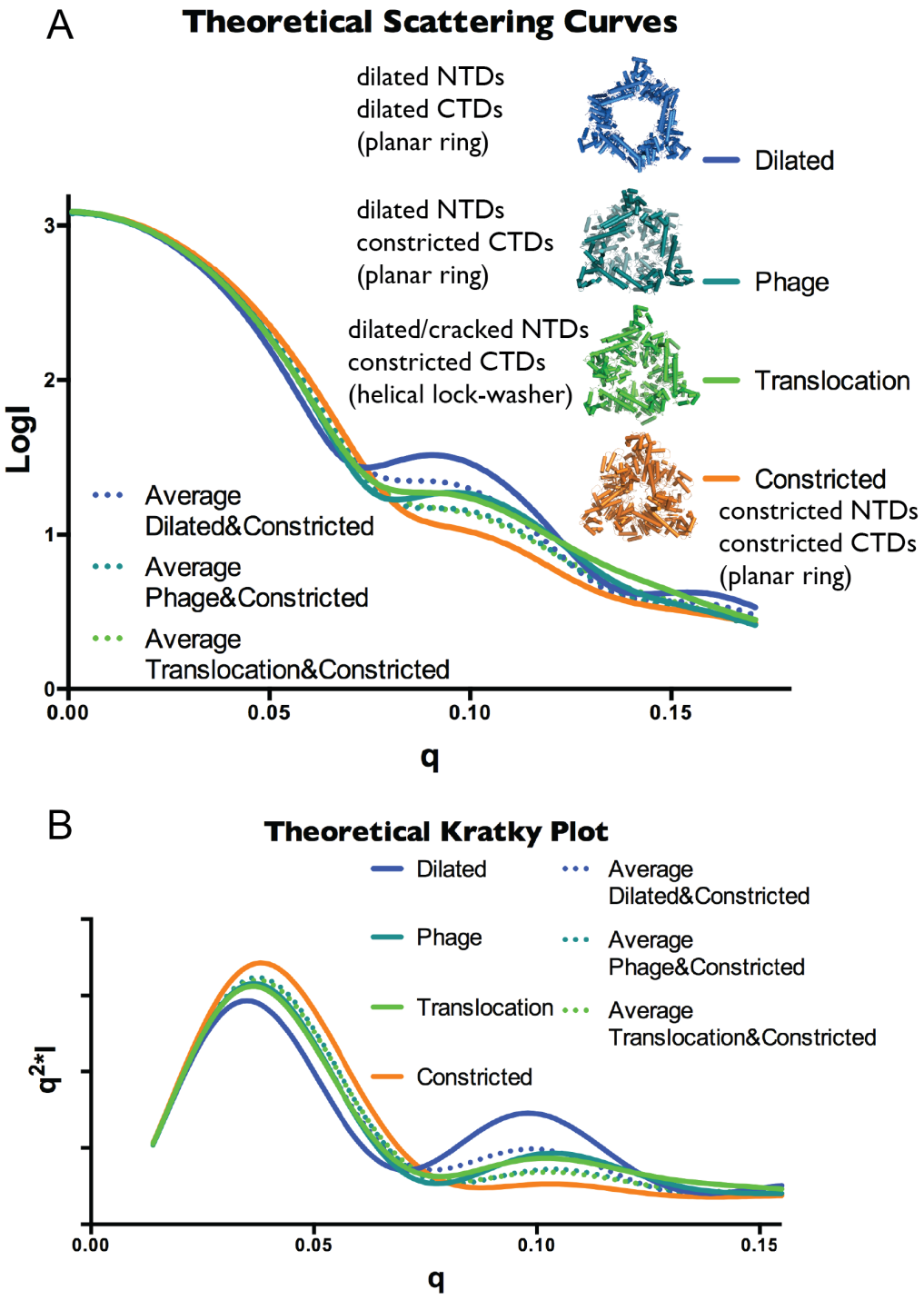


**Figure 4.4. Theoretical scattering profiles of the various crystal structures of DnaB helicase.** A) A plot of Log(Intensity) vs q, B) Kratky plot highlighting the distinctive dip and hump, visible from q=0.07-0.1 present in the structures with the dilated collar state, which flattens out in the constricted form.

**Figure 4.5**

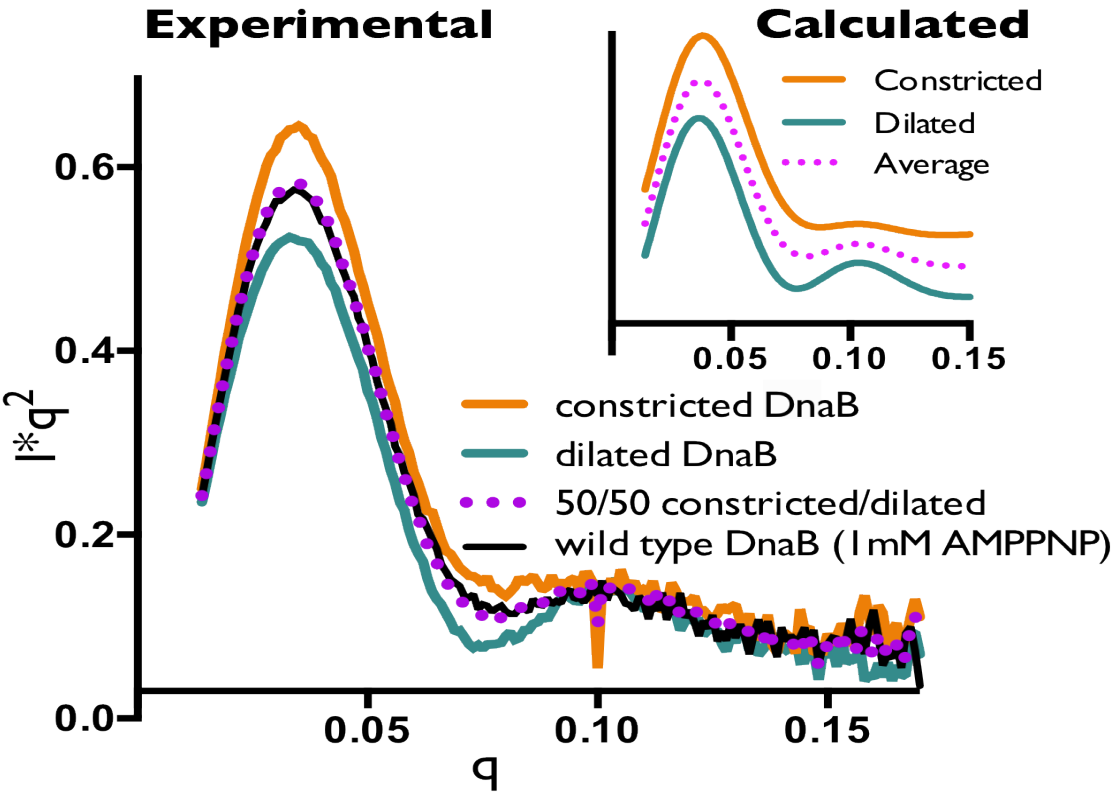


**Figure 4.5. Kratky plots:** Experimental SAXS curves of *Ec*DnaB with 1mM AMPPNP (black), constricted *Ec*DnaB (orange), dilated *Ec*DnaB (green) and average between the two states (pink dotted line). Inset: theoretical scattering curves of dilated (green) and constricted (orange) DnaB rings, as well as the average of the two models (pink dash) – curves are offset for clarity.

# Chapter 5 – Biochemical significance of the two states of DnaB helicase

## INTRODUCTION

Although the C-terminal domains of DnaB are well established as the helicase motor that hydrolyses ATP to power DNA unwinding (Biswas and Biswas, 1999; Biswas et al., 1994; Leipe et al., 2000; Nakayama et al., 1984), the structural and functional role of the N-terminal collar has been less clear. Some lines of evidence have indicated that the collar, like the motor domains, can bind single-stranded DNA (Bailey et al., 2007; Lo et al., 2009), as well as serve as a scaffolding element that helps stabilize DnaB hexamers (Biswas et al., 1994) and possibly maintain ring planarity (Wang et al., 2008). However, biochemical studies showing that the collar is both important for DNA unwinding and for binding specific partner proteins have hinted at a more complex role for this element in helicase function (Bailey et al., 2007; Bird et al., 2000; Biswas and Biswas, 1999; Biswas et al., 1994; Chang and Marians, 2000; Nakayama et al., 1984; Seitz et al., 2000; Xie and He, 2009). For example, the binding of the DnaB collar to DnaG is important for controlling both priming activity and frequency (Johnson et al., 2000; Koepsell et al., 2006; Mitkova et al., 2003; Tougu and Marians, 1996). Conversely, DnaG binding appears to antagonize the association of the helicase with DnaC (Makowska-Grzyska and Kaguni, 2010), an ATP-dependent helicase-loading factor that interacts with the C-terminal face of DnaB opposite the collar (Arias-Palomo et al., 2013; Galletto et al., 2003). Interestingly, whereas DnaG has been shown to engage the collar in a conformation seen in apo crystal structures of DnaB (Bailey et al., 2007), the collar takes on a markedly different conformation when the helicase associates with nucleotide-bound DnaC. The functional implications of these two collar states for DnaB helicase activity and the factors that lead to their interconversion are not known.

Although our structural data highlighted the existence of a two-state collar transition in DnaB, the functional significance of the dilated and constricted forms was not immediately apparent. We therefore set out to assess the consequences of the two states on DnaB activity, using our mutants to bias the helicase into one collar state or the other.

Interactions with specific factors are required for helicase loading. The closed-ring structure adopted by DnaB presents a topological impediment to the binding of ssDNA within a newly-melted replication origin during the initiation of strand synthesis (Davey and O'Donnell, 2003). In *E. coli*, this challenge is overcome by the DnaC protein, which acts on DnaB to allow the binding of ssDNA in the central pore (Davey et al., 2002; Fang et al., 1999; Marszalek and Kaguni, 1994; Wickner and Hurwitz, 1975). Recent findings indicate that DnaC not only facilitates ssDNA binding by physically opening a preformed helicase hexamer, but also appears to cause a structural rearrangement in DnaB that

correlates with unwinding efficiency (Arias-Palomo et al., 2013). Why DnaB might require DnaC to potentiate its activity has yet to be determined.

In addition to unwinding double-stranded (ds) DNA, DnaB collaborates with a number of other replication factors. For example, the enzyme responsible for synthesizing RNA primers during the initiation of replication and lagging-strand synthesis (the DnaG primase) has been shown to directly associate with DnaB (Bailey et al., 2007; Lu et al., 1996; Marians, 1992; Tougu et al., 1994; Zechner et al., 1992). DnaG binds DnaB in a 3:6 complex trough its C-terminal domain (Bird et al., 2000; Thirlway and Soultanas, 2006; Thirlway et al., 2004), which engages the N-terminal collar of the helicase (Bailey et al., 2007; Bird et al., 2000; Chang and Marians, 2000). This interaction places DnaG in close proximity to the lagging DNA strand as it emerges from the central pore of DnaB, thereby facilitating the binding of exposed template and primer synthesis. DnaG from *Escherichia coli* and other mesophilic bacteria associates with DnaB transiently, in a manner coupled to its priming activity (Johnson et al., 2000; Koepsell et al., 2006; Mitkova et al., 2003; Zechner et al., 1992), resulting in a periodicity of the lagging-strand synthesis known as the replication fork clock (Tougu and Marians, 1996). How this timing is controlled, and whether the relative placement of DnaG changes with respect to DnaB during translocation, is not understood. Replicative helicase is further coupled to the replicative polymerase via interaction with the C-terminal domain of τ subunit of the clamp-loader complex that also interacts with the α subunit of polymerase (Dallmann et al., 2000; Kim et al., 1996). This interaction between DnaB helicase and τ subunit is essential for maintaining a fast rate of replication fork progression and it enhances DnaB translocation rates by more than 10-fold (Kim et al., 1996). The mechanism of this helicase activation is not understood but could potentially be due to conformational rearrangements within the DnaB motor.

## RING CONSTRICTION AND DILATION AIDS IN DISTINGUISHING BETWEEN SINGLE AND DOUBLE STRANDED DNA SUBSTRATES

Although our structural data presented in Chapters 2-3 highlighted the existence of a two-state collar transition in DnaB, the functional significance of the dilated and constricted forms was not immediately apparent. We therefore set out to assess the consequences of the two states on DnaB activity, using the mutants described in Chapter 4 to bias the helicase into one collar state or the other.

### DNA binding

When assessed for single-stranded DNA binding using fluorescence anisotropy, with substrates ranging from 15 to 60 nulceotides in length, the constricted and dilated *Ec*DnaB mutants (discussed in Chapter 4) both showed a similar affinity compared to the wild-type enzyme (**Figure 5.1**). However, when double-stranded DNA substrates long enough to span the full length of the

central channel were investigated, the dilated mutant showed a >2-fold increase in binding affinity relative to the wild type protein, whereas the constricted conformation displayed a >2-fold decrease ($K_D$s of 28nM, 70nM and 180nM respectively, **Figure 5.1**). These results indicate that both conformations of DnaB helicase can accommodate single DNA strands equally well inside the helicase pore, but that the constricted conformation of the helicase is less able to engage duplex substrates.

## ATP hydrolysis

We next compared the basal, as well as single- and double-stranded DNA stimulated, ATP hydrolysis rates of the mutant and wild type proteins, utilizing a coupled enzyme assay and DNA substrates identical to those used in the DNA-binding experiments. The constricted mutant and wild-type DnaB helicase had very similar basal hydrolysis rates that were both greatly stimulated by the addition of single-stranded DNA (**Figure 5.2A**). In agreement with its reduced affinity for double-stranded DNA, the constricted conformation showed negligible stimulation of hydrolysis by duplex oligos (**Figure 5.2B**). By contrast, the dilated mutant displayed basal hydrolysis rates equivalent to the DNA-stimulated rates of wild type and constricted DnaB. Moreover, these rates were relatively unaffected by the addition of DNA (**Figure 5.2**), indicating that stabilization of the N-terminal collar in a dilated state uncoupled ATPase activity from DNA binding. Interestingly, a similar decoupling has been observed when mutations have been introduced into the DnaB **T**ransducer **H**elix (TH) that forms the interface between the N-terminal collar and the C-terminal ATPase ring (Biswas and Biswas, 1999).

## Translocation along dsDNA

To further understand the functional impact of a change in DnaB collar state, we measured the ability of both mutant and wild type DnaBs to translocate along dsDNA substrates; although DnaB is thought to move along a single-DNA strand when acting as a helicase (Jezewska et al., 1998; Kaplan and Steitz, 1999; LeBowitz and McMacken, 1986), it also can drive the powered movement of DNA duplexes (Kaplan, 2000; Kaplan and O'Donnell, 2002). Using a fluorescent assay outlined in **Figure 5.3A**, we found that whereas wild-type and dilated DnaB helicases were able to translocate along double-stranded DNA, the constricted mutant could not (**Figure 5.3B**). Taken together with our DNA-binding and ATP-hydrolysis data, these observations not only reveal that the structural disposition of the N-terminal collar directly helps coordinate nucleotide turnover with DNA binding, but also show that changes in collar state can control whether DnaB can translocate along dsDNA, likely by sterically preventing duplex DNA entry into the motor when the collar is constricted.

## Fork unwinding

As a final assessment of the effects of collar state on internal DnaB functions, we next looked at the unwinding of duplex DNA by the helicase. On short model duplexes, DnaB family enzymes are most active when one oligonucleotide end bears a single-stranded fork (Kaplan, 2000; Kaplan and Steitz, 1999); *E. coli* DnaC, a helicase loader, further stimulates the action of its cognate DnaB on these substrates (Arias-Palomo et al., 2013). As seen previously (Arias-Palomo et al., 2013), wild-type DnaB displayed relatively little unwinding activity in the absence of the helicase loader (**Figure 5.5**). The behavior of dilated mutant largely mirrored that of the native enzyme; however, the constricted mutant actually showed a moderately elevated degree of basal unwinding (**Figure 5.5**), indicating that this construct is not an inherently crippled motor. When the dilated and constricted mutants were tested in a single-turnover, fork-unwinding assay with DnaC, all the conformations were able to unwind the simple forked substrate.

# DIFFERENTIAL INTERACTION AND RESPONSE OF CONSTRICTED AND DILATED DNAB CONFORMERS WITH REPLISOMAL PARTNER PROTEINS

## Helicase loader DnaC

Although, as mentioned previously, both dilated and constricted mutants were able to unwind short forked DNA duplexes they differed in terms of rates and total performance. The dilated mutant was able to produce ~20% more unwound product as the wild type helicase, and did so at a slightly faster rate (**Figure 5.6**). By contrast, while the constricted mutant could generate a comparable amount of single-stranded DNA as wild-type DnaB, it took longer to do so (**Figure 5.6**). These observed differences in how the mutants promote product formation show that the collar can have an unexpectedly profound effect on the kinetics of helicase action. Interestingly, *Bst*DnaB has been seen to form a cracked, but dilated, N-terminal collar conformation when bound both to nucleotide and to a single-stranded DNA substrate proposed to reflect a translocation substrate (Itsathitphaisarn et al., 2012). This structural finding suggests that the elevated unwinding rates seen with a dilated collar could result from an ability of the mutant helicase to more stably retain a translocation-competent configuration. If true, then the moderate pace of the wild-type enzyme might result from continuous interconversion between this state and a slower moving form, one our data suggest could derive from a constricted collar configuration. Alternatively, 3D EM reconstructions of an *Ec*DnaB•DnaC complex have shown that upon binding of DnaC, contacts between the globular domains of the DnaB N-terminal collar rearrange into a cracked, but constricted, configuration (Arias-Palomo et al., 2013). Given that DnaC is known to prevent DnaB from unwinding DNA when it stays associated with the helicase (Biswas et al., 1986; Wahle et al., 1989), the observed differences in rate between wild-type and mutant DnaBs seen here could derive from a change in the relative affinity of

DnaC for the helicase depending on the state of the collar. In this view, a constricted collar state would favor DnaC binding, slowing release of the loader from the helicase and leading to a long lag that precedes unwinding. By contrast, a dilated collar would disfavor interactions with DnaC, speeding loader release to relieve inhibition of the helicase and promote more rapid unwinding. Future efforts will be needed to distinguish between these possibilities.

## Tau subunit of the clamp loader

As with DnaC, *E. coli* τ has been reported to bind to the C-terminal motor domains of DnaB (Haroniti et al., 2004; Martinez-Jimenez et al., 2002); mass-spectrometry studies have further found that domains III and IV of τ associate more strongly with DnaB in the presence of ATP and $Mg^{2+}$ (Afonso et al., 2013), conditions shown here to promote collar constriction. To test whether τ could distinguish between different N-terminal domain conformations of DnaB, we examined the effect of its helicase-binding domains on DNA unwinding by the *E. coli* helicase. Notably, the presence of τ domains III-IV stimulated strand separation by all DnaB constructs tested. However, the highest degree of stimulation was actually exhibited by the constricted DnaB mutant, with levels approaching those seen for the dilated DnaB mutant when activated by DnaC (compare **Figures 5.6**). Thus, as with DnaC, τ also appears capable of distinguishing between different DnaB collar states. How τ reads out the collar confirmation of DnaB is not clear: the protein could recognize a cryptic binding site on the N-terminal domains that is revealed upon collar constriction, or movements in the collar might allosterically remodel the existing τ binding site in DnaB's C-terminal motor region to favor more productive interactions.

## DnaG primase

Yet another replisomal factor that binds to DnaB is the DnaG primase (Bailey et al., 2007; Bird et al., 2000; Chang and Marians, 2000). In a co-crystal structure of *Bst*DnaB bound to the C-terminus of DnaG (Bailey et al., 2007), the helicase-interaction domain of primase, which is itself a structural homolog of the DnaB N-terminal domain (Chintakayala et al., 2007; Oakley et al., 2005; Syson et al., 2005), can be seen to bind non-equivalently to two adjacent, but distinct, globular heads of a dilated DnaB collar (**Figure 5.7**A). Interestingly, the disposition of DnaG-binding sites is dramatically different in the constricted state, with one site rendered sterically inaccessible and the other repositioned far from the central pore of the helicase (**Figure 5.7B**).

The change in DnaG-binding site configurations between the two collar states suggested to us that DnaG might preferentially associate with DnaB when the helicase collar is dilated compared to when it is constricted. To test this idea, we assessed the ability of different DnaB collar mutants to stimulate primer synthesis by DnaG, a well-characterized activity that can be monitored in an M13 priming assay by titrating different amounts of helicase against a fixed concentration of primase (Johnson et al., 2000; Koepsell et al., 2005; Lu et al.,

1996). Notably, we observed that while the dilated mutant enhanced primer synthesis to the same degree as wild-type *Ec*DnaB, the constricted helicase was completely unable to stimulate DnaG activity (**Figure 5.8**). These findings not only corroborate prior structural data showing that primase associates with a dilated form of the DnaB N-terminal domains (Bailey et al., 2007), but also demonstrate that the conformational state of the collar can directly control the efficiency of primer formation.

## CONCLUSIONS

Taken together, our data indicate that the N-terminal collar may serve as a locus for sensing interactions with DNA and controlling the diameter of the central channel of DnaB helicase to accommodate DNA substrates with different numbers of nucleic acid strands. The interconversion between the dilated and constricted states of the N-terminal collar appears to be also relayed onto the C-terminal ATPase domains, affecting the rate of ATP hydrolysis and thus potentially rates of translocation.

Our biochemical data also imply the existence of a close allosteric relationship between the N- and C-terminal tiers of the helicase. The conformation of the N-terminal collar appears to have a profound impact on the various functions of the helicase, particularly on the binding and unwinding of DNA, which is carried out by the C-terminal RecA domains. Furthermore, it is possible that interactions of other replication factors with the C-terminal tier of the helicase affect the conformation of the N-terminal collar, thus allowing the helicase to sense and respond to the changes in replisome state. Based on these results, it is tempting to envisage, a complex allosteric mechanism by which the function of the helicase and its partners within the replisome can be tightly regulated.

## MATERIALS AND METHODS

*DNA substrates*

HPLC-purified DNA oligonucleotides were purchased from Integrated DNA Technologies (for a list of substrates refer to **Figure 5.9**). Buffer containing 10 mM Tris-HCl, 1 mM EDTA, and 100 mM NaCl, pH 7.5 was used in all annealing reactions. All substrates were run on pre-cast Tris-borate/EDTA gradient polyacrylamide gels purchased from Invitrogen by Life Technologies to ensure correct size and annealing. Gels containing substrates labeled with fluorescein, Cy3 and Cy5 were imaged on a Typhoon scanner (GE Healthcare Life Sciences) (**Figure 5.3C**).

*DNA binding assays*

DNA and protein were resuspended in buffer containing 20 mM HEPES-KOH pH 7.5, 5 mM magnesium acetate, 50 mM potassium glutamate, 5 % glycerol, 0.2 mg/mL BSA and 0.5mM AMPPNP. Each binding reaction contained 10 μL of 20 nM fluorescent DNA substrate and 10 μL of DnaB hexamer. Two-fold

protein dilutions were carried out starting at 2μM concentration and working down to 0 mM (12 total data points). Fluorescent polarization of each reaction was measured at 37°C on a Victor $^3$V plate reader (Perking Elmer) immediately after mixing and following 5min incubation. Data, converted to fluorescent anisotropy, were fitted to one-site specific binding with a Hill slope equation:

$$Y=Bmax*X^h/(Kd^h + X^h),$$

where **Bmax** is the maximum extrapolated specific binding in the same units as Y, **Kd** is the ligand concentration needed to achieve a half-maximum binding at equilibrium (expressed in the same units as X), and **h** is the Hill slope.

*ATPase assay*

Wild-type and mutant ATPase activities were measured using an established enzyme-coupled assay in which hydrolysis of ATP to ADP is coupled to the oxidation of NADH to $NAD^+$ (Lindsley, 2001; Tamura and Gellert, 1990; Webb, 1992). To determine $K_m$ and $V_{max}$, 25 nM DnaB hexamers were incubated at 37° C with 0-1.6 mM ATP (3-fold dilutions for a total of 8 points) in 100μL reactions. Reactions contained 2 mM phosphoenol pyruvate (PEP), 0.6 mM β-nicotinamide adenine dinucleotide (NADH), and an excess of pyruvate kinase and lactate dehydrogenase (Sigma). The oxidation of NADH to $NAD^+$ was monitored by measuring absorbance at 340 nm in a Victor $^3$V plate reader (Perking Elmer). The rate of decrease in absorbance was converted to μmol of ATP hydrolyzed to ADP by using an NADH standard curve and the assumption that one ATP is hydrolyzed for every NADH oxidized. ATPase rate as a function of ATP concentration was fit using Michaelis-Menten kinetics in PRISM (GraphPad). DNA stimulation of ATPase activity was measured by addition of 500nM unlabeled ss/dsDNA substrates used in DNA binding assays.

*dsDNA translocation*

DNA substrate was formed by annealing 10 μM Cy3-labeled 4c oligonucleotide with a 2-fold excess of 4a and 3-fold excess of 4b oligonucleotides (**Figure 5.9**) to ensure full quenching of the fluorescent DNA. Additionally, we annealed a substrate where the 4b oligonucleotide carried a 3' Cy5 label to ensure that our annealing protocol resulted in formation of a desired substrate where every piece of DNA with Cy3 label would also have the initial double-stranded DNA region. DnaB helicase and DnaC loader proteins were premixed and incubated on ice for 10min, followed by addition of DNA and another 10min incubation on ice. 1mM ATP was added together with DNA capture strand complementary to the Cy3 labeled DNA piece and reaction was transferred to 37°C to be monitored for the increase of Cy3 fluorescence using a Victor $^3$V plate reader (Perkin Elmer). 20 μl reactions contained 200 nM DnaB hexamer and equimolar concentration of DnaC (1.2 μM DnaC monomer), 100 nM DNA substrate, 200 nM capture strand and 1 mM ATP in the same buffer that was used for DNA binding and ATP hydrolysis experiments. Each reaction was measured six separate times to generate robust statistics. Data were first processed in Excel (Microsoft) and plotted using PRISM (GraphPad). As a control we tested DnaB for unwinding of a blunt fork lacking the 3' flap region that mimicked the first half of our dsDNA translocation substrate (oligonucleotides

3ab, **Figure 5.9**), and observed minimal activity even in the presence of DnaC loader (**Figure 5.3D**). We also measured duplex DNA translocation on the doubly-labeled substrate that contained Cy5 label on 3' end of the 4b oligonucleotide and 5' Cy3 label on the 4c oligonucleotide (**Figure 5.3E**); the observed trends were similar to the duplex DNA translocation measured on a substrate without the additional Cy5 label, but DnaB was significantly less efficient on the doubly-labeled substrate.

*Forked substrate helicase assay*

The forked DNA substrate was formed by annealing oligonucleotides 5a and 5b (**Figure 5.9**) at 20μM concentration of the Cy3 labeled substrate with 1.2-molar excess of the Black hole quencher-labeled DNA. Helicase and loader were premixed on ice for 10 min, followed by addition of the forked substrate and another 10min incubation step. A DNA capture strand (complementary to the base-paired region of the Cy3-labeled oligonucleotide) was then added together with ATP and the reaction was transferred to 37° C and immediately monitored for the increase of Cy3 fluorescence using a Victor $^3$V plate reader (Perkin Elmer). 20 μl reactions contained 200 nM DnaB hexamer, 100 nM forked DNA, 200 nM capture strand and 1 mM ATP. Helicase loader was added at equimolar concentration (1.2 μM DnaC monomer), while τ domains III and IV were added at 2 fold excess (2.4 μM final concentration of τ monomer). All proteins and DNA were resuspended in the buffer used for DNA binding experiments (without the AMPPNP). Each reaction was measured six separate times to generate robust statistics. Background correction and normalization was conducted in Excel (Microsoft), while PRISM (GraphPad) was used to generate final plots.

*Fluorometric de novo primer synthesis assay*

For analysis of DnaB-stimulation of primer synthesis by DnaG, all components were brought up in RNase free water, individual solutions of ATP, UTP, CTP and GTP were purchased at 100 mM concentration (certified as RNase free, New England Biolabs), and RNase free buffer components were purchased from Teknova. DnaB, DnaC and DnaG were diluted down into reaction buffer containing 100 mM potassium glutamate, 20 mM HEPES-KOH pH 7.5, 10 mM magnesium acetate and 0.2 mg/ml BSA. DnaB and DnaC were mixed in equimolar concentration and preincubated on ice for 10 min; 10μl of $Dna(BC)_6$ was then mixed with 10 μl of DnaG and incubated for 1 min at 37° C. 10 μl of nucleotides combined with single stranded M13 DNA in the reaction buffer was then added to facilitate priming. Following a 5 min incubation at 37° C reactions were quenched with 30 μl of 1:100 Pico Green stock solution (Invitrogen) in 20 mM Tris-HCl, 50 mM EDTA (pH 7.5). Stopped reactions were incubated in the dark for 5 min and raw fluorescence was measured in a Victor $^3$V plate reader (Perking Elmer). All reactions were carried out in triplicate, fluorescent data was background corrected by subtracting raw fluorescence of reactions that lacked DnaG and $Dna(BC)_6$ proteins. Obtained data was plotted using PRISM (GraphPad)

**Figure 5.1**

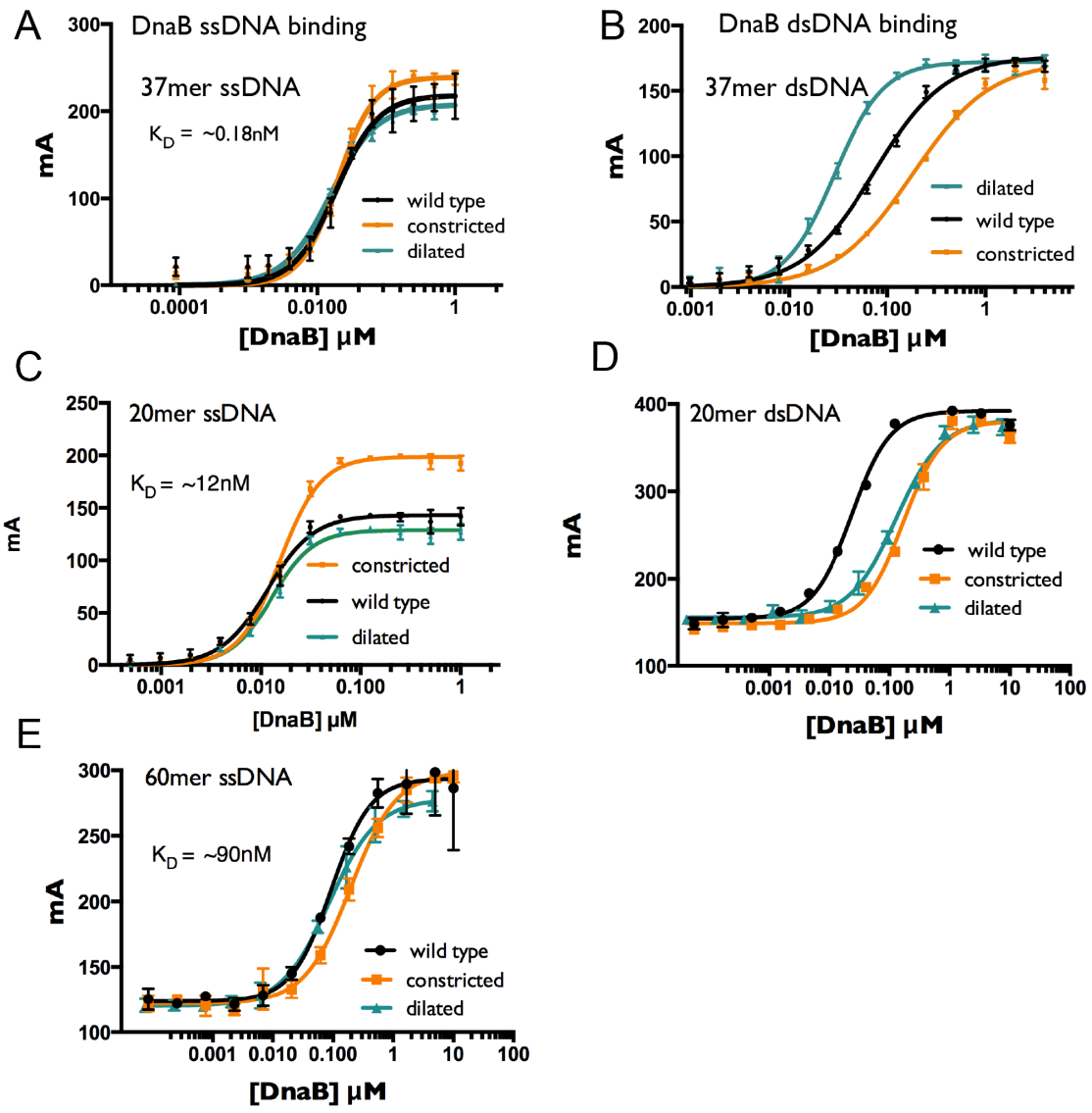


**Figure 5.1. The N-terminal collar conformation affects helicase interactions with DNA.** Panels (A) and (B) correspond to single-stranded DNA binding and duplex DNA binding by wild type (black), constricted (orange) and dilated (green) *Ec*DnaB, respectively, as measured by fluorescence anisotropy for pieces of DNA 37nucleotides long. Panels (C) and (E) show that wild type DnaB and both of the mutants bind ssDNA equally well regardless of the DNA length but the $K_D$ values increase with the length of DNA. Panel (D) shows that the dilated mutant does not appear to bind dsDNA better than the wild type DnaB if the DNA is not long enough to span the full length of DnaB helicase.

**Figure 5.2**

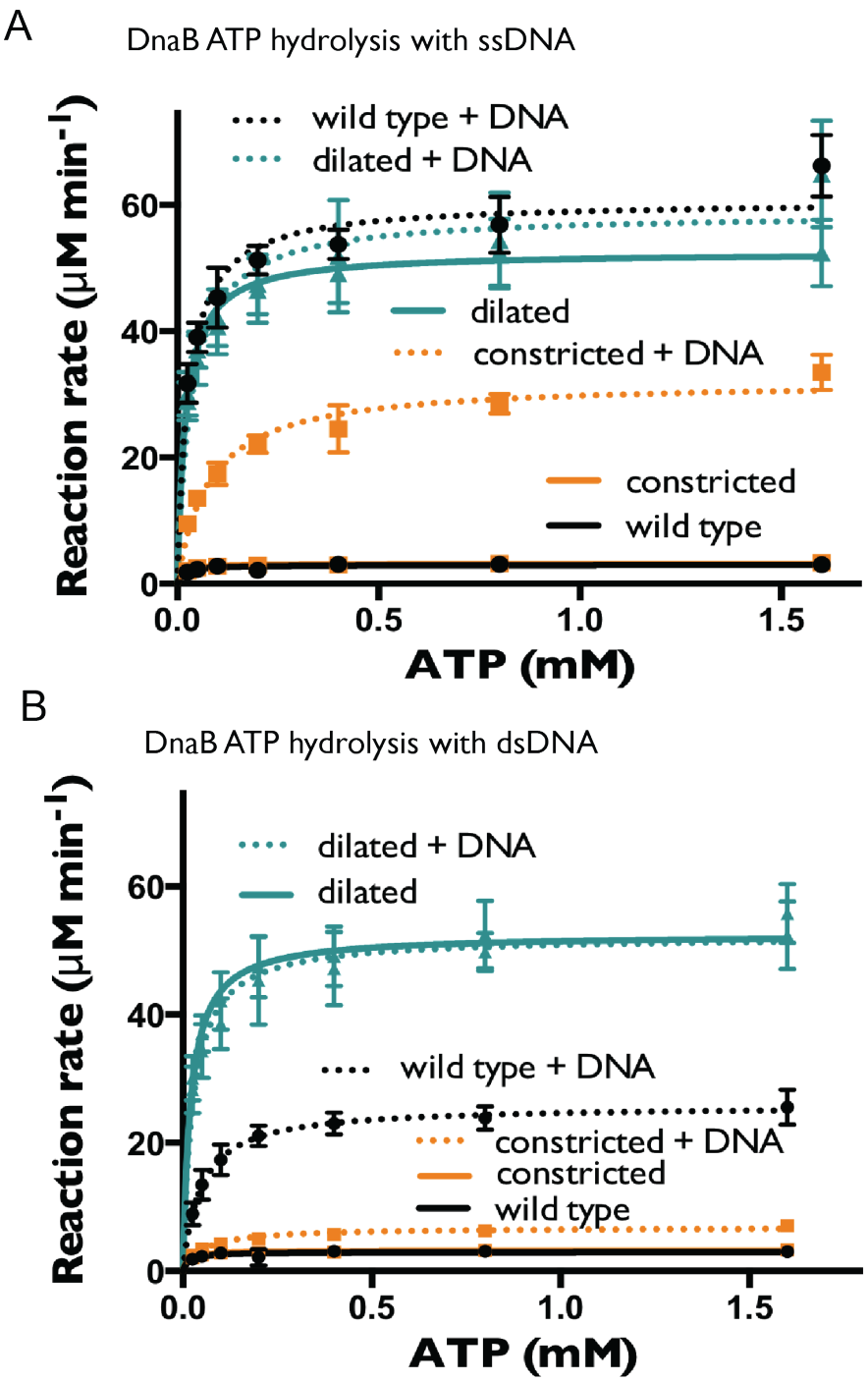


**Figure 5.2. The N-terminal collar conformation affects helicase ATPase rate.** Panels (A) and (B) correspond to ATP hydrolysis in the presence of single-stranded DNA and duplex DNA, respectively.

**Figure 5.3**

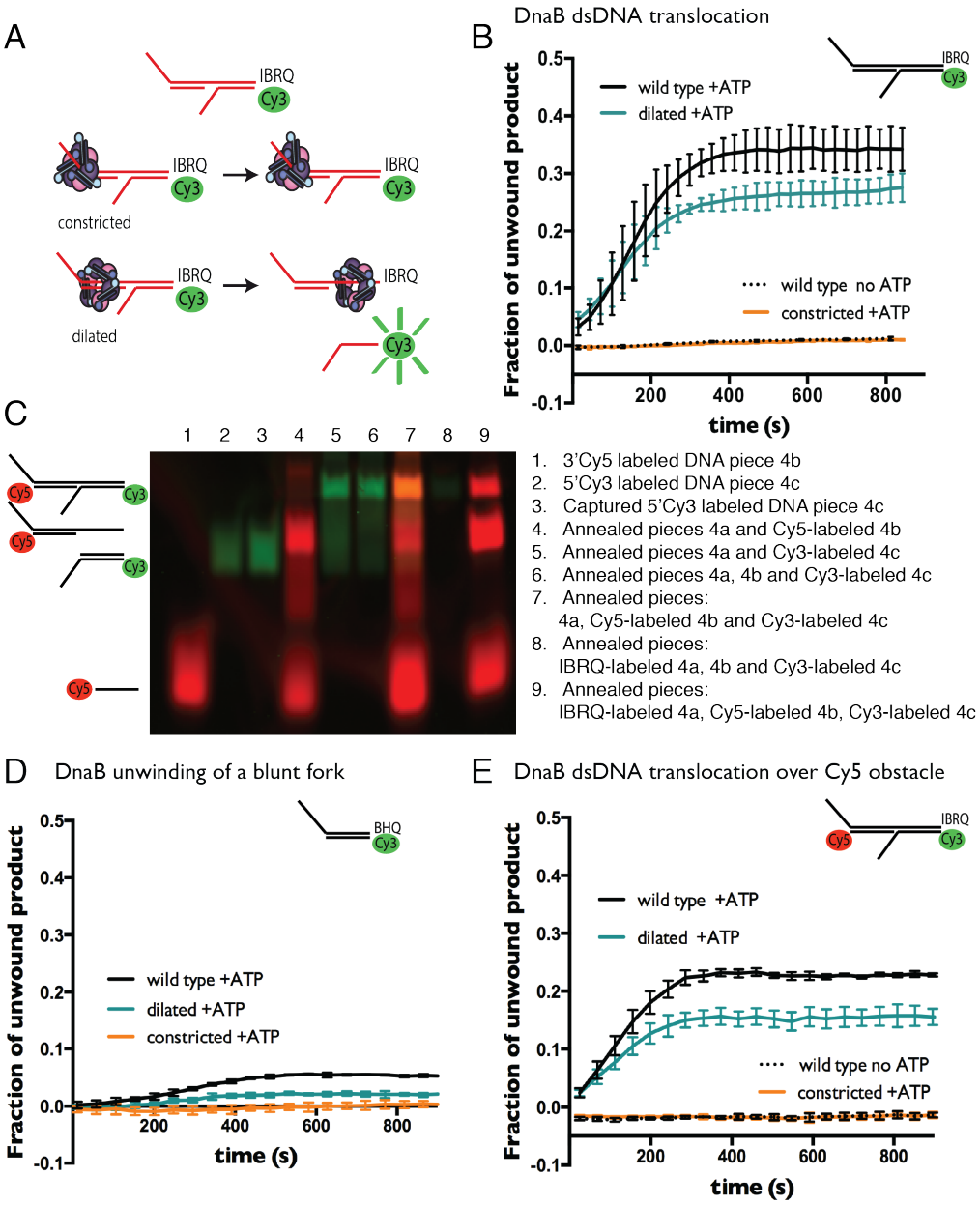


**Figure 5.3. Only helicases that can access a dilated state can move along double-stranded DNA** A) Schematic outline of experiment assaying translocation along duplex DNA. B) Control experiment showing that a blunt fork does not get unwound by DnaB (wild type or mutant) even in the presence of DnaC. C) Annealing of substrates for dsDNA translocation experiments, translocation was tested on substrates from lanes 8 and 9, DNA substrates were additionally incubated for 10min at 37°C following incubation to ensure that they would not fall apart in a plate-reader assay. D) dsDNA translocation tested on the doubly labeled substrate from lane 9 of the gel from C). E) Kinetic data showing the ability of wild type (black), constricted (orange) and dilated (green) *Ec*DnaB to translocate along duplex DNA.

**Figure 5.4**

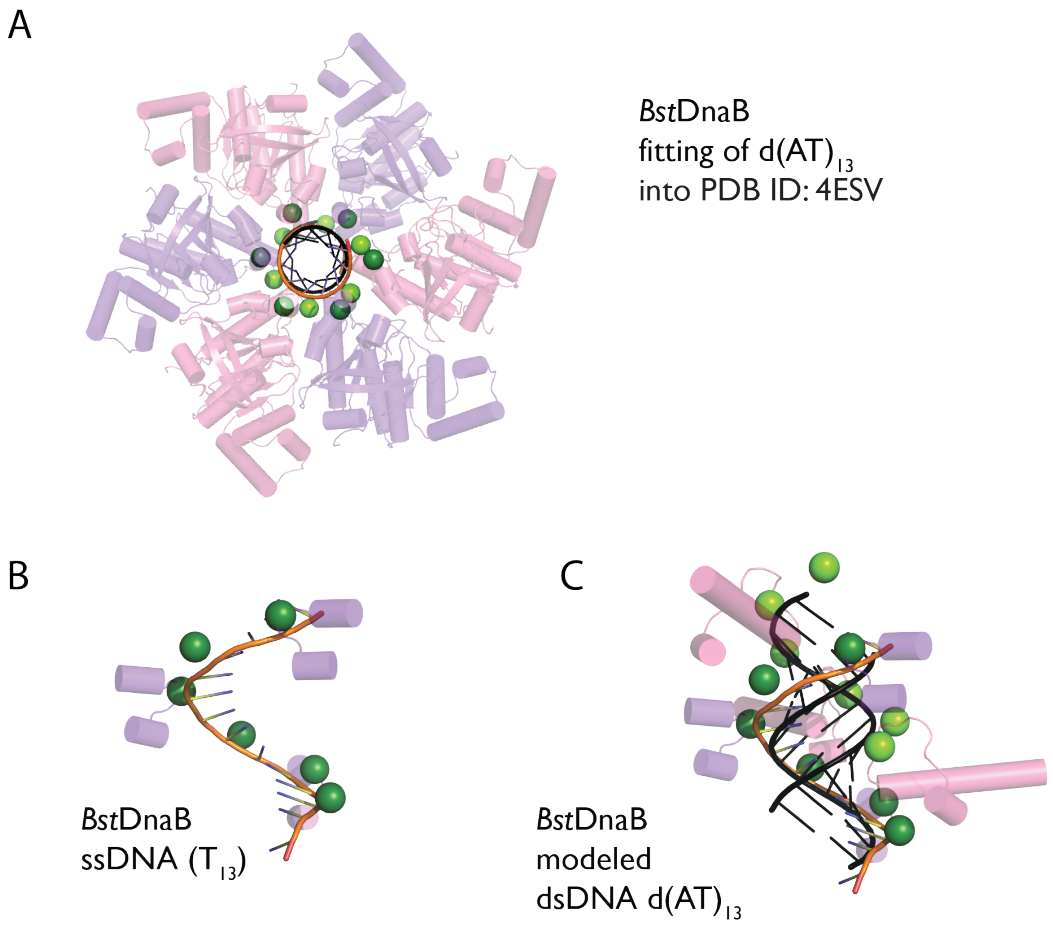


**Figure 5.4. Fitting of dsDNA inside the central channel of *Bst*DnaB.** A) Top view of the fit of dsDNA inside the central channel of DnaB from the structure of *Bst*DnaB bound to ssDNA (PDB ID 4SEV). B) Side view of the ssDNA inside the central channel of DnaB helicase from the structure of BstDnaB (PDB ID: 4SEV), residues forming specific contacts are shown as dark green spheres. C) Modeled dsDNA (black) superposed onto ssDNA (orange) inside the DnaB central channel, light green spheres represent residues already positioned to form contacts with the second DNA strand.

**Figure 5.5**

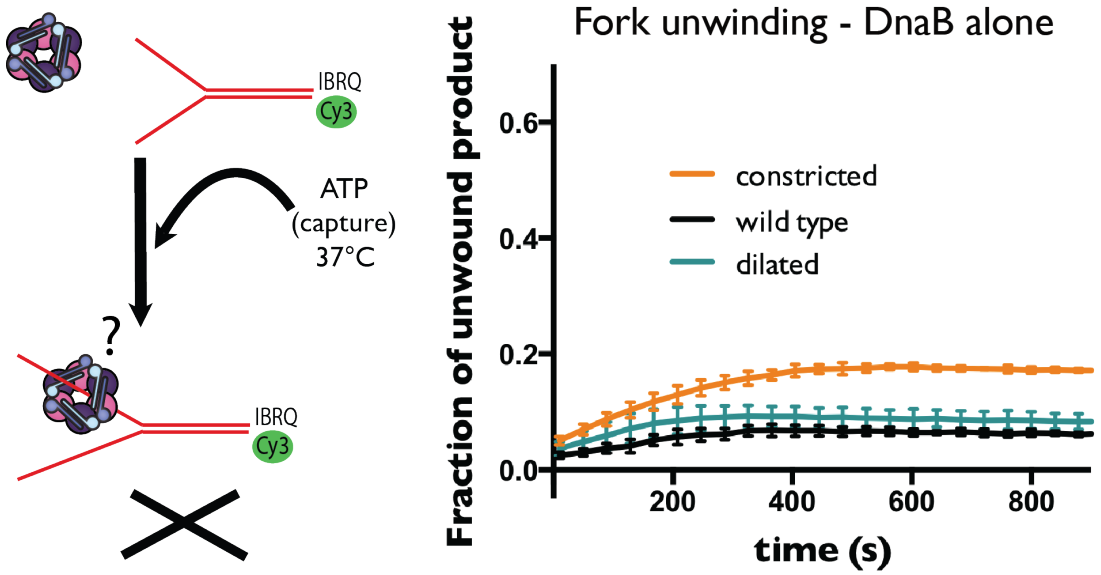


**Figure 5.5. DNA unwinding is influenced by collar state.** Cartoon representation of the unwinding assay and basal unwinding levels of a short forked substrate by wild type *Ec*DnaB (black) and both constricted (orange) and dilated (green) DnaB mutants.

**Figure 5.6**

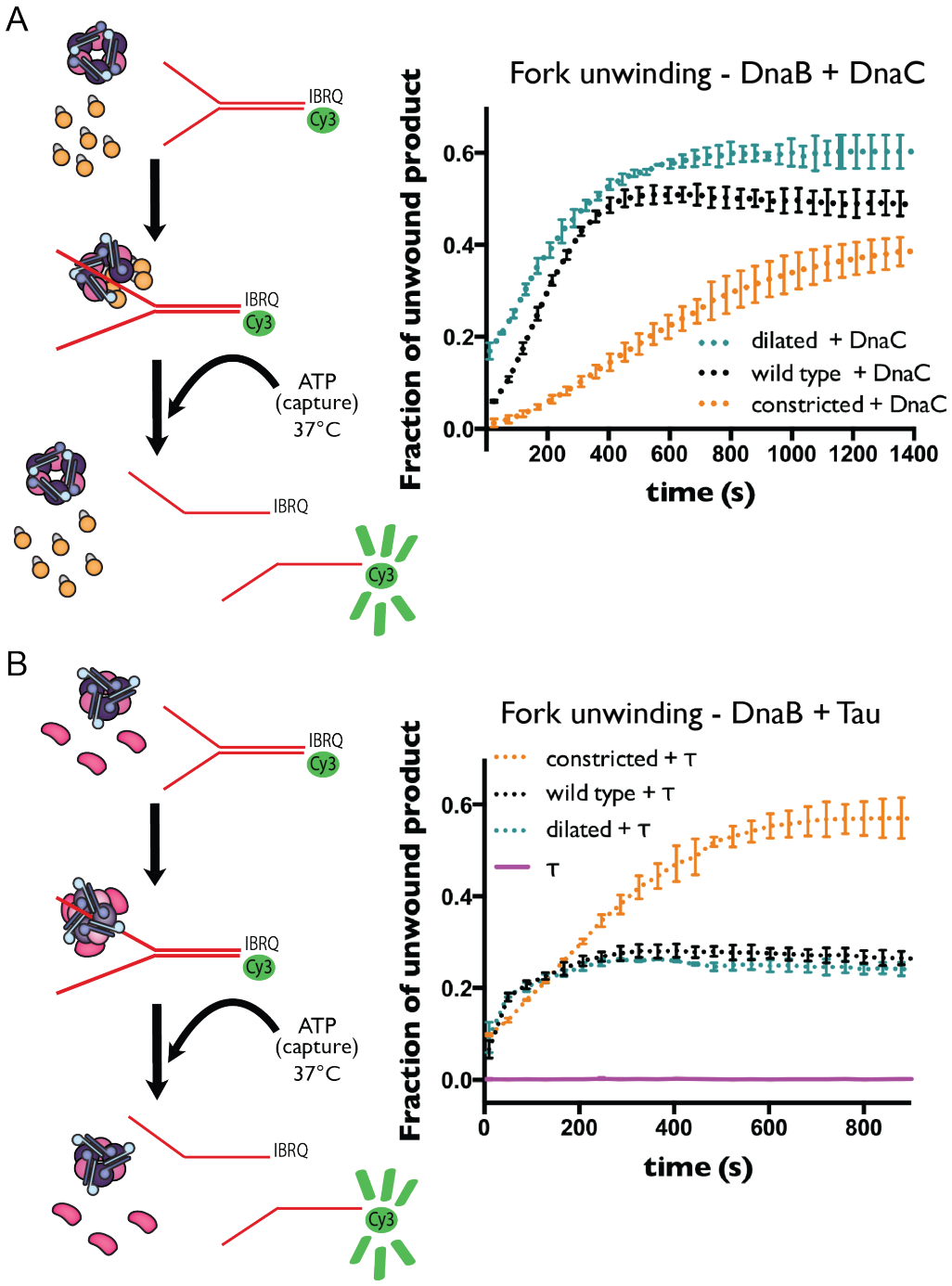


**Figure 5.6. DNA unwinding and DnaB-partner interactions are influenced by collar state.** A) DnaC-dependent activation of DNA unwinding by DnaB and both constricted and dilated DnaB mutants. DnaC preferentially activates DNA unwinding by DnaB helicases that can access a dilated collar conformation. B) Effect of τ on DNA unwinding by DnaB. τ preferentially activates DNA unwinding by DnaB when the helicase favors a constricted collar conformation.

**Figure 5.7**

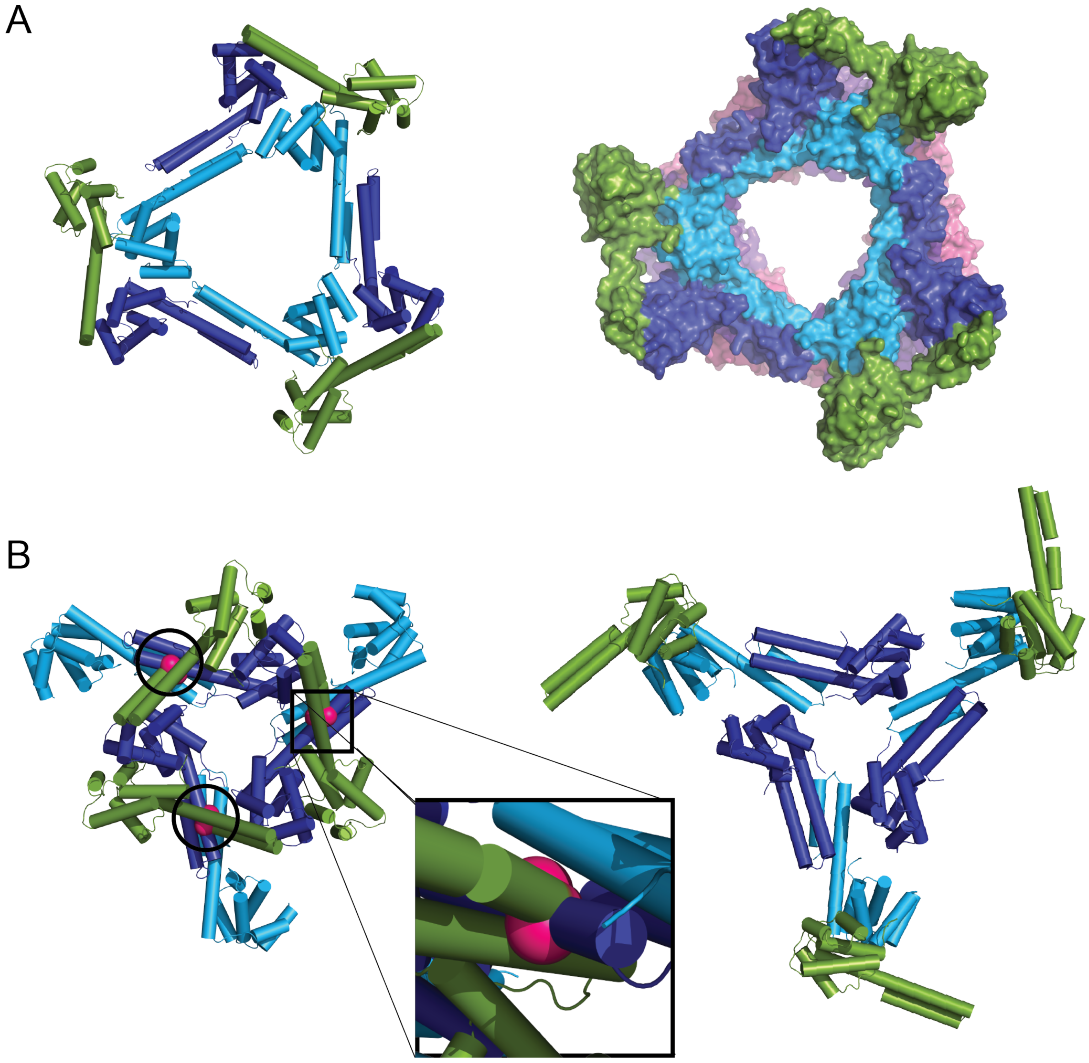


**Figure 5.7. DnaB-DnaG interactions via the N-terminal collar.** A) DnaG binds to two adjacent globular head subdomains when DnaB is in the dilated ring state (PDB ID: 2R6A). B) The DnaG helicase-binding domain can access only one of its two DnaB N-terminal domain binding sites when the collar is constricted, resulting in a loss of nearly half of the binding surface area (change from 1198Å2 /monomer to 617Å2) Clashes indicated by pink spheres and circled. Inset: close-up view of clashes.

**Figure 5.8**

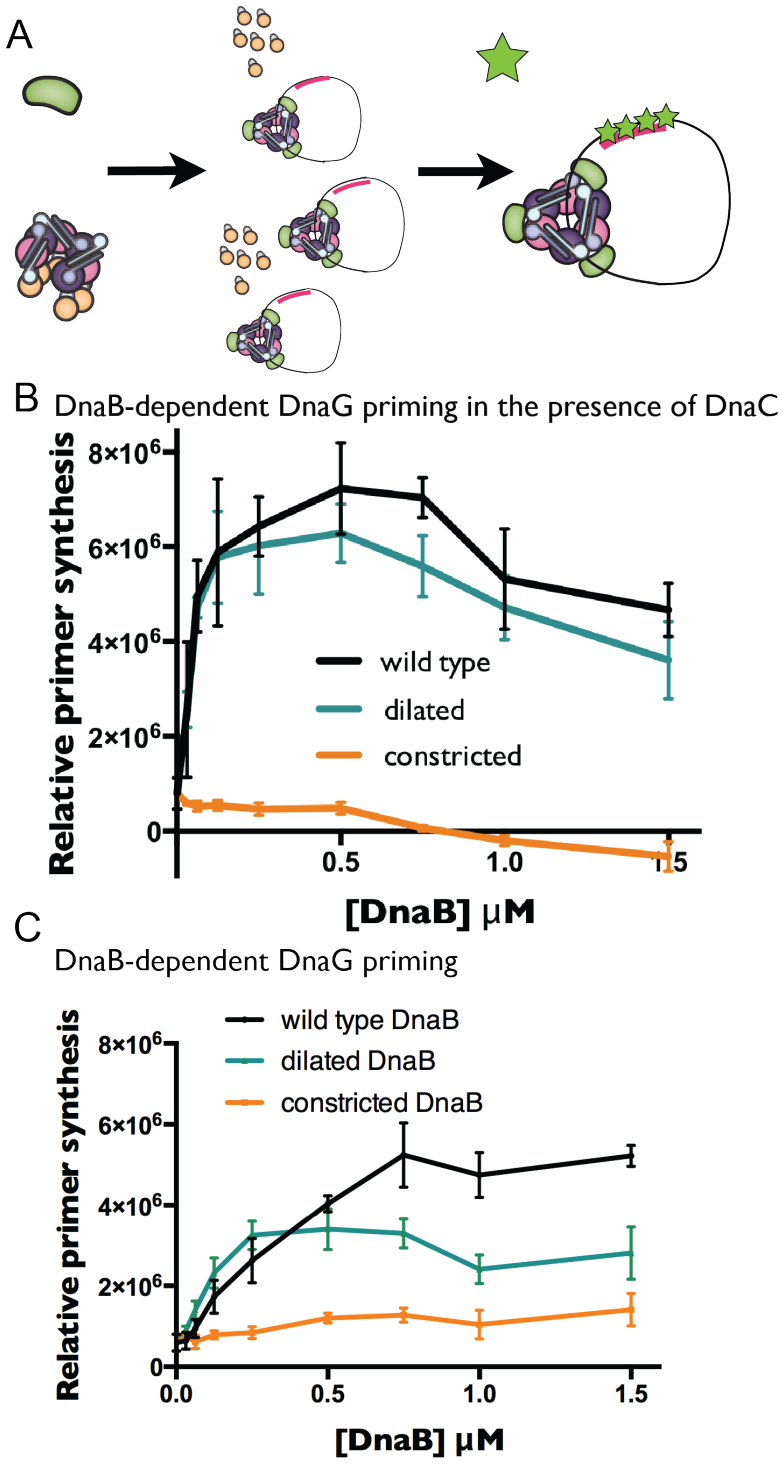


**Figure 5.8. DnaB-DnaG interactions are influenced by collar state.** A) Cartoon representation of the priming assay. B) C)Primer synthesis by DnaG in the presence of wild type and collar mutants of *Ec*DnaB in the presence (B) or absence of DnaC loader (C). Only helicases that can adopt a dilated collar stimulate primer synthesis.

## Figure 5.9

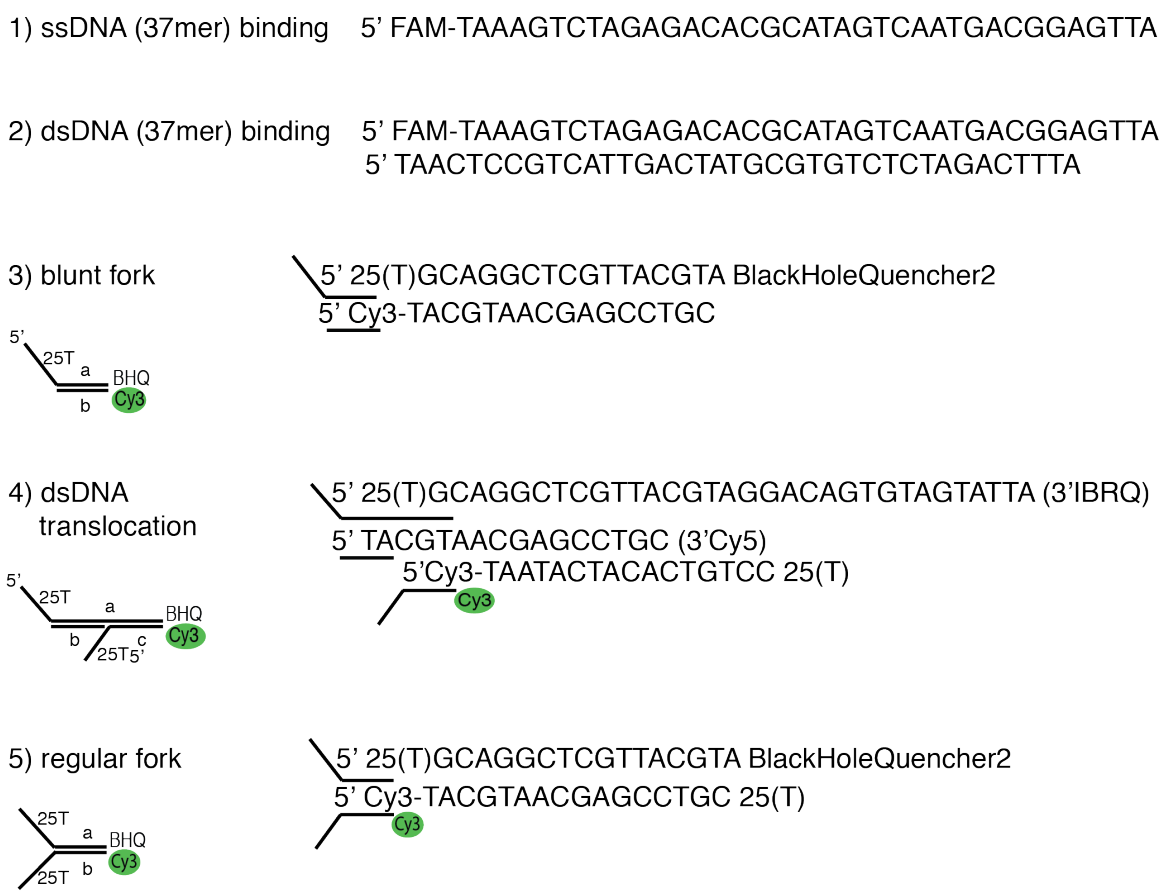


**Figure 5.9. Substrates for biochemistry assays**. DNA substrates for DNA binding experiments (1,2), fork unwinding assays (5) and translocation along dsDNA (3,4).

# Chapter 6 – Bacterial replicative helicase: Conclusions and Future Directions

## THE N-TERMINAL COLLAR IS A CONTROL LOCUS FOR REGULATING DNAB STRUCTURE AND FUNCTION

All bacteria rely on a DnaB family helicase for DNA replication (Ilyina et al., 1992; Leipe et al., 2000). Although the translocation and unwinding activity of the DnaB C-terminal domains is well appreciated (Bird et al., 2000; Biswas and Biswas, 1999; Nakayama et al., 1984), the function of the DnaB N-terminal collar has remained enigmatic. To date, the collar has been shown both to stabilize DnaB hexamers (Biswas et al., 1994) and to sterically impede aberrant loading onto DNA (Arias-Palomo et al., 2013). Some lines of evidence have also indicated that the collar, like the motor domains, can bind single-stranded DNA (Bailey et al., 2007; Lo et al., 2009). Whether the N-terminal domains might play a more fundamental part of DnaB function other than as a basic scaffolding element has been, however, unresolved.

The structural and mutagenesis data presented in Chapters 2-5 establish a new and unexpected role for the N-terminal collar as a nucleotide-actuated locus for controlling DnaB conformation. Our data further show that these states can regulate both intrinsic helicase functions, such as double-stranded DNA translocation, and the interplay between DnaB and its associated replication factors. Consideration of these data in light of the known activities of DnaB reveals a rich pattern by which structural interconversions in the helicase could be used to help direct a myriad of replication-dependent processes (**Figure 6.1**). For example, a dilated form of the collar not only supports DnaG-dependent priming, but also appears to help repress helicase activity in the absence of any binding partners (possibly as a means to prevent inopportune replication onset). By contrast when constricted, the collar appears to favor interactions with DnaC (Arias-Palomo et al., 2013) (likely to promote loading onto replication origins during initiation), and is furthermore uniquely responsive to τ (a property that may aid with clamp loader recruitment during fork progression). Consistent with these notions, the association of DnaG with DnaB has been shown to help displace DnaC from the helicase during initiation (Makowska-Grzyska and Kaguni, 2010). We posit that this activity likely derives from an ability of primase to stabilize a dilated collar conformation that allosterically antagonizes DnaC binding to DnaB, and that DnaG and τ might similarly alter the relative binding of each other by promoting the formation of different helicase states.

A distinct preference of DnaG, DnaC and τ for a specific state of DnaB could ensure correct order of events during replication initiation and fork progression. Our data suggests that DnaB exists in a dynamic equilibrium

between the constricted and dilated conformations. Upon binding, DnaC either drives the conversion of DnaB to a constricted state or simply stabilizes this arrangement, which appears required for efficient ring cracking and loading onto single-stranded DNA. Once the helicase is deposited onto the melted origin of replication, interaction with DNA and/or ATP hydrolysis within DnaC filament results in ejection of the loader allowing the N-terminal collar of DnaB to revert to the dilated and now slightly cracked conformation observed in the fully-liganded *Bst*DnaB crystal structure (Itsathitphaisarn et al., 2012) that has been proposed to depict a translocation competent intermediate. Following this event DnaG can bind the collar, with the contacts formed between the helicase interaction domain of primase stabilizing DnaB in the dilated state (**Figure 5.7**) serve to help maintain this configuration of the helicase throughout the formation of Okazaki fragments. Once primer synthesis is complete, DnaG is thought to dissociate from DnaB through an interaction with the single-stranded DNA binding protein (Yuzhakov et al., 1999). This event would liberate the DnaB collar from DnaG, possibly also through τ-assisted constriction of the N-terminal collar. DnaG would be predicted to act in a similar manner during helicase loading, remodeling the collar of DnaB into a dilated form, and antagonizing the action of DnaC (which we find binds to and opens DnaB when the collar is constricted) to favor dissociation of the loader from the helicase. A preference of DnaG for a specific state of DnaB may help to further explain some puzzling observations published previously. For example, it has been shown that primer synthesis leads to a transient pausing of T7 bacteriophage replisome and it slows down *E. coli* replisome progression *in vitro* (Tanner et al., 2008). It is possible that during replisome progression (while bound to τ and coupled to the replicative polymerase), DnaB translocates along single-stranded DNA in a constricted state, and that primase can only weakly bind to this state. At some point, the helicase transitions to a dilated state and pauses (or slows down), either as a result of primase activity or as a prerequisite to promoting primer formation. The additional contacts formed between the helicase interaction domain of primase and DnaB in the dilated state would serve to both stabilize their interaction with one another and maintain a dilated configuration of the helicase.

A need for DnaC not just in DnaB loading, but also in activation, may explain why the collar appears to take on a different structural organization in DnaB orthologs that derive from bacterial species (such as *Helicobacter pylori*) that lack a DnaC homolog (Stelter et al., 2012); in these instances the helicase may not possess a cognate loading factor to overcome the repressive effects of the collar. A close analysis of the arrangement of RecA and N-terminal domains of DnaB reveals an additional advantage of DnaB N-terminal collar constriction. When the particle is in a constricted conformation cracking the ring results in a continuous straight path for single-stranded DNA entry (**Figure 6.2**). On the other hand in the dilated helicase the globular head of each N-terminal domain is positioned above the neighboring C-terminal domain producing a zigzagging channel when the ring is cracked thus possibly impeding helicase loading (**Figure 6.2**).

A second unanticipated outcome of this work is the finding that while both DnaB collar states can support helicase activity, and hence translocation along single-stranded DNA, only helicases that can access a dilated state can move along double-stranded DNA. This observation indicates that the dilated conformation recently seen for *Bst*DnaB when bound to single-stranded DNA and nucleotide (Itsathitphaisarn et al., 2012) may also be accessed by the helicase when binding duplex substrates. Interestingly, dilated and constricted DnaB mutants also appear to differ in their relative rates of unwinding. Although this difference (which is most apparent in reactions that rely on DnaC to promote unwinding) may derive from a preference of the helicase loader for one state of DnaB over another, it is possible that constricted and dilated forms could also translocate along DNA at different rates.

## FUTURE DIRECTIONS

### Activity of the two conformations in the context of the fully assembled replisome

To elucidate whether the conformational rearrangements of DnaB helicase play a significant role during DNA replication in bacteria, the two mutants should be studied in the context of the fully assembled replisome. The interactions of these different conformations with other replication factors could be studied *in vitro* using a reconstituted replication fork of *E. coli* in a rolling circle-type DNA replication system (Wu et al., 1992a; Wu et al., 1992b; Wu et al., 1992c; Zechner et al., 1992a, b). In this setup, the synthesis of DNA strands is carried out by the DNA polymerase III holoenzyme while the action of primosome in the presence of SSBs results in Okazaki fragment synthesis on the lagging-strand. The reconstituted replication forks move at rates comparable to those measured *in vivo* and can produce comparable amounts of leading and lagging-strand DNA. Using this system, we could study the effects of the DnaB N-terminal collar rearrangements on the cycle of Okazaki fragment synthesis at the replication fork. To gain an even deeper understanding of the kinetics of the replisome in the presence of either of the two DnaB helicase mutants a more complex single-molecule assay could be used. Synthesis of primers, pauses caused by protein-protein interactions at the replication fork, and looping of a lagging strand can be monitored on hydrodynamically stretched DNA molecules (Geertsema and van Oijen, 2013; Tanner et al., 2008) or by following fluorescently labeled replication factors and freshly synthesized DNA in *in vitro* assays or in live cells (Lia et al., 2012; Loparo et al., 2011).

### Activity of the two conformations *in vivo*

The biological relevance of the two conformations of the N-terminal collar could be further investigated by *in vivo* complementation assays utilizing a number of previously characterized temperature sensitive DnaB-strains (obtained strains are listed in **Table 6.1**). Efforts have already been directed at cloning the constricted mutant for expression without the N-terminal tag and

using induction with either IPTG or Arabinose for tighter control. Unfortunately, a number of cloning and mutagenesis strategies have so far failed, suggesting that this mutation may be too toxic for DNA plasmid preparation in an XLBlue strain. Furthermore, a different dilated mutant would have to be characterized, since disulfide cross-linking is not likely to occur under *in vivo* conditions. One of the dilated mutants described in Chapter 4 could prove useful, provided it was fully characterized with SAXS or EM. Preliminary experiments have been carried out in strains PC6 and E107 to verify that wild type DnaB could rescue temperature sensitive mutations taking advantage of the leaky expression from T7 promoter - based vectors when IPTG is omitted during cell growth.

**Table 6.1.**

| CGSC Strain# | Strain designation | Chromosomal DnaB marker | Specific mutation | Affected functions |
|---|---|---|---|---|
| 5945 | PC6 | dnaB 6 | | |
| 5947 | PC8 | dnaB 8 | A130V | Negligible primer synthesis, ATPase or unwinding activity |
| 4013 | FA22 | dnaB 22 | | |
| 3596 | χ909 | dnaB 43 | A130V | Negligible primer synthesis, ATPase or unwinding activity |
| 4017 | HfrH 165/70 | dnaB 70 | M242I | Dead helicase |
| 5647 | E107 | dnaB 107 | | |
| 6349 | RS162 | dnaB 252 | G299D | Priming, unwinding and ATP hydrolysis not affected; possibly affects interaction with DnaC |
| 3644 | CR34/313 | dnaB 313 | | |
| 3639 | CR34/454 | dnaB 454 | A130V | Negligible primer synthesis, ATPase or helicase activity |
| 4002 | AB4002 | dnaB 500 | | |

## DnaB-DnaC interaction

Based on the 3D EM reconstruction of the *E. coli* DnaBC complex we know that when DnaB helicase is bound to its loader, the N-terminal domains adopt a constricted conformation (Arias-Palomo et al., 2013). However it remains unclear whether the loader specifically drives the conformational rearrangement or just preferentially binds to the constricted conformation. Both a recently published structure of the primosome with *Bst*DnaB in complex with DnaC from *B. subtilis* (Liu et al., 2013) and a yet unpublished structure of DnaBC complex from *A. aeolicus* (personal communication within the Berger Laboratory) show DnaC in

complex with a dilated conformation of DnaB. Whether the differences in those EM reconstructions reflect different intermediates along a single path or a specific difference between mesophilic *E. coli* proteins and their thermophilic homologues remains to be established. Additionally constricted *E. coli* DnaB mutant could serve as a good crystal target to obtain a co-crystal structure of the *E. coli* DnaB- DnaC complex and further our understanding of the specific interactions between the helicase and its loader.

## Interactions with other replication factors

The DnaB helicase plays a major role during initiation of bacterial replication, where interactions with DnaC loader, as well as with the replication initiation protein DnaA, result in loading of two helicases at the origin of replication, each facing the opposite way to form a bi-directional fork (Abe et al., 2007; Marszalek and Kaguni, 1994; Seitz et al., 2000; Sutton et al., 1998). During replication fork progression, DnaB is further stimulated by its interactions with the primase DnaG and the τ subunit of Polymerase III, while the single-stranded binding protein (SSB) is thought to be involved in the release of primase from DnaB ring. Thus far, we investigated effects of the helicase's N-terminal collar rearrangements on the interactions with the loader, primase and τ, but we have yet to look at the effects of binding to DnaA and SSB. Furthermore, DnaB is involved in the restart of stalled forks, as well as with the termination of replication, and thus the N-terminal collar arrangements could have significant impact on the interactions with PriC helicase and Tus/Ter complex. In addition to investigating effects of N-terminal collar states on stimulation of helicase function by various replication factors, interactions of DnaB mutants with all the binding partners could be studied through pull-down experiments and Biacore studies to test for changes in binding affinities and dissociation rates.

## Mechanochemical properties of the two conformations of DnaB

Apart from differences in DNA binding, ATP hydrolysis and translocation along double-stranded DNA, the two conformations of DnaB could differ in key biophysical properties such as processivity, velocity and pausing behavior, and step-size during translocation along single-stranded DNA and during duplex unwinding. Interestingly, when bound to single-stranded DNA, *Bst*DnaB adopts an extended spiral structure that binds two nucleotides per subunit (Itsathitphaisarn et al., 2012). By contrast, other helicases such as the Rho transcription termination factor and the papilloma virus E1 protein form more compact rings in which each protomer engages only a single nucleotide (Enemark and Joshua-Tor, 2006; Thomsen and Berger, 2009), a configuration approximated by the ADP-bound *Aa*DnaB structure presented in Chapter 2. It is tempting to speculate that the rate differences between different collar states could also reflect a true difference in translocation rate that results from a change in helicase step size. Additional studies specifically in a single molecule set up with the use of optical tweezers could be used to fully characterize

machanochemical properties of the dilated and constricted mutants and compare them to the wild type helicase. Alternatively, fluorescent stop-flow or microfluidic experiments could be utilized to measure rates of translocation of the two DnaB conformations in bulk.

### Cross-linked DnaB hexamer and hand-over-hand translocation mechanism

A recently published structure of *Bst*DnaB bound to single-stranded DNA and nucleotide was the basis for a hand-over-hand DnaB translocation mechanism, where DnaB hexamer adopts a helical subunit arrangement around the DNA strand and sequential nucleotide hydrolysis is coupled to translocation of the hexamer subunits along the DNA. This model predicts that the top subunit of DnaB would slide towards 3' end of the lagging strand in a single step to occupy the bottom position in the ATPase domain staircase resulting in a ~30Å drop. This model differs from the mechanisms proposed for the two related helicases, E1 and Rho, where the substrate translocation is thought to be perpetrated by the movement of nucleic acid binding loops that protrude into the central channel of the helicase, while the ATPase domains (compared to DnaB ATPase domains) remain relatively planar and are not thought to translocate along large distances as nucleotide hydrolysis progresses around the ring. This model could be tested using the cross-linked conformation of the DnaB helicase, since locking the N-terminal domains in place through disulfide bonds or with slightly longer maleimide cross-linkers would prevent large vertical motions of the subunits within the helicase ring. However, to fully test previously proposed translocation mechanism, we would have to adjust the cross-linking conditions to obtain a population where ideally all of the three globular head dimers are cross-linked within each hexamer (under current conditions, only 30% or one dimer in each hexamer are cross-linked). This could be achieved either by screening for a pair of opposing residues that would more readily form a disulfide bond when mutated to cysteines or by using a longer meleimide linker that could span the ~5Å distance between positions 86 and 121 more efficiently and link the majority of the dimers.

## FINAL REMARKS

The work described here reveals the existence of a new structural configuration and ATP-responsive autoregulatory locus in bacterial DnaB-family helicases. Coupled with biochemical analyses, these findings not only provide unanticipated insights into the molecular action of DnaB, but also demonstrate that the structural and functional responses of DnaB to its substrates and partner proteins are more varied and nuanced than previously established. In particular, the enzyme can interconvert between a number of distinct global conformations, each of which exhibits distinct biochemical properties that could be exploited differentially to support and regulate alternate replication events such as initiation and elongation. This complexity highlights an unexpected but convergently evolved parallel between the replicative helicases of bacteria and

eukaryotes, in which the MCM2-7 complex is subject to analogous –albeit mechanistically distinct – levels of structural and functional control (**Figure 6.3**) (Brewster and Chen, 2010; Costa et al., 2013; Remus and Diffley, 2009). Both, DnaB and MCM helicases, appear to exist in equilibrium of states that can be partially controlled by addition of nucleotide (Lyubimov et al., 2012). Furthermore, both helicases have distinct conformations that bind single versus double stranded DNA and they both require interactions with other replication factors for not only loading but also activation. Future experiments with the presented N-terminal collar mutants could potentially reveal an even greater complexity of the bacterial replicative machinery. Additionally, the periplasmic expression system, developed to purify the constricted mutant of *E. coli* DnaB, provides us with a powerful tool to study other toxic mutations that up till now remained inaccessible.

**Figure 6.1**

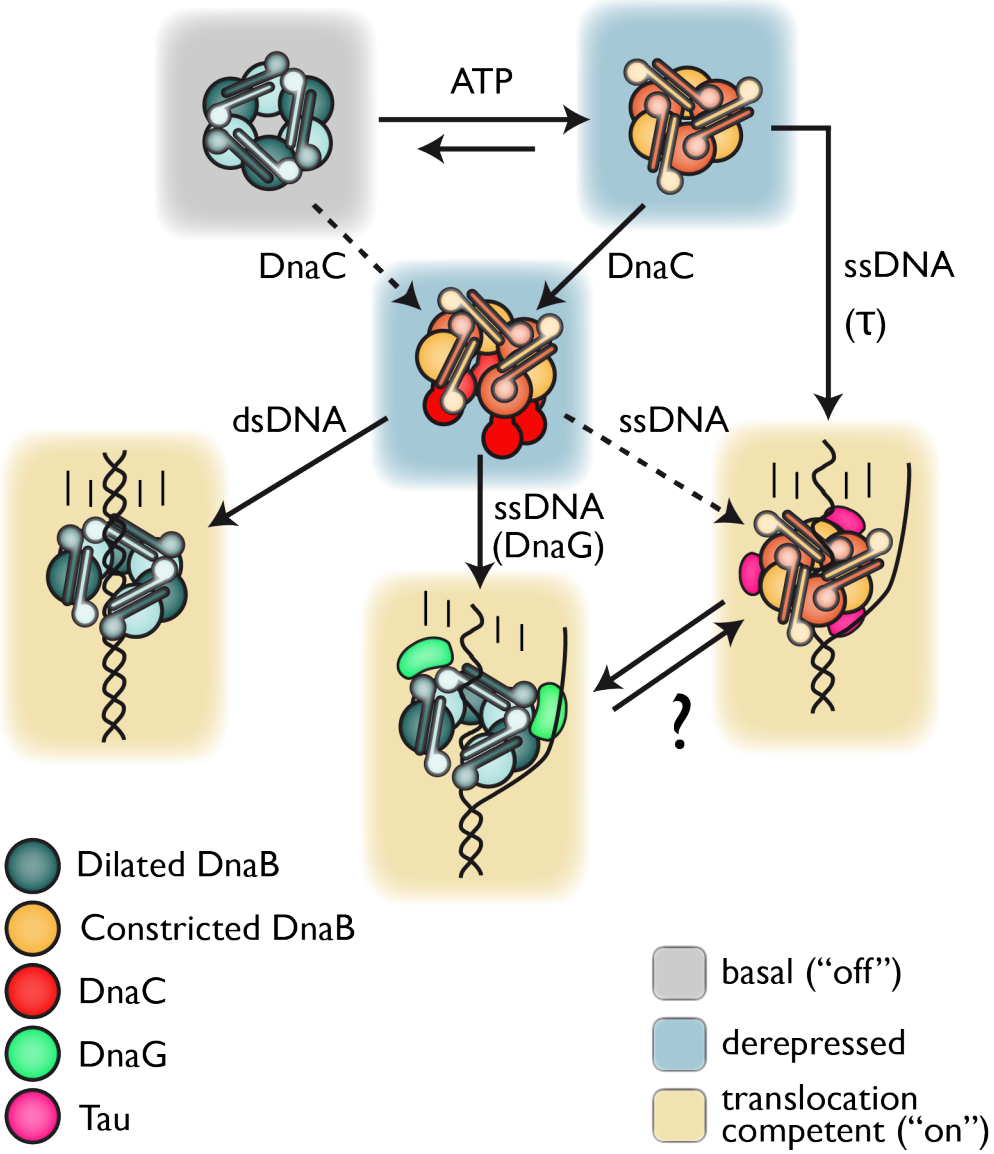


**Figure 6.1. Potential roles for conformational switching in the N-terminal collar as a means to regulate DnaB function.** Schematic illustrating how DnaB could use different collar states to switch from basal, low-activity states into translocation-competent forms, and how both substrates and partner proteins preferentially interact with and/or help control collar transitions and ring opening. Dashed lines represent less favored transitions based on data presented in Chapters 2-5 and from the literature.

**Figure 6.2**

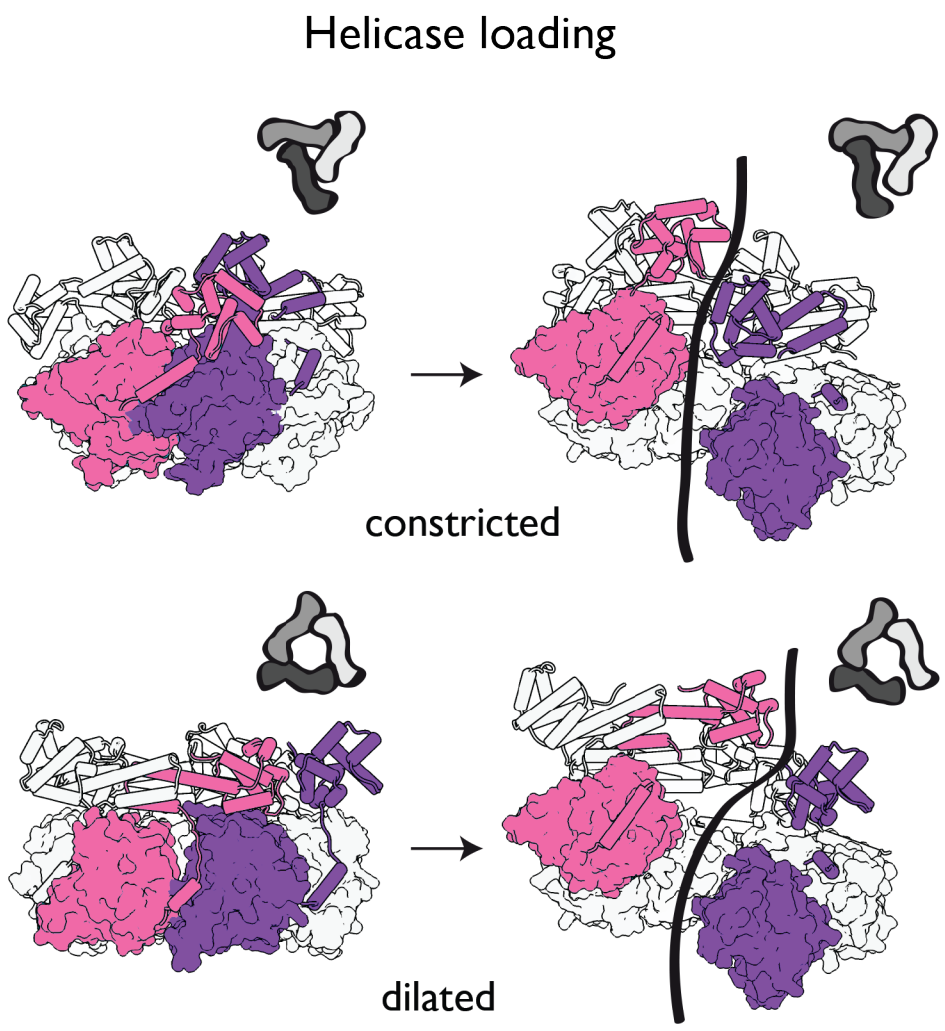


**Figure 6.2. Cracking DnaB helicase ring in a constricted and dilated conformation.** When the constricted DnaB ring is cracked, a continuous straight path across the ring is available to ssDNA. Cracking of a dilated ring results in a zigzagging path due to the organization of the N-terminal domains that in the dilated conformation lie on top of their neighboring C-terminal domains instead of in line with their own ATPase centers.

**Figure 6.3**

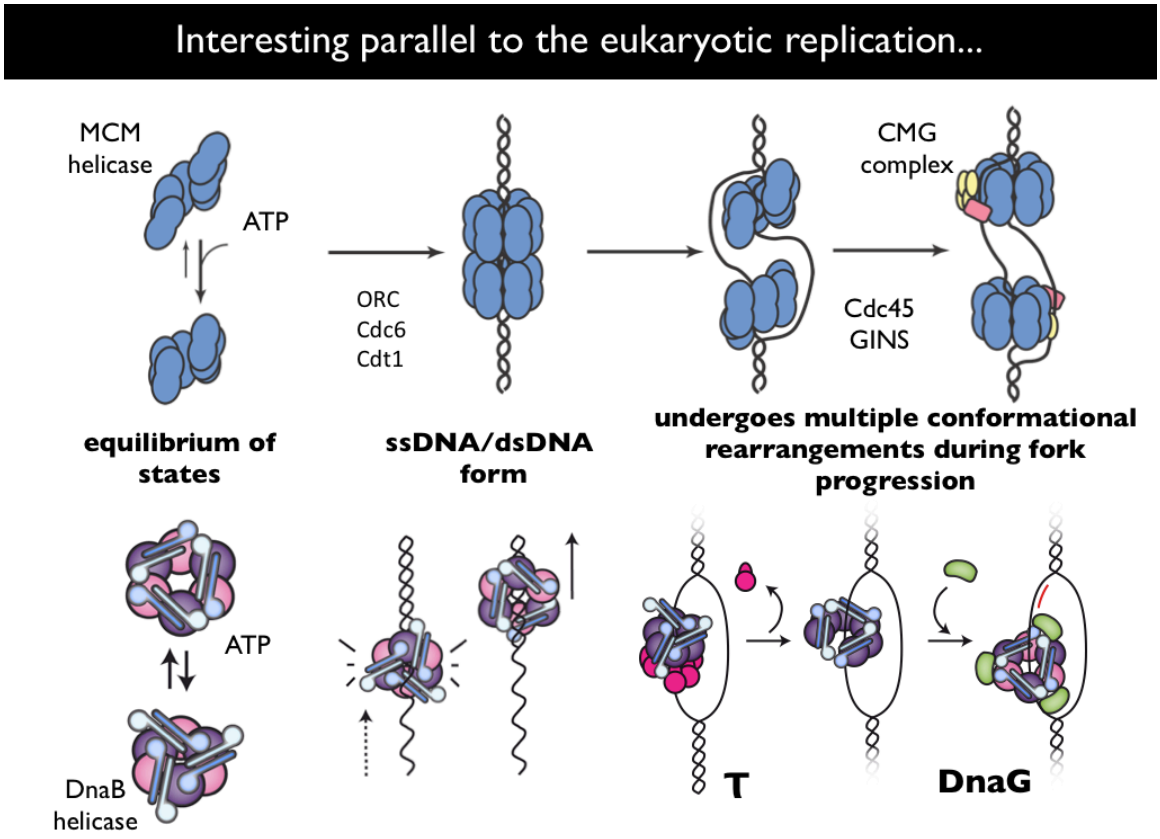


**Figure 6.3. Structural and mechanistic parallels between bacterial and eukaryotic DNA replication.** The complexity of conformational switching involved in regulation of DnaB helicase highlights an unexpected, and convergently evolved, parallel between the replicative helicases of bacteria and eukaryotes, where the MCM2-7 helicase similarly accesses multiple conformational and functional states in a manner controlled by different types of regulatory factors

# Chapter 7 – Structural and Biochemical studies of McrB motor

## INTRODUCTION

### McrBC function and structure

McrBC is a multisubunit GTP-dependent restriction endonuclease from *Escherichia coli* K-12 (Sutherland et al., 1992). The complex is encoded by two genes: *mcrB*, from which two proteins – $McrB_L$ (full length version) and $McrB_S$ (N-terminal truncation) – are expressed; and *mcrC*, which codes for McrC endonuclease subunit. Although the restriction behavior of McrBC resembles that of Type I and Type III restriction enzymes, it cannot be classified in either of these groups structurally or phylogenetically. Instead, the $McrB_{L/S}$ subunit shares sequence similarity with members of the AAA+ (ATPases associated with various cellular activities) family of proteins (Neuwald et al., 1999). As shown in **Figure 7.1**, AAA+ enzymes comprise a subgroup of the ASCE superfamily of NTPases, specifically the Helix 2 - insert clade (Erzberger and Berger, 2006). Like many ASCE motors, McrB (both short and long versions) has been shown to assemble into a ring-shaped structure, and contains a central channel about 3 nm in diameter (Panne et al., 2001).

$McrB_L$ is a 54kDa protein with a GTP-binding motif in its C-terminal region and an N-terminal DNA binding domain that recognizes methylated cytosines preceded by a purine ($R^mC$) (Gast et al., 1997; Kruger et al., 1995; Pieper et al., 1999b). $McrB_S$ lacks 162 N-terminal residues and cannot bind specifically to DNA, however, it is still a functional GTPase (Pieper et al., 1999b) (**Figure 7.1**). Although the two products of *mcrB* gene are expressed at equimolar ratios in the cells (Dila et al., 1990; Ross et al., 1989), the $McrB_L$ subunit is necessary and sufficient for DNA cleavage *in vitro* in the presence of McrC, GTP and $Mg^{2+}$ (Sutherland et al., 1992). $McrB_S$ is thought to regulate the interactions of $McrB_L$ with the McrC endonuclease (Panne et al., 1998) and may serve to sequester excess endonuclease. McrC is a 39kDa nuclease of an unknown fold that cleaves DNA, but only when it is found in complex with McrB. McrC does not bind to DNA on its own and its activity is not supported by McrB mutants deficient in GTP hydrolysis (Gast et al., 1997; Pieper et al., 1997; Pieper and Pingoud, 2002).

### Proposed mechanism of McrBC cleavage and McrB DNA translocation

McrBC recognizes and cleaves methylated DNA in a reaction that requires GTP hydrolysis (GTPγS does not support cleavage)(Sutherland et al., 1992). Cleavage requires the presence of at least two $R^mC$ recognition sites that need to be separated by as few as 30bp and can be as far apart as 3kb (Stewart and Raleigh, 1998). DNA cleavage occurs in multiple locations, but is always close to

one of the recognition sites (Panne et al., 1999; Stewart and Raleigh, 1998) and shows a characteristic 10 bp repeat cleavage pattern (Pieper et al., 2002). Based on these results, a mechanism of McrBC cleavage has been proposed by Panne et al. (**Figure 7.2**), whereby in the presence of GTP, $McrB_L$ assembles into a translocation-active oligomeric ring (most likely a heptamer) that can autonomously load onto DNA. The DNA binding domain of $McrB_L$ recognizes an $R^mC$ site and tightly binds to it. Energy from GTP hydrolysis is converted into mechanical force that allows the motor to translocate, while the DNA binding domains continue to hold onto the recognition sequence; the interaction of this complex with McrC further stimulates GTP hydrolysis. DNA cleavage occurs when two translocating complexes (each bound to one of the two $R^mC$ sites) collide with one another. When two complexes run into one another, McrC subunit is somehow brought into contact with DNA and a double stranded break is catalyzed. Because a random road block (such as a Lac repressor) can also cause DNA cleavage, it is thought that specific interactions between the two translocating McrBC complexes are not required to promote cutting (Panne et al., 1999).

## COMPLEX PREPARATION

$McrB_S$ and $McrB_L$ constructs were cloned into a pET28b – TEV (LIC modified vector) with a hexa-Histidine tag and Kanamycin resistance. Each plasmid was transformed into BL21 RIL Codon+ cells and the protein was overexpressed in 2xYT media by induction at an $OD_{600}$ of 0.6 with 0.5 mM IPTG at 37°C for 3 hours. Cells were harvested by spinning at 5000rpm for 10min and resuspended in 20 mM HEPES-KOH pH 7.5, 0.5M NaCl, 10% Glycerol, 5 mM $MgCl_2$, 10 mM Imidazole, 5mM β-mercaptoethanol, 1 μM Pepstatin-A, 1 μM leupeptin and 1 mM PMSF, and lysed by sonication. Crude lysate was applied to a Ni-column, washed with resuspension buffer followed by a wash with a buffer containing 1M NaCl to remove nuclease contamination. Protein was eluted in 0.5 M NaCl with a gradient of Imidazole and digested with TEV protease for 3 hours at RT in the presence of 1mM GTP. Digested fractions were separated from the $His_6$ tag and TEV protease by a second Nickel column and incubated with GTP in order to assemble active oligomers. Final step of purification was gel filtration: an S200 column in the absence of GTP to obtain monomers or an S300 column in 1mM GTP to obtain oligomeric rings. Gel filtration buffer contained 0.5M NaCl, 10% Glycerol, 20mM Hepes pH 7.5, 5mM $MgCl_2$, 1mM DTT, 1mM GTP and 1 μM Pepstatin-A, 1 μM leupeptin and 1 mM PMSF. **Figure 7.3** shows example traces from S200 and S300 columns and analysis of purity on SDS-Page gels. Assembled oligomers were dialyzed into buffers used for the biochemical or single molecule experiments and stored as small aliquots at -80°C, while fresh protein was used for crystallography. It is also possible to assemble $McrB_L$ rings using a non-hydrolyzable GTP analog such as GTPγS. This produces stalled rings that can be activated for translocation by chasing with GTP (Stewart et al., 2000).

## McrB RING: A HEPTAMER OR A HEXAMER?

### Cross-linking gels

During purification in the presence of GTP on a sizing column, McrB appeared to form an oligomeric structure. However, based on the gel-filtration profile it was unclear whether the protein assembled into hexameric or heptameric rings, so we performed cross-linking experiments using glutaraldehyde, Sulfo-EGS or $BS_3$ as cross-linking reagents. Full length protein was dialyzed into 50mM NaCl, 10mM Hepes pH 7.5, 10% Glycerol, 10mM $MgCl_2$, 1mM TCEP and 1mM GTP. 1μM $McrB_L$ aliquots of protein were incubated with increasing amount of cross-linking reagents (from 0 to 5mM) for up to 30min; heat denatured samples were then loaded on a 4% Phosphate gel and run at 30V for 4-6 hours (see cross-linking protocol in the Appendix). Protein bands were visualized with silver staining. Experiments with all three cross linkers resulted in band patterns from 1 to 6 bands total, indicating that McrB motor forms a hexamer in solution in the presence of GTP (**Figure 7.4**). Addition of 1μM dsDNA (19mer with a single recognition $R^mC$ site) did not affect the band distribution.

### Negative stain electron microscopy

We next attempted to further characterize oligomeric state of the protein using negative stain electron microscopy. With the help of Vincent Ramey from the Nogales Laboratory, 2D class averages were obtained that clearly showed a ring-shaped structure with a central channel and often additional density on the outside of the ring that could possibly correspond to the N-terminal DNA-binding domains of $McrB_L$. Matlab software was used to generate autocorrelation plots where each ring representing a single 2D class average was compared to itself to enhance periodicity of the features; the peaks on the autocorrelation plots thus correspond to the possible number of subunits forming the rings. Based on this analysis, most of the class averages appeared to represent 7-membered rings (**Figure 7.5**). Changing the dimensions of the mask (removing electron density outside of the main ring that could compromise the analysis of the ring-forming AAA+ motor region of the McrB complex) eliminated 3, 4, 9 and 11-membered rings. However, peaks for 5, 6 and 7 were still observed with 7 giving the highest peak (~ 40% of data, but at an insufficient level to provide a definite answer).

### Small Angle X-ray Scattering (SAXS)

Structural characterization of $McrB_{L/S}$ was also attempted via SAXS. Good scattering curves were obtained at the Advanced Light Source, however, analysis proved difficult. Without a clear model it was problematic to even deduce exact molecular weight and a correct oligomeric state of the protein. Scattering curves were processed with ATSAS suite programs DAMMIN and Gasbor to attempt *ab initio* shape determination by applying various symmetries. For the full length protein DAMMIN reconstructions with both 6 and 7-fold symmetry yielded

reasonably looking shapes similar to other ring-shaped translocases (**Figure 7.6A**). However analysis of the truncated $McrB_S$ protein produced reasonable shapes only under no or 7-fold symmetry, while 6-fold symmetry did not result in a ring-like envelope (**Figure 7.6B**).

## Conclusions

In summary, although McrB protein purified in the presence of GTP formed an oligomeric structure on the S300 sizing column and was seen to assemble into a ring-shaped structure with a clear central channel by EM, the exact oligomeric state of the protein could not be confirmed. Glutaraldehyde cross-linking experiments suggested a hexameric ring, whereas both SAXS and EM hinted of the possibility of a distribution between hexa- and heptameric rings, with a slight bias in favor of heptamers. While majority of AAA+ proteins form hexameric rings, the protein that bears the closest similarity to McrB motor, the Nitrogen regulatory protein C (NtrC), can adopt heptameric ring conformation (Lee et al., 2003). Furthermore, NtrC bears not only structural resemblance to McrB, but also appears to act through a similar mechanism, in which DNA looping is used to bring enhancer and promoter regions together during transcription. Whether a heptameric conformation is important or necessary for the specific function of either NtrC or McrB has not been yet determined. A number of other ASCE motor proteins have been seen to form different oligomeric states under specific conditions; for example, the archeal MCM helicase (a AAA+ motor) and the RecA-type bateriophage T7 gp4 helicase both operate as hexameric rings, but have been shown to also assemble into heptameric oligomers (Gomez-Llorente et al., 2005; Pape et al., 2003; Singleton et al., 2000; Toth et al., 2003; Yu et al., 2002). The heptamers of T7 gp4 have been proposed to either translocate along dsDNA (Toth et al., 2003) or to serve as the loading intermediate, while hexamers are thought to thread only a single strand of DNA through the protein's central channel; however so far there is little experimental evidence directly linking the diverse oligomeric states of ASCE rings to specific functions. Additional structural and biochemical analyses will be needed to fully understand McrB's oligomeric state, its potential heterogeneity and how it correlates with the motor function or the assembly of an active McrBC restriction enzyme.

# ATTEMPTS AT CRYSTALLIZING MCRB MOTOR

## DNA constructs

The DNA constructs presented in **Figure 7.7** were designed to be 19 basepairs long, a length consistent with the DNA footprint of McrB (Pieper et al., 2002; Stewart et al., 2000). Designed substrates have "double" recognition sites (two $R^mC$ on the opposing strands) to enhance the binding affinity. The 62mer duplex is supposed to encourage crystal packing of two active complexes trapped during translocation.

## Crystallization trials

Following extensive optimization of the purification protocol to prevent protein from inadvertently precipitating out of solution, high protein yields could be consistently achieved. Unlike the previous attempts from a former student in the Berger Laboratory (Jacob Corn) that focused on trying to assemble McrB complexes just shortly before setting crystal trays, I was able to assemble complexes during purification and verify their size as well as ring-like shape through cross-linking experiments and electron microscopy. The assembled complexes were seen to remain stable for at least 3 days under 4°C and could be dialyzed into low salt buffers without protein precipitation. Crystal trays were set with full-length oligomers of McrB ($McrB_L$) as well as the $McrB_S$ truncation (amino acids 162-455). An initial crystal hit for the $McrB_S$ oligomer was obtained in Mosquito trays using a well solution condition containing 20% PEG 3350 and 200mM Potassium Acetate that was mixed 1:1 with 10 mg/mL $McrB_S$ dialyzed into 200mM NaCl, 10mM Hepes pH 7.5, 1mM TCEP and 1mM GTP. Diffraction data for these crystals were collected at Advanced Light Source and indexed with Elves in P2 spacegroup with the following unit cell dimensions: a = 93.4, b = 125.4, C = 152.5 Å, $\alpha = 90°$, $\beta = 95.6°$, $\gamma = 90°$ (**Figure 7.7**). Further optimization of the crystals yielded a number of data sets with diffraction up to 3.8 – 4.0Å, that indexed in space group $P2_1$ (dimensions: a/b/c = 96.24, 128.60, 154.60Å; $\alpha/\beta/\gamma = 90, 94.45, 90°$). Unfortunately, molecular replacement with other known AAA+ structures did not provide a solution. $McrB_S$ was expressed in the presence of seleno-methionine and similar crystal hits were obtained to those of native protein, however, they diffracted only to ~5Å. We noted that each monomer contained 8 methionines, giving 48 selenium sites per hexamer (or 56 per heptamer); calculation of the unit cell dimensions and Mathews coefficient predicted two oligomers in the asymmetric unit, further increasing the number of selenium sites to over a hundred, which unfortunately would be too many to assign at 5Å resolution. A significant amount of time was devoted to improving the resolution of the crystals, including additive screens, microbatch, hanging and sitting drop set-up with variable drop sizes and at different temperatures, screening protein concentration in 0.5mg/ml increments, changing initial dialysis buffer conditions, and adding different DNA substrates and nucleotides together with their nonhydrolyzable analogues (GTP and ATP, as well as excess of GDP and ADP). Bigger crystals were obtained when extra water was added to the wells following mixing of mother liquor with the protein solution; however those crystals diffracted only to 9-12Å. Crystals from trays set at 4mg/ml and 5mg/ml were very small and grew off the skin and in heavy precipitate; when harvested they diffracted well but exhibited significant problems with multiple lattices. Crystals grown in the presence of ATP and its analogues did not diffract at all, while crystals from trays containing GTP with an excess of GDP were showing large variability in the quality of diffraction ranging from 16Å to occasionally 4Å. Two additional new crystal forms were also identified from these attempts. A second crystal form of the $McrB_S$ complex was observed in the presence of DNA oligonucleotides and a completely new hit was found when trays were set with a hydrolysis-enhanced mutant of full length McrB (R337A) in the presence of GDP-

$BeF_3$ and dsDNA. Those hits were not pursued as I moved on to work on the DnaB helicase.

## BIOCHEMICAL CHARACTERIZATION OF MCRB

Some of the basic features used to describe a motor that translocates along DNA include its rate (which is often coupled to nucleotide turnover kinetics), directionality, processivity and step size. Knowing these properties enables us to design models that can describe both the motor's mechanism and the mechanochemical cycle employed to transform chemical energy of nucleotide hydrolysis into mechanical motion. Once we have characterized a number of various motors we can compare their properties and mechanisms and look for common principles that underline their function. Using a combination of bulk biochemistry and Atomic Force Microscopy (AFM) we began to characterize a number of biochemical features of the McrB motor.

### DNA and nucleotide binding

$McrB_L$ (the full length protein containing sequence specific DNA binding domain) and $McrB_S$ (a truncation containing only the AAA+ domain) were tested for DNA binding, NTP binding and hydrolysis, and translocation along dsDNA using a triplex displacement assay. Oligomers (in the presence of GTP) and monomers (in the absence of any nucleotide) of $McrB_L$ were measured to have roughly 200nM affinity for a dsDNA oligonucleotide with a single methylated recognition sequence (**Figure 7.8A**). $McrB_L$ protein and a hydrolysis-enhanced R337A mutant were also observed to interact with a random ssDNA, resulting in a small gel-shift of a labeled DNA oligonucleotide under different nucleotide conditions (**Figure 7.8B**). The affinity of $McrB_{L/S}$ for GTP was measured by fluorescence anisotropy to be around 3μM (**Figure 7.9A**), while binding coefficients for ATP were in the 30-40μM range (**Figure 7.9B**). The results of GTP binding experiments are in agreement with a previously published affinity of $10^6 M^{-1}$ (Pieper et al., 1997), however the same study found the affinity for ATP to be three orders of magnitude lower than for GTP, while we found it to be only 10-fold less.

### Nucleotide hydrolysis

GTP-hydrolysis rates of McrB motor were previously measured as approximately 0.5/min – 40/hour (Gast et al., 1997; Panne et al., 1999; Pieper et al., 1999a) with 30-fold stimulation in the presence of McrC. However, these experiments were not carried out on assembled complexes and were not coupled to activity assays. I performed hydrolysis measurements using coupled enzyme assay (Tamura and Gellert, 1990) and obtained hydrolysis rates as high as 40 GTP molecules/minute, with similar results when ATP was used (**Figure 7.9C**). To observe hydrolysis, the protein first had to be dialyzed out of the final sizing buffer that contained 1mM GTP into a lower nucleotide concentration.

## Translocation along dsDNA

While McrBC has been proposed to translocate along dsDNA (Panne et al., 1999), the exact mechanism of its action has not been verified experimentally. In my experiments, I used a triplex displacement assay (Firman and Szczelkun, 2000; McClelland et al., 2005) to try to observe translocation of McrB motor along dsDNA. A 3kb piece of DNA (either linear or a plasmid) was cloned with a triplex binding site that anneals with a short fluorescently-labeled oligonucleotide through the formation of Hoogsteen base-pairs to form a triplex DNA substrate under low pH conditions (pH 5.5). Translocation assays were performed between pH 7 - 8.5, so as to prevent re-annealing of the short fluorescent triplex-forming oligonucleotide. Wild type McrB was not observed to displace a triplex forming oligonucleotide in this assay. However, when a hydrolysis-enhanced R337A mutant was used, both full-length and truncated McrB were seen to displace a triplex in a buffer containing 50mM NaCl, 10mM $MgCl_2$, 10mM Tris-HCl pH 7.9, 1mM DTT and 1mM GTP (**Figure 7.10**). McrB appears to be especially sensitive to the pH of the reaction, as no translocation was observed in the identical buffer at pH 7.5 (**Figure 7.10A**). The R337A mutation has been shown in the past to mimic the enhancement of hydrolysis caused by McrC (a nuclease subunit of the McrBC restriction enzyme) (Pieper et al., 1999a). Displacement of the triplex was observed in the presence of GTP and ATP on a linear DNA, as well as on a plasmid (**Figure 7.10B-C**), These studies provide the first direct evidence of McrB translocation along a DNA duplex.

## Does McrB motor loop DNA during translocation?

Indirect pieces of evidence suggest that McrB enzyme binds specific recognition sequences and holds onto them while translocating along DNA so as to bring the two motifs together (Panne et al., 1999). This type of mechanism should lead to generation of DNA loops associated with the position of the protein complex on DNA. In collaboration with Dr. Marta Kopaczynska, a postdoctoral fellow in the Bustamante Laboratory, we used Atomic Force Microscopy to look for the formation of DNA loops. In these experiments, assembled $McrB_L$ complexes were incubated with 1mM GTP and pieces of DNA with 0, 1 or 2 recognition sites for different periods of time; translocation reactions were then stopped by depositing the protein-DNA complexes onto Mica surfaces. Imaging was performed using Nanoscope V (Veeco Instruments Inc.). The preliminary AFM experiments showed that $McrB_L$ oligomers could load onto dsDNA and were found distributed randomly along DNA pieces instead of being associated predominantly with the recognition sites (**Figure 7.11**). By comparing the contour lengths of naked DNA with McrB-bound DNA, we deduced that binding of the motor did not involve extensive wrapping of the DNA as the length of the DNA pieces did not greatly change. Furthermore, when we used DNA containing McrB recognition sequences, DNA loops were observed to form underneath McrB oligomers that appeared to originate around the enzyme's recognition sites (**Figure 7.12**). Combined with the dsDNA translocation experiments the formation of loops observed via AFM would appear to

corroborate McrBC restriction mechanism proposed by (Panne et al., 1999). Unfortunately insufficient data were collected to provide strong statistical evidence for this behavior.

## CONCLUSIONS

In summary, the AAA+ motor McrB was successfully purified with reproducibly high yields, and in the presence of GTP was seen to form an oligomeric structure on the S300 sizing column. The oligomeric state of the protein was further investigated with glutaraldehyde cross-linking experiments, electron microscopy and SAXS. While it remained unclear whether the protein formed hexa- or heptamers, we observed a ring-shaped structure with a central channel in negative-stain EM experiments. We further verified that McrB could bind and hydrolyze both GTP and ATP, as well as double-stranded DNA with a specific recognition site. Triplex displacement assays performed with a hydrolysis-stimulated mutant (R337A) provided preliminary evidence of McrB's ability to translocate along dsDNA. Furthermore, with the use of AFM, we observed loading onto dsDNA and formation of loops originating underneath the motor complexes that appeared to be specifically associated with the enzyme's known recognition sites.

Ultimately, the McrBC project was abandoned due to slow hydrolysis rates and difficulty in showing robust and reproducible translocation along dsDNA. The triplex displacement assays with the R337A carried out after work had already began work on the new DnaB helicase system and were not pursued further due to progress in that system.

**Figure 7.1**

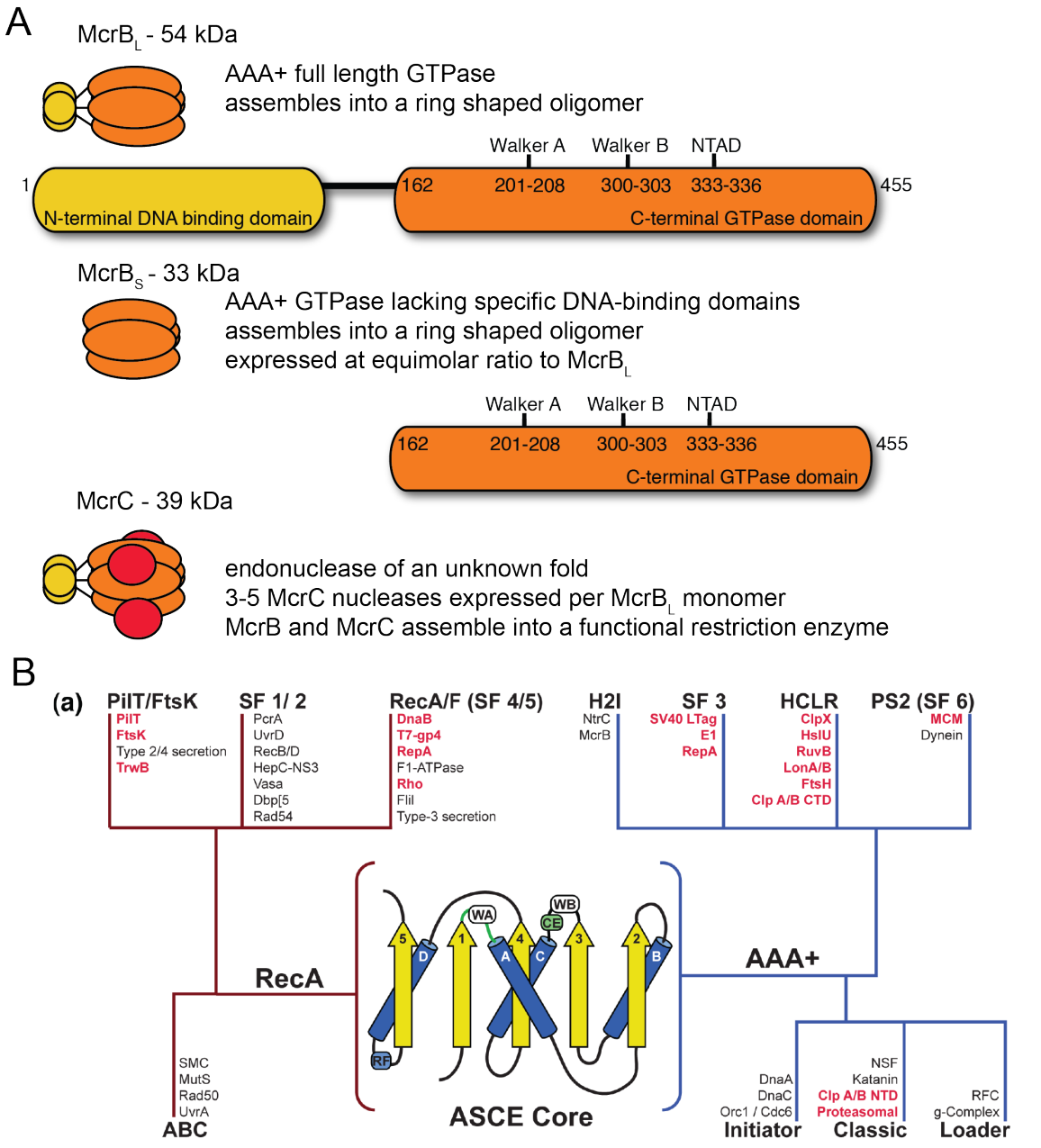


**Figure 7.1. McrB motor.** A) A cartoon representation of proteins involved in the formation of the McrBC enzyme complex. B) A phylogenetic tree showing the main clades of the RecA-type (red) and AAA+ (blue) subgroups of the ASCE superfamily. McrB motor can be found in the H2I clade of the AAA+ subgroup with its closest relative NtrC. (Reproduced from (Lyubimov et al., 2011) with authors' permission).

**Figure 7.2**

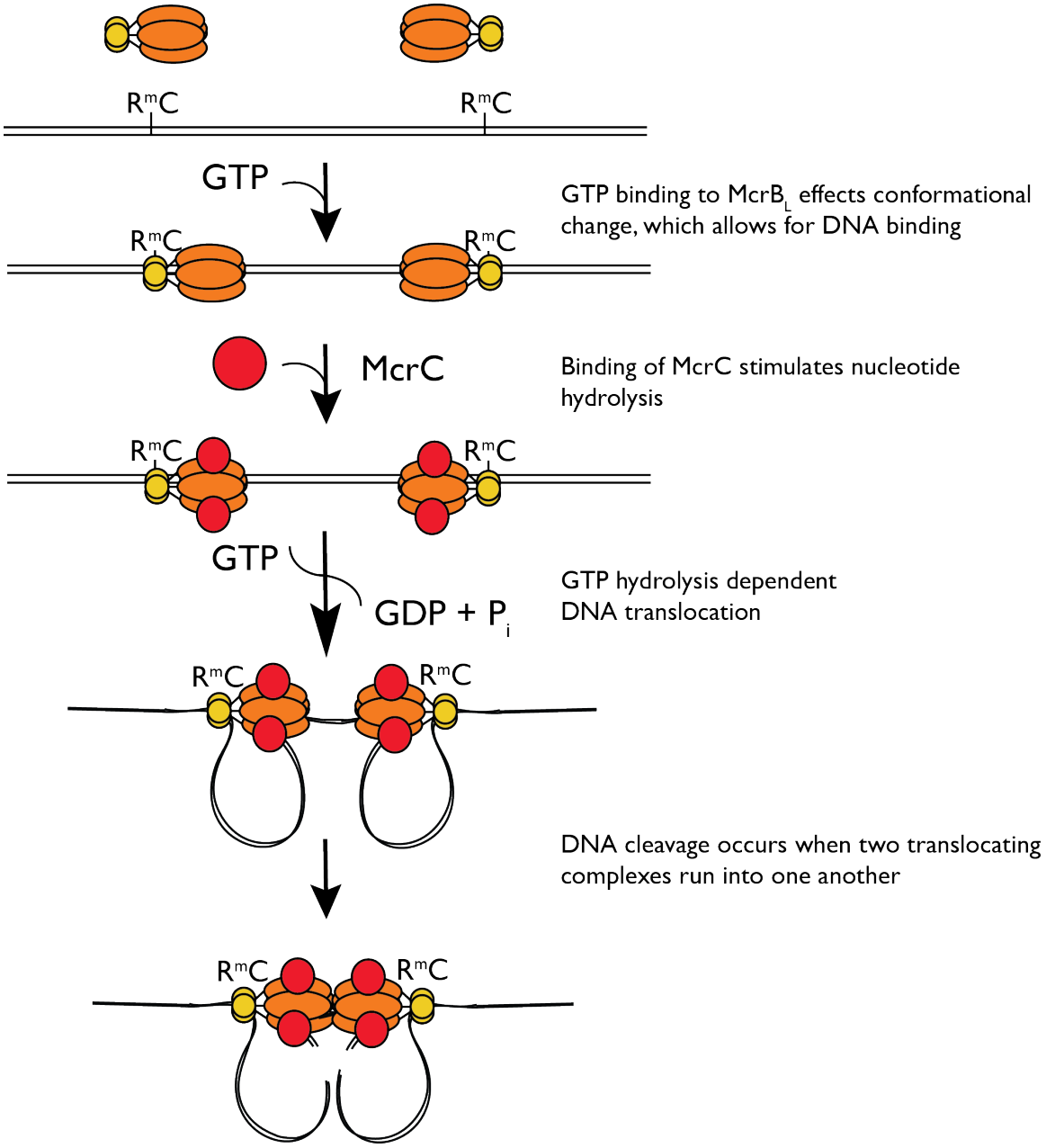


**Figure 7.2. Proposed mechanism of McrBC restriction enzyme**

**Figure 7.3**

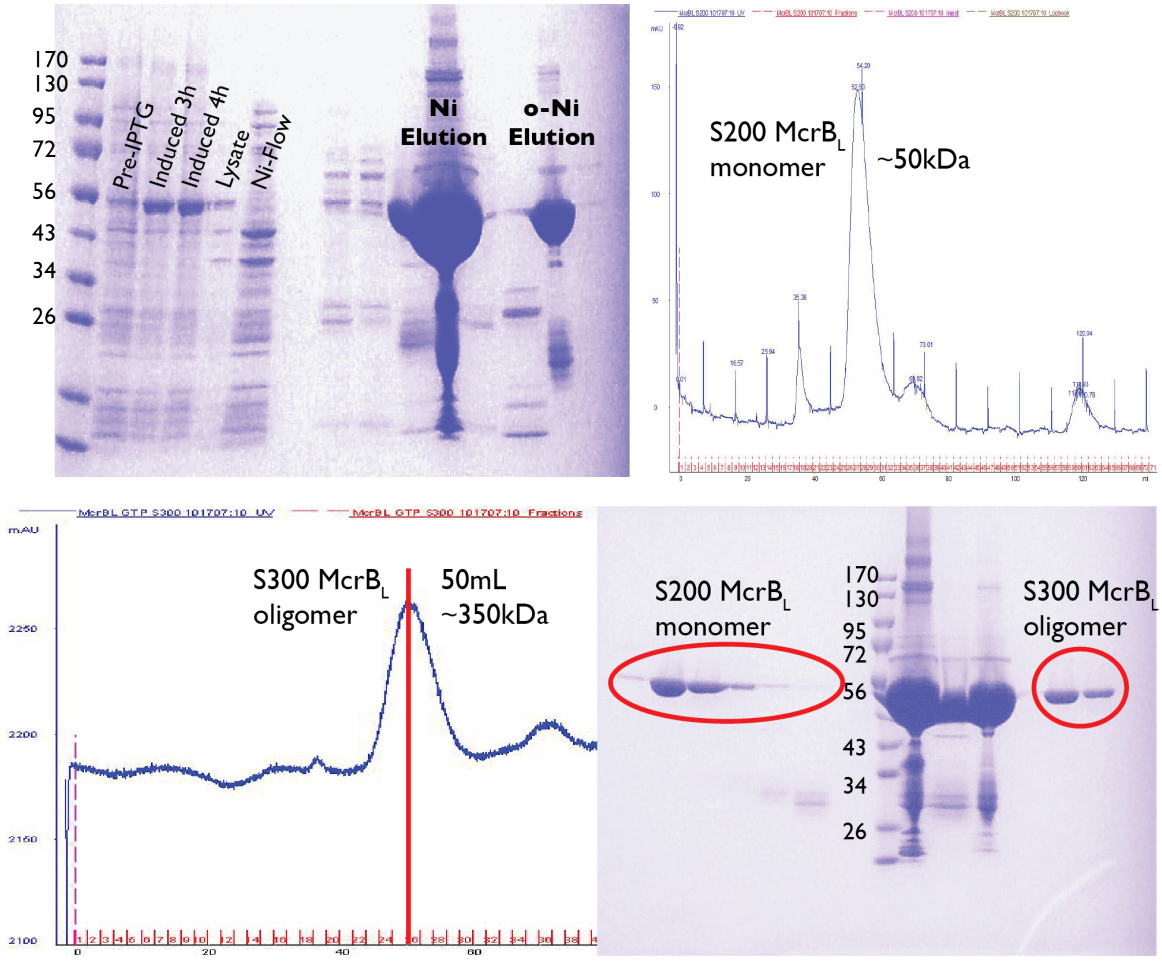


**Figure 7.3 Purification scheme for McrB.** SDS-Page protein gels showing $McrB_L$ monomer after each stage of purification. Example traces from gel-filtration experiments, where in the absence of the nucleotide $McrB_L$ migrates as a monomer on an S200 column, while in the presence of 1mM GTP it assembles into ~350kDa oligomer**.**

**Figure 7.4**

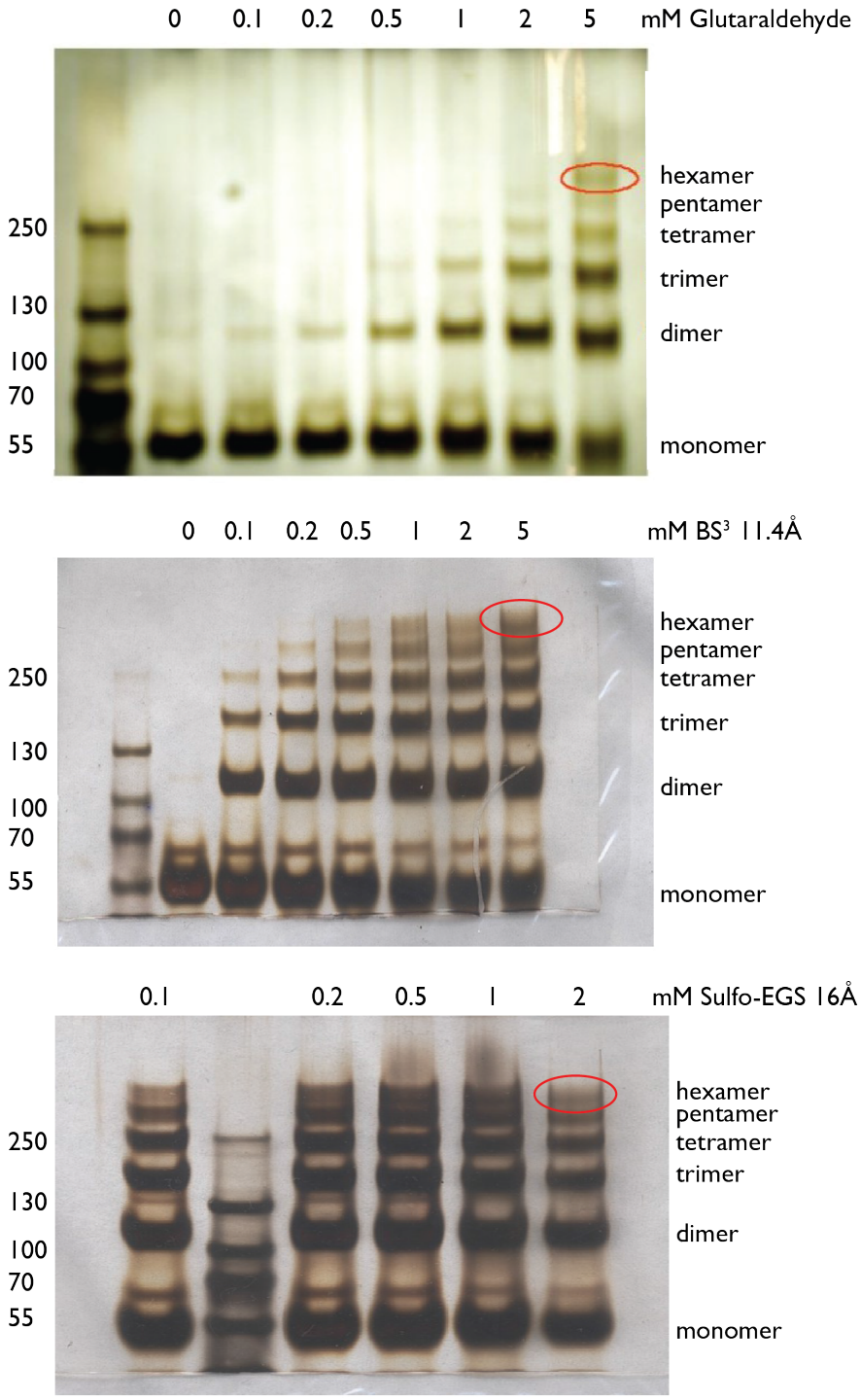


**Figure 7.4. Cross-linking McrB ring.** Example gels showing stable oligomers of $McrB_L$ in the presence of different cross-linking reagents.

**Figure 7.5**

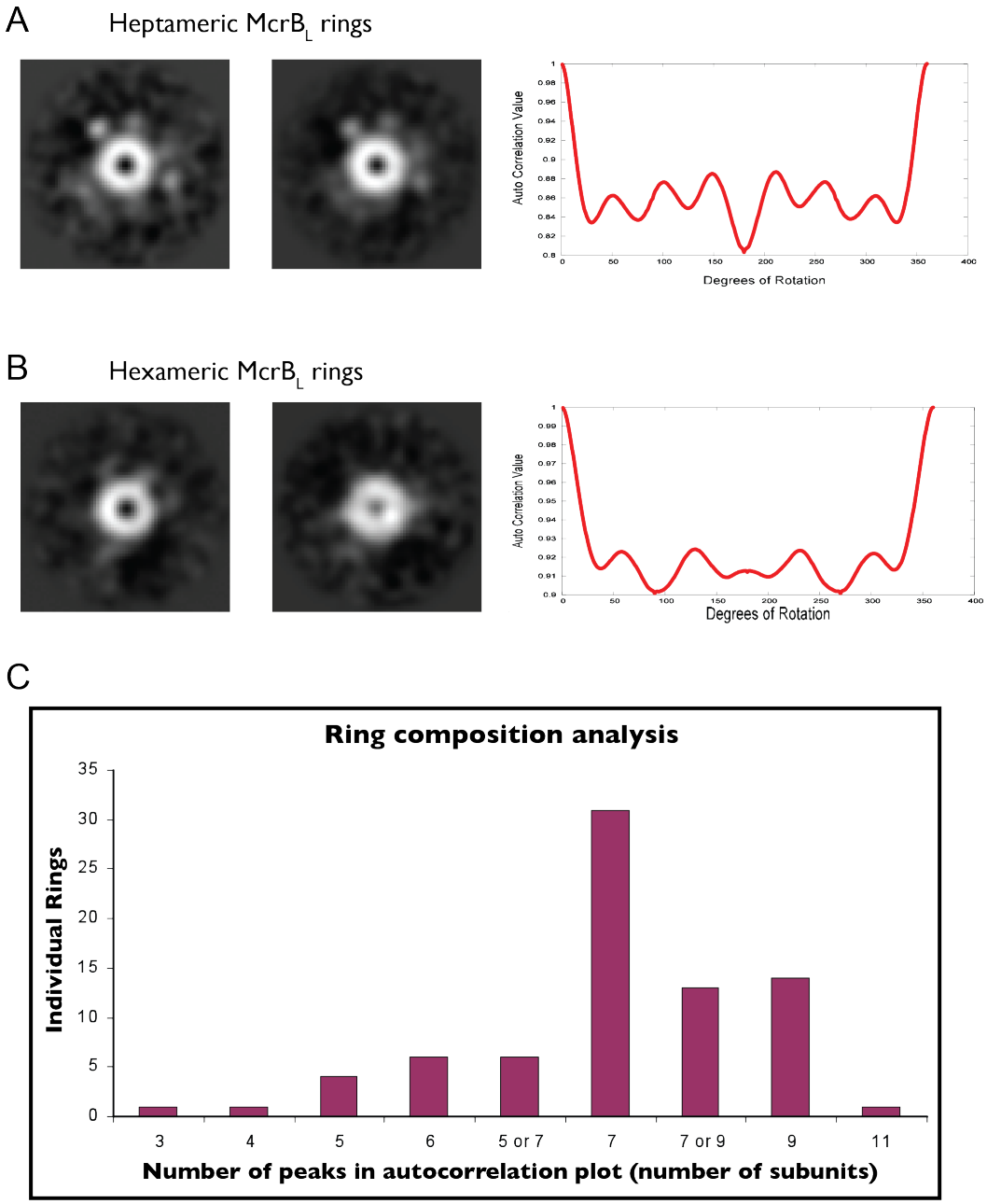


**Figure 7.5. Electron Microscopy analysis of McrB ring.** A) Two examples of 2D class averages of the McrBL ring with an accompanying auto-correlation analysis revealing 7 peaks that likely correspond to 7 protomers within the ring. B) Two examples of 2D class averages of the McrBL ring with an accompanying auto-correlation analysis revealing 6 peaks that likely correspond to 6 protomers within the ring. C) A histogram representation of all the observed 2D class averages and the distribution of the number of protomers in each ring calculated with the use of auto-correlation plots.

**Figure 7.6**

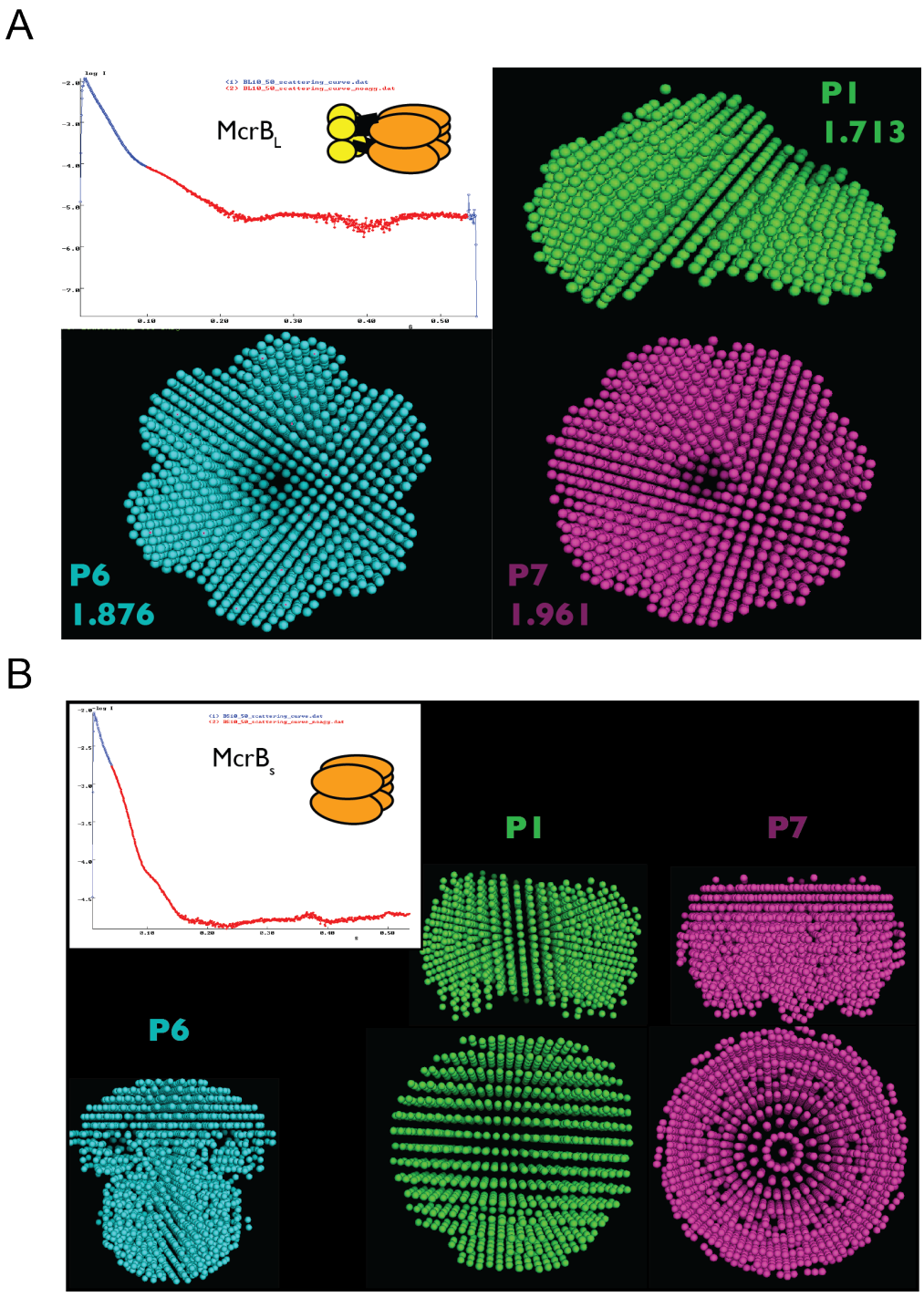


**Figure 7.6. SAXS experiments with McrB.** A) Scattering curve of McrB$_L$ oligomer and obtained DAMMIN envelopes with different imposed symmetries. Applying both 6- and 7-fold symmetry appears to generate a ring-like shape of roughly correct dimensions. B) Scattering curve of McrB$_S$ and obtained DAMMIN reconstructions. In this case applying 6-fold symmetry results in an unrealistic shape, while 7-fold symmetric reconstruction reproduces a ring like envelope.

**Figure 7.7**

A

1. GCG CAG $^{m}$CCG G CT GCG AGC G
   CGC GTC GGC $^{m}$CGA CGC TCG C — 19mer duplex, 2 $^{m}$C and no overhang matches footprinting single site

2. GCG CAG $^{m}$CCG GCT GCG AGC G
   CGC GTC GGC CGA CGC TCG C — 19mer duplex, 1 $^{m}$C and no overhang matches footprinting single site

3. GCG CAG $^{m}$CCG GCT GCG G
   CGC GTC GGC $^{m}$CGA CGC C — 16mer duplex, 2 $^{m}$C and no overhang

4. CCGCG CAG $^{m}$CCG GCT GCG AGC G
   CGC GTC GGC $^{m}$CGA CGC TCG CGG — 19mer duplex, 2 $^{m}$C, 2GG/CC overhang

5. GCG CAG $^{m}$CCG GCT GCG AGC GTC GCA GTC ACT GCA GTG ACT GC GAC G CTC GCA G$^{m}$CC G GC TGC GC
   CGC GTC GGC $^{m}$CGA CGC TCG CAG CGT CAG TGA CGT CAC TGA CG CTG C GAG CGT CGG C$^{m}$CG ACG CG
   Construct designed to self anneal into a 62mer duplex with 4 $^{m}$C, overhang marked by black line

B

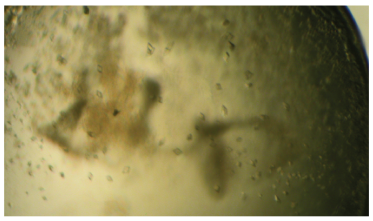

Initial hits: 20% PEG 3350, 200mM KOAc
10 mg/mL McrB$_S$

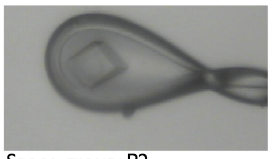

Space group: P2
Resolution: 3.8Å (best spots)
Dimensions: 93.4, 125.4, 152.5
90, 95.6, 90

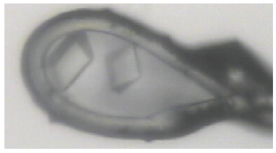

Space group: P21
Dimensions: 96.24, 128.60, 154.60
90, 94.45, 90
Resolution: 4Å
Molecular Replacement did not work.
Se-Met crystals did not diffract past 5Å

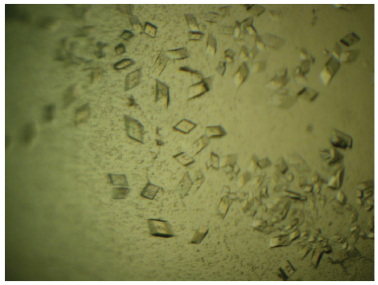

Improved hits: 22% PEG 3350, 5%MPD,
200mM KOAc, 25% MPD for cryoprotection
7.5 mg/mL McrB$_S$

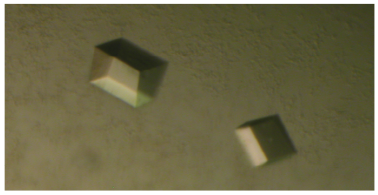

Grown in the presence of ATP
(no diffraction)

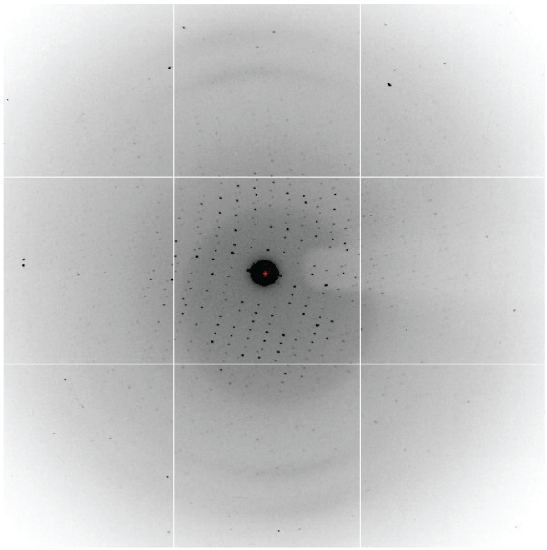

**Figure 7.7. Crystallography efforts with McrB.** A) List of DNA substrates used for crystallography. B) Examples of grown crystals and diffraction of McrBs oligomer.

**Figure 7.8**

A

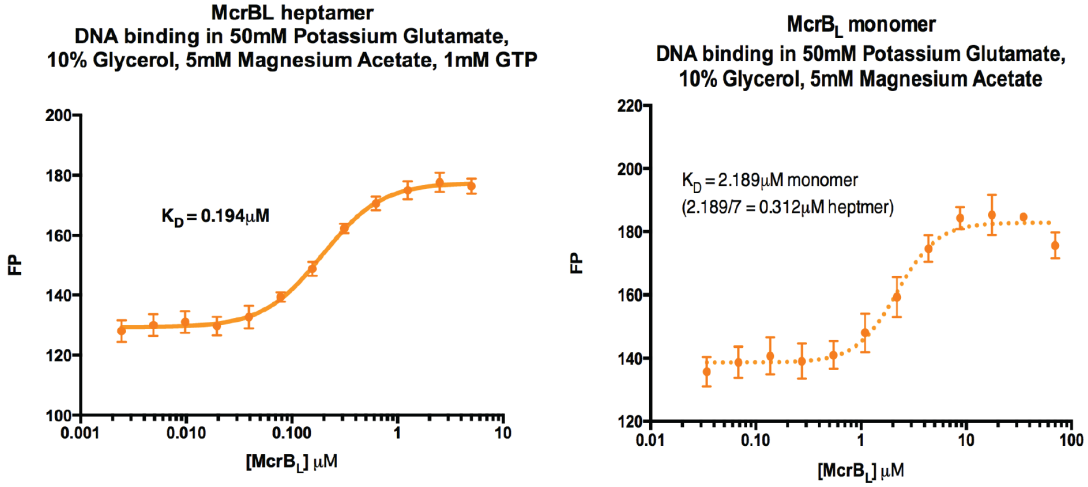


B

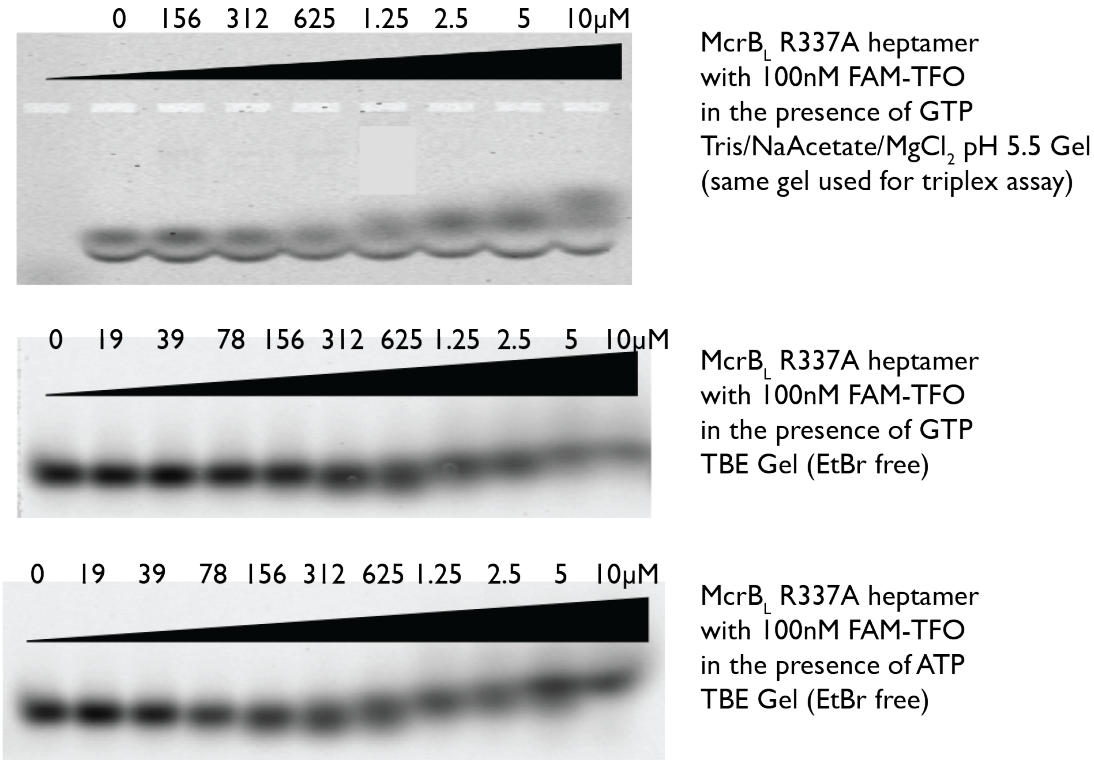


**Figure 7.8. McrB binds dsDNA with recognition sequence and random ssDNA.** A) DNA binding curves for McrBL oligomer and monomer measured with fluorescence anisotropy for labeled dsDNA oligonucleotide with a single recognition sequence. B) Gel shifts of McrBL mutant (R337A) and ssDNA oligonucleotide used to form DNA triplexes in double stranded translocation assays.

**Figure 7.9**

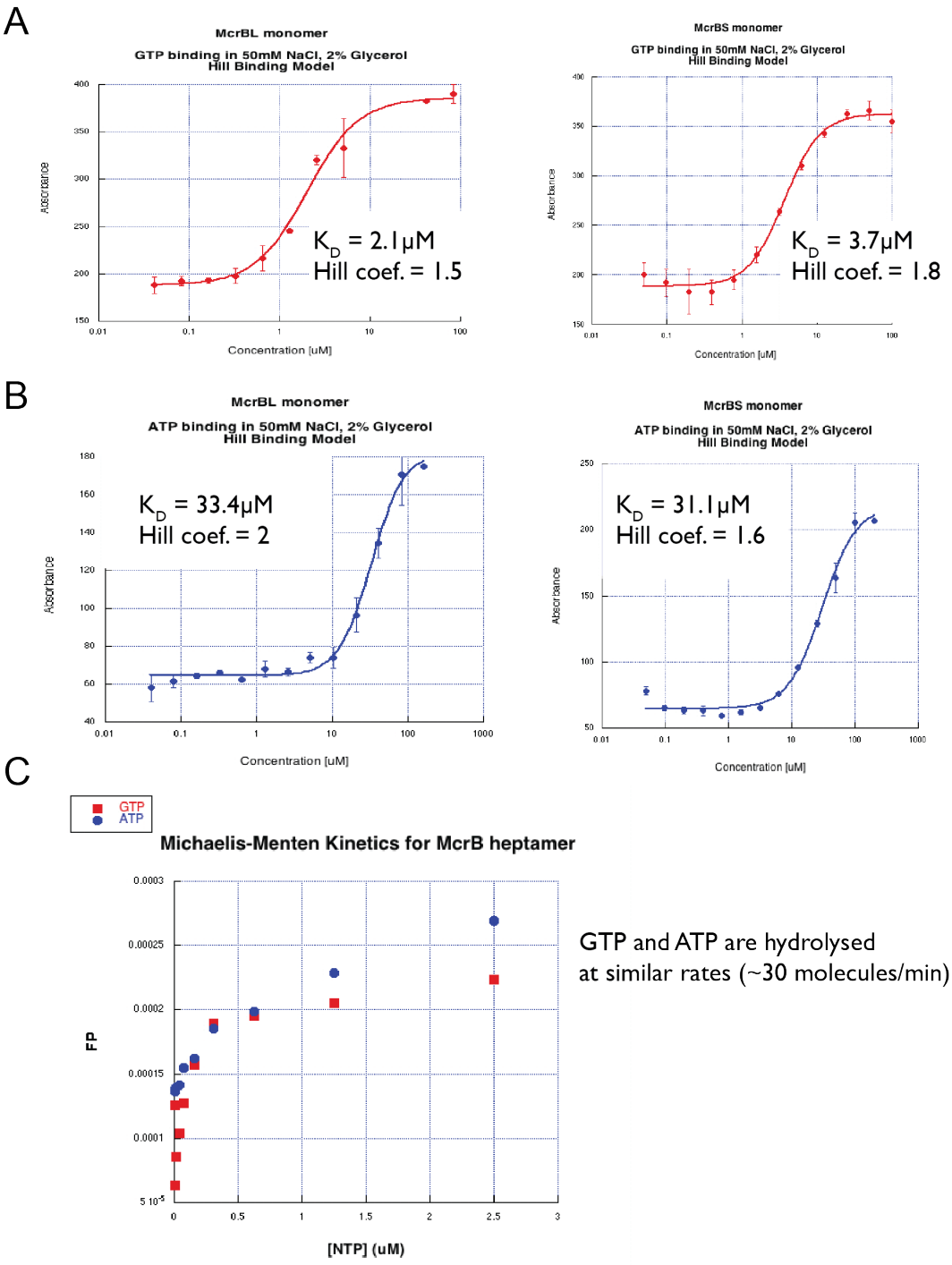


**Figure 7.9. Nucleotide binding and hydrolysis by McrB motor.** A) Binding curves for GTP measured with fluorescence anisotropy. B) Binding curves for ATP measured with fluorescence anisotropy. C) $McrB_L$ oligomer can hydrolyze ATP and GTP at roughly similar rates.

**Figure 7.10**

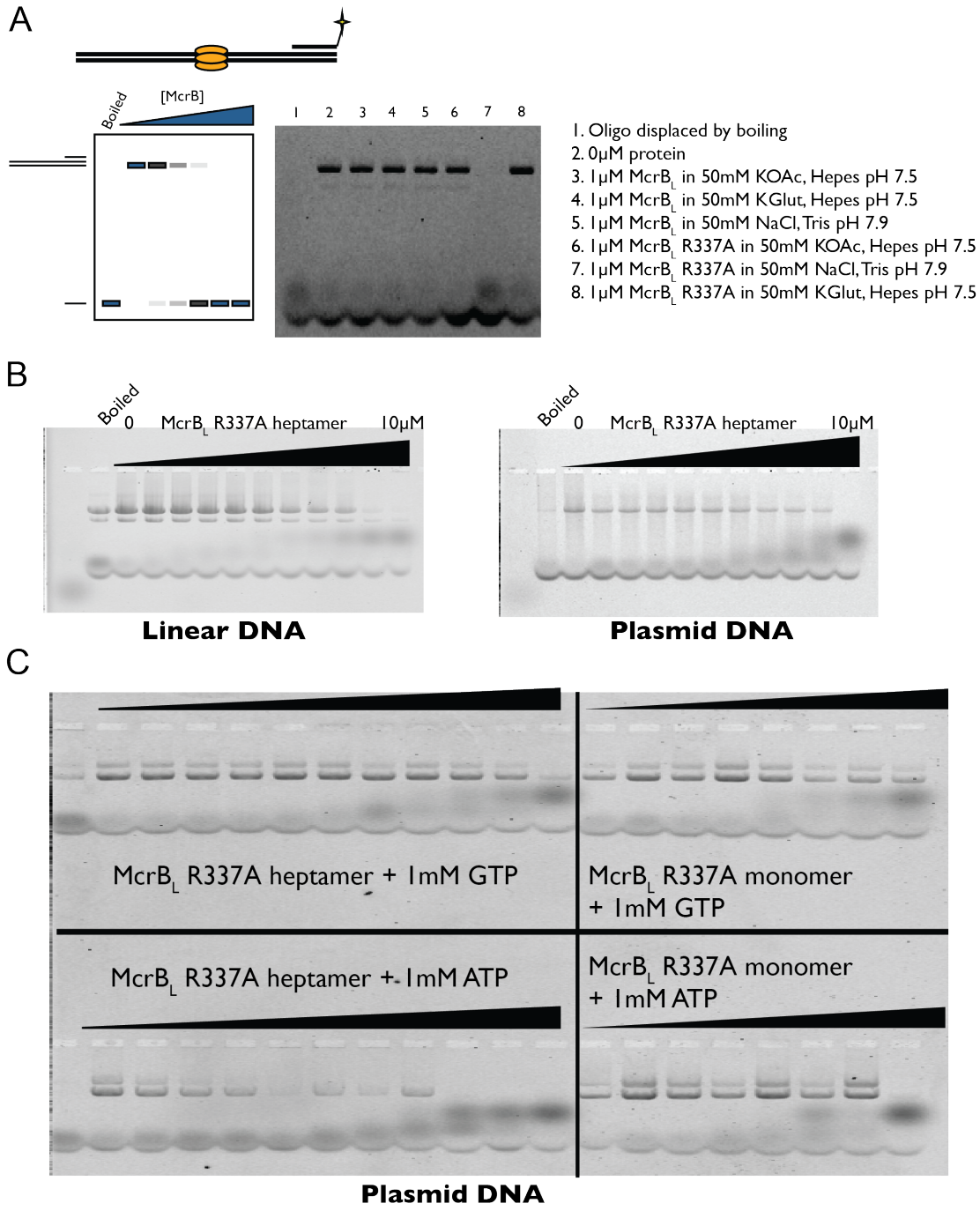


**Figure 7.10. Translocation along dsDNA measured with triplex displacement assay.** A) Identified conditions that result in triplex displacement, only hydrolysis-enhanced mutant of McrB appears able to displace a triplex forming oligonucleotide. B) Triplex displacement measured on linear and plasmid DNA substrates – McrB does not appear to require a free DNA end to load onto in order to translocate along dsDNA. C) Triplex displacement observed on plasmid DNA substrates in the presence of GTP but also ATP.

**Figure 7.11**

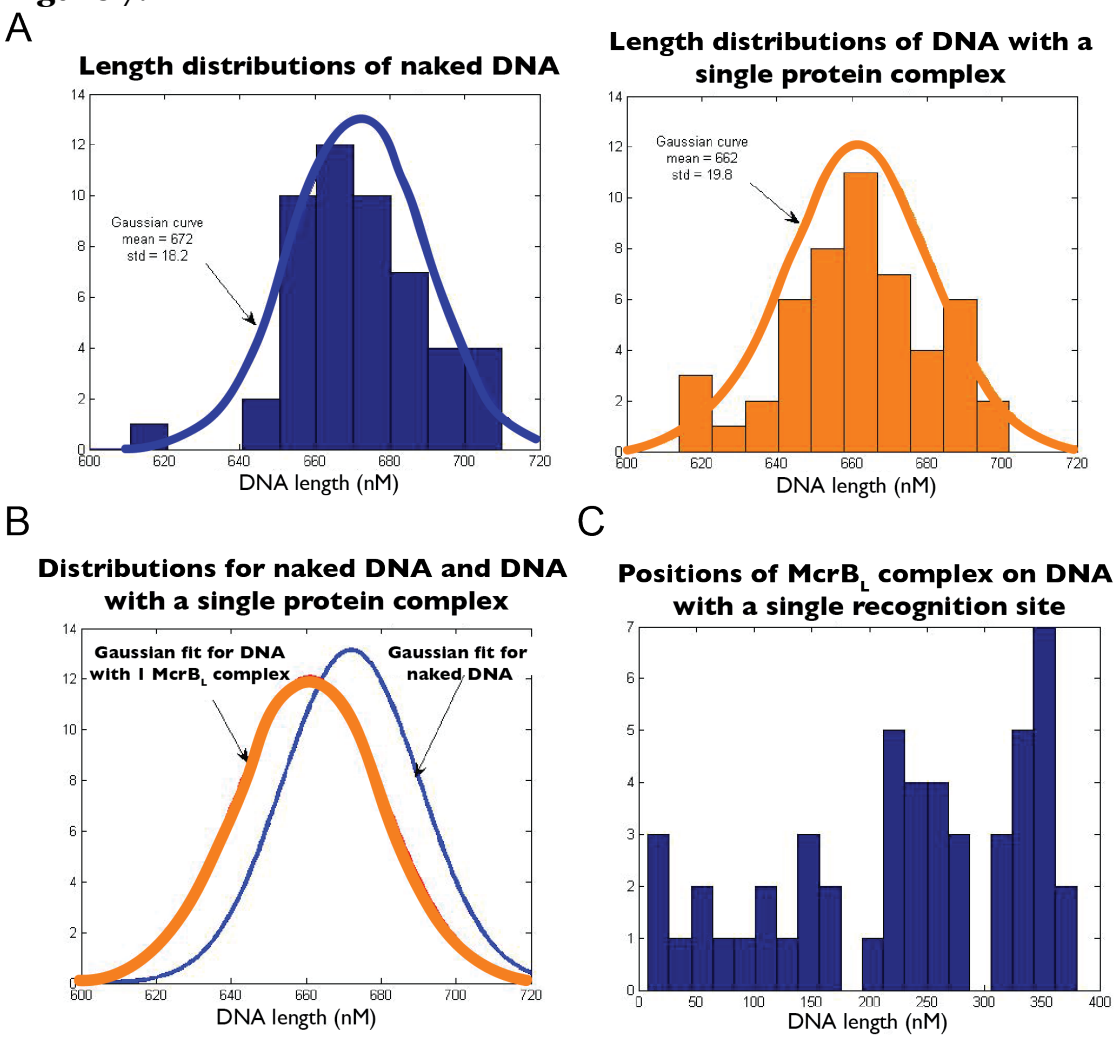


**Figure 7.11. McrB motor loads randomly onto dsDNA and does not wrap it.** A) Length distribution histograms of naked DNA and DNA pieces with a single protein complex. B) Overlapping the two distributions shows that the contour length of DNA did not dramatically decrease with the binding of the McrB complex. While it is possible that the enzyme wraps DNA it does not occur on a large scale. C) Histogram showing distribution of McrB complexes on a piece of DNA with a single recognition site. Position of the protein complex does not appear to correlate with the location of the recognition site suggesting that the enzyme can load randomly and does not assemble specifically around its recognition sequence.

**Figure 7.12**

A

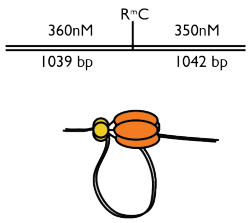


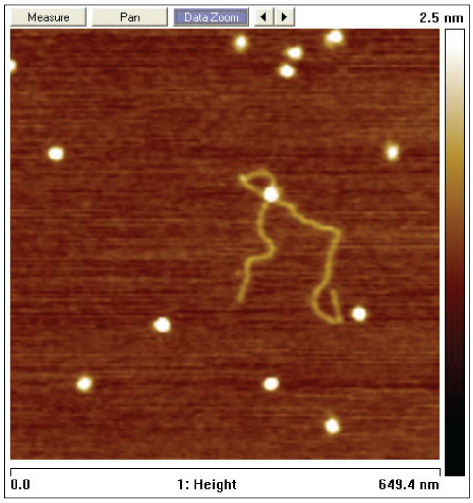


| Loop | Start site |
|---|---|
| 1 | 317 |
| 2 | 305 |
| 3 | 350 |
| 4 | 347 |
| 5 | 324 |
| 6 | 330 |
| 7 | 355 |
| 8 | 337 |
| 9 | 345 |
| 10 | 327 |
| Mean | **333.7** |
| Std | 15.95166 |

B

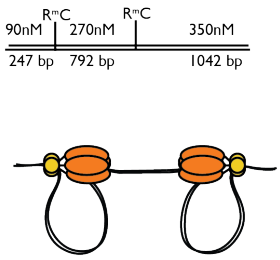


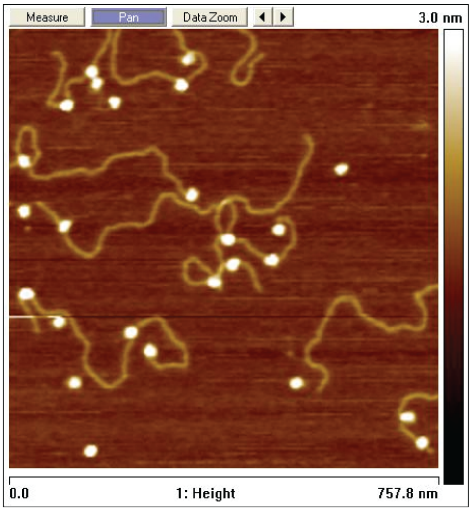


| Loop | Start site |
|---|---|
| 1 | 78 |
| 2 | 29 |
| 3 | 101 |
| 4 | 33 |
| 5 | 91 |
| 6 | 66 |
| 7 | 63 |
| 8 | 108 |
| 9 | 56 |
| 10 | 45 |
| **Mean** | **67** |
| Std | 27.4 |

| Loop | Start site |
|---|---|
| 1 | 384 |
| 2 | 326 |
| 3 | 345 |
| 4 | 360 |
| 5 | 306 |
| 6 | 371 |
| **Mean** | **348.7** |
| Std | 29.1 |

**Figure 7.12. McrB motor appears to loop DNA during translocation while it remains bound to its recognition sequence.** A) Cartoon representation of the experiment on a piece of DNA with a single recognition site together with an example of an AFM image showing a single loop and a table summarizing obtained data. All 10 loops observed along a piece with a single recognition site appeared to originate around the recognition sequence. B) Cartoon representation of the experiment on a piece of DNA with two recognition sites together with an example of an AFM image showing two loops on a single piece of DNA and a table summarizing obtained data. All loops observed along a piece with two recognition sites appeared to originate around one or the other recognition sequence.

# References


Aathavan, K., Politzer, A.T., Kaplan, A., Moffitt, J.R., Chemla, Y.R., Grimes, S., Jardine, P.J., Anderson, D.L., and Bustamante, C. (2009). Substrate interactions and promiscuity in a viral DNA packaging motor. Nature *461*, 669-673.

Abe, Y., Jo, T., Matsuda, Y., Matsunaga, C., Katayama, T., and Ueda, T. (2007). Structure and function of DnaA N-terminal domains: specific sites and mechanisms in inter-DnaA interaction and in DnaB helicase loading on oriC. J Biol Chem *282*, 17816-17827.

Abrahams, J.P., Leslie, A.G., Lutter, R., and Walker, J.E. (1994). Structure at 2.8 A resolution of F1-ATPase from bovine heart mitochondria. Nature *370*, 621-628.

Adachi, K., Yasuda, R., Noji, H., Itoh, H., Harada, Y., Yoshida, M., and Kinosita, K., Jr. (2000). Stepping rotation of F1-ATPase visualized through angle-resolved single-fluorophore imaging. Proc Natl Acad Sci U S A *97*, 7243-7247.

Adams, P.D., Grosse-Kunstleve, R.W., Hung, L.W., Ioerger, T.R., McCoy, A.J., Moriarty, N.W., Read, R.J., Sacchettini, J.C., Sauter, N.K., and Terwilliger, T.C. (2002). PHENIX: building new software for automated crystallographic structure determination. Acta Crystallogr D Biol Crystallogr *58*, 1948-1954.

Adelman, J.L., Jeong, Y.J., Liao, J.C., Patel, G., Kim, D.E., Oster, G., and Patel, S.S. (2006). Mechanochemistry of transcription termination factor Rho. Mol Cell *22*, 611-621.

Afonso, J.P., Chintakayala, K., Suwannachart, C., Sedelnikova, S., Giles, K., Hoyes, J.B., Soultanas, P., Rafferty, J.B., and Oldham, N.J. (2013). Insights into the structure and assembly of the Bacillus subtilis clamp-loader complex and its interaction with the replicative helicase. Nucleic Acids Res *41*, 5115-5126.

Arias-Palomo, E., O'Shea, V.L., Hood, I.V., and Berger, J.M. (2013). The bacterial DnaC helicase loader is a DnaB ring breaker. Cell *153*, 438-448.

Augustin, S., Gerdes, F., Lee, S., Tsai, F.T., Langer, T., and Tatsuta, T. (2009). An intersubunit signaling network coordinates ATP hydrolysis by m-AAA proteases. Mol Cell *35*, 574-585.

Bailey, S., Eliason, W.K., and Steitz, T.A. (2007a). The crystal structure of the Thermus aquaticus DnaB helicase monomer. Nucleic Acids Res *35*, 4728-4736.

Bailey, S., Eliason, W.K., and Steitz, T.A. (2007b). Structure of hexameric DnaB helicase and its complex with a domain of DnaG primase. Science *318*, 459-463.

Baker, T.A., Funnell, B.E., and Kornberg, A. (1987). Helicase action of dnaB protein during replication from the Escherichia coli chromosomal origin in vitro. J Biol Chem *262*, 6877-6885.

Barcena, M., Martin, C.S., Weise, F., Ayora, S., Alonso, J.C., and Carazo, J.M. (1998). Polymorphic quaternary organization of the Bacillus subtilis bacteriophage SPP1 replicative helicase (G40 P). J Mol Biol *283*, 809-819.

Bird, L.E., Pan, H., Soultanas, P., and Wigley, D.B. (2000). Mapping protein-protein interactions within a stable complex of DNA primase and DnaB helicase from Bacillus stearothermophilus. Biochemistry *39*, 171-182.

Biswas, S.B., Chen, P.H., and Biswas, E.E. (1994). Structure and function of Escherichia coli DnaB protein: role of the N-terminal domain in helicase activity. Biochemistry *33*, 11307-11314.

Biswas, E.E., and Biswas, S.B. (1999a). Mechanism of DNA binding by the DnaB helicase of Escherichia coli: analysis of the roles of domain gamma in DNA binding. Biochemistry *38*, 10929-10939.

Biswas, E.E., and Biswas, S.B. (1999b). Mechanism of DnaB helicase of Escherichia coli: structural domains involved in ATP hydrolysis, DNA binding, and oligomerization. Biochemistry *38*, 10919-10928.

Biswas, T., and Tsodikov, O.V. (2008). Hexameric ring structure of the N-terminal domain of Mycobacterium tuberculosis DnaB helicase. FEBS J *275*, 3064-3071.

Biswas, E.E., Biswas, S.B., and Bishop, J.E. (1986). The dnaB protein of Escherichia coli: mechanism of nucleotide binding, hydrolysis, and modulation by dnaC protein. Biochemistry *25*, 7368-7374.

Bochman, M.L., and Schwacha, A. (2008). The Mcm2-7 complex has in vitro helicase activity. Mol Cell *31*, 287-293.

Brennan, C.A., Dombroski, A.J., and Platt, T. (1987). Transcription termination factor rho is an RNA-DNA helicase. Cell *48*, 945-952.

Brewster, A.S., and Chen, X.S. (2010). Insights into the MCM functional mechanism: lessons learned from the archaeal MCM complex. Crit Rev Biochem Mol Biol *45*, 243-256.

Brunger, A.T., Adams, P.D., Clore, G.M., DeLano, W.L., Gros, P., Grosse-Kunstleve, R.W., Jiang, J.S., Kuszewski, J., Nilges, M., Pannu, N.S.*, et al.* (1998). Crystallography & NMR system: A new software suite for macromolecular structure determination. Acta Crystallogr D Biol Crystallogr *54*, 905-921.

Chang, P., and Marians, K.J. (2000). Identification of a region of Escherichia coli DnaB required for functional interaction with DnaG at the replication fork. J Biol Chem *275*, 26187-26195.

Chemla, Y.R., Aathavan, K., Michaelis, J., Grimes, S., Jardine, P.J., Anderson, D.L., and Bustamante, C. (2005). Mechanism of force generation of a viral DNA packaging motor. Cell *122*, 683-692.

Chen, V.B., Arendall, W.B., 3rd, Headd, J.J., Keedy, D.A., Immormino, R.M., Kapral, G.J., Murray, L.W., Richardson, J.S., and Richardson, D.C. (2010). MolProbity: all-atom structure validation for macromolecular crystallography. Acta Crystallogr D Biol Crystallogr *66*, 12-21.

Chintakayala, K., Larson, M.A., Grainger, W.H., Scott, D.J., Griep, M.A., Hinrichs, S.H., and Soultanas, P. (2007). Domain swapping reveals that the C- and N-terminal domains of DnaG and DnaB, respectively, are functional homologues. Mol Microbiol *63*, 1629-1639.

Costa, A., Hood, I.V., and Berger, J.M. (2013). Mechanisms for Initiating Cellular DNA Replication. Annual Review of Biochemistry, Vol 82 *82*, 25-+.

Crampton, D.J., Mukherjee, S., and Richardson, C.C. (2006). DNA-induced switch from independent to sequential dTTP hydrolysis in the bacteriophage T7 DNA helicase. Mol Cell *21*, 165-174.

Dallmann, H.G., Kim, S., Pritchard, A.E., Marians, K.J., and McHenry, C.S. (2000). Characterization of the unique C terminus of the Escherichia coli tau DnaX protein. Monomeric C-tau binds alpha AND DnaB and can partially replace tau in reconstituted replication forks. J Biol Chem *275*, 15512-15519.

Davey, M.J., Fang, L., McInerney, P., Georgescu, R.E., and O'Donnell, M. (2002). The DnaC helicase loader is a dual ATP/ADP switch protein. EMBO J *21*, 3148-3159.

Davey, M.J., and O'Donnell, M. (2003). Replicative helicase loaders: ring breakers and ring makers. Curr Biol *13*, R594-596.

DeLano, W.L. (2009). PyMOL molecular viewer: Updates and refinements. Abstr Pap Am Chem S *238*.

Dila, D., Sutherland, E., Moran, L., Slatko, B., and Raleigh, E.A. (1990). Genetic and sequence organization of the mcrBC locus of Escherichia coli K-12. J Bacteriol *172*, 4888-4900.

Dombroski, A.J., Brennan, C.A., Spear, P., and Platt, T. (1988). Site-directed alterations in the ATP-binding domain of rho protein affect its activities as a termination factor. J Biol Chem *263*, 18802-18809.

Donate, L.E., Llorca, O., Barcena, M., Brown, S.E., Dixon, N.E., and Carazo, J.M. (2000). pH-controlled quaternary states of hexameric DnaB helicase. J Mol Biol *303*, 383-393.

Emsley, P., and Cowtan, K. (2004). Coot: model-building tools for molecular graphics. Acta Crystallogr D Biol Crystallogr *60*, 2126-2132.

Enemark, E.J., and Joshua-Tor, L. (2006). Mechanism of DNA translocation in a replicative hexameric helicase. Nature *442*, 270-275.

Erzberger, J.P., and Berger, J.M. (2006). Evolutionary relationships and structural mechanisms of AAA+ proteins. Annu Rev Biophys Biomol Struct *35*, 93-114.

Fang, L., Davey, M.J., and O'Donnell, M. (1999). Replisome assembly at oriC, the replication origin of E. coli, reveals an explanation for initiation sites outside an origin. Mol Cell *4*, 541-553.

Fass, D., Bogden, C.E., and Berger, J.M. (1999). Crystal structure of the N-terminal domain of the DnaB hexameric helicase. Structure *7*, 691-698.

Firman, K., and Szczelkun, M.D. (2000). Measuring motion on DNA by the type I restriction endonuclease EcoR124I using triplex displacement. EMBO J *19*, 2094-2102.

Fuller, R.S., Kaguni, J.M., and Kornberg, A. (1981). Enzymatic Replication of the Origin of the Escherichia-Coli Chromosome. P Natl Acad Sci-Biol *78*, 7370-7374.

Gai, D., Zhao, R., Li, D., Finkielstein, C.V., and Chen, X.S. (2004). Mechanisms of conformational change for a replicative hexameric helicase of SV40 large tumor antigen. Cell *119*, 47-60.

Galletto, R., Jezewska, M.J., and Bujalowski, W. (2003). Interactions of the Escherichia coli DnaB helicase hexamer with the replication factor the DnaC protein. Effect of nucleotide cofactors and the ssDNA on protein-protein interactions and the topology of the complex. J Mol Biol *329*, 441-465.

Gast, F.U., Brinkmann, T., Pieper, U., Kruger, T., Noyer-Weidner, M., and Pingoud, A. (1997). The recognition of methylated DNA by the GTP-dependent restriction endonuclease McrBC resides in the N-terminal domain of McrB. Biol Chem *378*, 975-982.

Geertsema, H.J., and van Oijen, A.M. (2013). A single-molecule view of DNA replication: the dynamic nature of multi-protein complexes revealed. Curr Opin Struct Biol.

Glynn, S.E., Martin, A., Nager, A.R., Baker, T.A., and Sauer, R.T. (2009). Structures of asymmetric ClpX hexamers reveal nucleotide-dependent motions in a AAA+ protein-unfolding machine. Cell *139*, 744-756.

Gomez-Llorente, Y., Fletcher, R.J., Chen, X.S., Carazo, J.M., and San Martin, C. (2005). Polymorphism and double hexamer structure in the archaeal minichromosome maintenance (MCM) helicase from Methanobacterium thermoautotrophicum. J Biol Chem *280*, 40909-40915.

Hacker, K.J., and Johnson, K.A. (1997). A hexameric helicase encircles one DNA strand and excludes the other during DNA unwinding. Biochemistry *36*, 14080-14087.

Haroniti, A., Anderson, C., Doddridge, Z., Gardiner, L., Roberts, C.J., Allen, S., and Soultanas, P. (2004). The clamp-loader-helicase interaction in Bacillus. Atomic force microscopy reveals the structural organisation of the DnaB-tau complex in Bacillus. J Mol Biol *336*, 381-393.

Hohn, M., Tang, G., Goodyear, G., Baldwin, P.R., Huang, Z., Penczek, P.A., Yang, C., Glaeser, R.M., Adams, P.D., and Ludtke, S.J. (2007). SPARX, a new environment for Cryo-EM image processing. J Struct Biol *157*, 47-55.

Ilves, I., Petojevic, T., Pesavento, J.J., and Botchan, M.R. (2010). Activation of the MCM2-7 helicase by association with Cdc45 and GINS proteins. Mol Cell *37*, 247-258.

Ilyina, T.V., Gorbalenya, A.E., and Koonin, E.V. (1992). Organization and evolution of bacterial and bacteriophage primase-helicase systems. J Mol Evol *34*, 351-357.

Itsathitphaisarn, O., Wing, R.A., Eliason, W.K., Wang, J., and Steitz, T.A. (2012). The hexameric helicase DnaB adopts a nonplanar conformation during translocation. Cell *151*, 267-277.

Iyer, L.M., Leipe, D.D., Koonin, E.V., and Aravind, L. (2004). Evolutionary history and higher order classification of AAA+ ATPases. J Struct Biol *146*, 11-31.

Jezewska, M.J., Rajendran, S., Bujalowska, D., and Bujalowski, W. (1998). Does single-stranded DNA pass through the inner channel of the protein hexamer in the complex with the Escherichia coli DnaB Helicase? Fluorescence energy transfer studies. J Biol Chem *273*, 10515-10529.

Johnson, S.K., Bhattacharyya, S., and Griep, M.A. (2000). DnaB helicase stimulates primer synthesis activity on short oligonucleotide templates. Biochemistry *39*, 736-744.

Kabsch, W. (2010). Xds. Acta Crystallogr D Biol Crystallogr *66*, 125-132.

Kaguni, J.M., Fuller, R.S., and Kornberg, A. (1982). Enzymatic Replication of Escherichia-Coli Chromosomal Origin Is Bidirectional. Nature *296*, 623-627.

Kaplan, D.L. (2000). The 3'-tail of a forked-duplex sterically determines whether one or two DNA strands pass through the central channel of a replication-fork helicase. J Mol Biol *301*, 285-299.

Kaplan, D.L., Davey, M.J., and O'Donnell, M. (2003). Mcm4,6,7 uses a "pump in ring" mechanism to unwind DNA by steric exclusion and actively translocate along a duplex. J Biol Chem *278*, 49171-49182.

Kaplan, D.L., and O'Donnell, M. (2002). DnaB drives DNA branch migration and dislodges proteins while encircling two DNA strands. Mol Cell *10*, 647-657.

Kaplan, D.L., and Steitz, T.A. (1999). DnaB from Thermus aquaticus unwinds forked duplex DNA with an asymmetric tail length dependence. J Biol Chem *274*, 6889-6897.

Kashav, T., Nitharwal, R., Abdulrehman, S.A., Gabdoulkhakov, A., Saenger, W., Dhar, S.K., and Gourinath, S. (2009). Three-dimensional structure of N-terminal domain of DnaB helicase and helicase-primase interactions in Helicobacter pylori. PLoS One *4*, e7515.

Katoh, K., Asimenos, G., and Toh, H. (2009). Multiple alignment of DNA sequences with MAFFT. Methods Mol Biol *537*, 39-64.

Kim, S., Dallmann, H.G., McHenry, C.S., and Marians, K.J. (1996). Coupling of a replicative polymerase and helicase: a tau-DnaB interaction mediates rapid replication fork movement. Cell *84*, 643-650.

Koepsell, S.A., Hanson, S., Hinrichs, S.H., and Griep, M.A. (2005). Fluorometric assay for bacterial primases. Anal Biochem *339*, 353-355.

Koepsell, S.A., Larson, M.A., Griep, M.A., and Hinrichs, S.H. (2006). Staphylococcus aureus helicase but not Escherichia coli helicase stimulates S. aureus primase activity and maintains initiation specificity. J Bacteriol *188*, 4673-4680.

Konarev, P.V., Volkov, V.V., Sokolova, A.V., Koch, M.H.J., and Svergun, D.I. (2003). PRIMUS: a Windows PC-based system for small-angle scattering data analysis. J Appl Crystallogr *36*, 1277-1282.

Kruger, T., Wild, C., and Noyer-Weidner, M. (1995). McrB: a prokaryotic protein specifically recognizing DNA containing modified cytosine residues. EMBO J *14*, 2661-2669.

Lander, G.C., Stagg, S.M., Voss, N.R., Cheng, A., Fellmann, D., Pulokas, J., Yoshioka, C., Irving, C., Mulder, A., Lau, P.W.*, et al.* (2009). Appion: an integrated, database-driven pipeline to facilitate EM image processing. J Struct Biol *166*, 95-102.

LeBowitz, J.H., and McMacken, R. (1986). The Escherichia coli dnaB replication protein is a DNA helicase. J Biol Chem *261*, 4738-4748.

Lee, S.Y., De La Torre, A., Yan, D., Kustu, S., Nixon, B.T., and Wemmer, D.E. (2003). Regulation of the transcriptional activator NtrC1: structural studies of the regulatory and AAA+ ATPase domains. Genes Dev *17*, 2552-2563.

Lee, C., Schwartz, M.P., Prakash, S., Iwakura, M., and Matouschek, A. (2001). ATP-dependent proteases degrade their substrates by processively unraveling them from the degradation signal. Mol Cell *7*, 627-637.

Leipe, D.D., Aravind, L., Grishin, N.V., and Koonin, E.V. (2000). The bacterial replicative helicase DnaB evolved from a RecA duplication. Genome Res *10*, 5-16.

Leipe, D.D., Koonin, E.V., and Aravind, L. (2003). Evolution and classification of P-loop kinases and related proteins. J Mol Biol *333*, 781-815.

Lia, G., Michel, B., and Allemand, J.F. (2012). Polymerase exchange during Okazaki fragment synthesis observed in living cells. Science *335*, 328-331.

Lindsley, J.E. (2001). Use of a real-time, coupled assay to measure the ATPase activity of DNA topoisomerase II. Methods Mol Biol *95*, 57-64.

Lisal, J., Kainov, D.E., Lam, T.T., Emmett, M.R., Wei, H., Gottlieb, P., Marshall, A.G., and Tuma, R. (2006). Interaction of packaging motor with the polymerase complex of dsRNA bacteriophage. Virology *351*, 73-79.

Liu, B., Eliason, W.K., and Steitz, T.A. (2013). Structure of a helicase-helicase loader complex reveals insights into the mechanism of bacterial primosome assembly. Nat Commun *4*, 2495.

Lo, Y.H., Tsai, K.L., Sun, Y.J., Chen, W.T., Huang, C.Y., and Hsiao, C.D. (2009). The crystal structure of a replicative hexameric helicase DnaC and its complex with single-stranded DNA. Nucleic Acids Res *37*, 804-814.

Loparo, J.J., Kulczyk, A.W., Richardson, C.C., and van Oijen, A.M. (2011). Simultaneous single-molecule measurements of phage T7 replisome composition and function reveal the mechanism of polymerase exchange. Proc Natl Acad Sci U S A *108*, 3584-3589.

Lu, Y.B., Ratnakar, P.V., Mohanty, B.K., and Bastia, D. (1996). Direct physical interaction between DnaG primase and DnaB helicase of Escherichia coli is

necessary for optimal synthesis of primer RNA. Proc Natl Acad Sci U S A *93*, 12902-12907.

Ludtke, S.J., Baldwin, P.R., and Chiu, W. (1999). EMAN: semiautomated software for high-resolution single-particle reconstructions. J Struct Biol *128*, 82-97.

Lyubimov, A.Y., Costa, A., Bleichert, F., Botchan, M.R., and Berger, J.M. (2012). ATP-dependent conformational dynamics underlie the functional asymmetry of the replicative helicase from a minimalist eukaryote. Proc Natl Acad Sci U S A *109*, 11999-12004.

Lyubimov, A.Y., Strycharska, M., and Berger, J.M. (2011). The nuts and bolts of ring-translocase structure and mechanism. Curr Opin Struct Biol *21*, 240-248.

MacDowell, A.A., Celestre, R.S., Howells, M., McKinney, W., Krupnick, J., Cambie, D., Domning, E.E., Duarte, R.M., Kelez, N., Plate, D.W.*, et al.* (2004). Suite of three protein crystallography beamlines with single superconducting bend magnet as the source. J Synchrotron Radiat *11*, 447-455.

Makowska-Grzyska, M., and Kaguni, J.M. (2010). Primase directs the release of DnaC from DnaB. Mol Cell *37*, 90-101.

Mancini, E.J., Kainov, D.E., Grimes, J.M., Tuma, R., Bamford, D.H., and Stuart, D.I. (2004). Atomic snapshots of an RNA packaging motor reveal conformational changes linking ATP hydrolysis to RNA translocation. Cell *118*, 743-755.

Marians, K.J. (1992). Prokaryotic DNA replication. Annu Rev Biochem *61*, 673-719.

Marszalek, J., and Kaguni, J.M. (1994). DnaA protein directs the binding of DnaB protein in initiation of DNA replication in Escherichia coli. J Biol Chem *269*, 4883-4890.

Martin, A., Baker, T.A., and Sauer, R.T. (2005). Rebuilt AAA + motors reveal operating principles for ATP-fuelled machines. Nature *437*, 1115-1120.

Martinez-Jimenez, M.I., Mesa, P., and Alonso, J.C. (2002). Bacillus subtilis tau subunit of DNA polymerase III interacts with bacteriophage SPP1 replicative DNA helicase G40P. Nucleic Acids Res *30*, 5056-5064.

Massey, T.H., Mercogliano, C.P., Yates, J., Sherratt, D.J., and Lowe, J. (2006). Double-stranded DNA translocation: structure and mechanism of hexameric FtsK. Mol Cell *23*, 457-469.

McClelland, S.E., Dryden, D.T., and Szczelkun, M.D. (2005). Continuous assays for DNA translocation using fluorescent triplex dissociation: application to type I restriction endonucleases. J Mol Biol *348*, 895-915.

McCoy, A.J., Grosse-Kunstleve, R.W., Adams, P.D., Winn, M.D., Storoni, L.C., and Read, R.J. (2007). Phaser crystallographic software. J Appl Crystallogr *40*, 658-674.

Mindell, J.A., and Grigorieff, N. (2003). Accurate determination of local defocus and specimen tilt in electron microscopy. J Struct Biol *142*, 334-347.

Mitkova, A.V., Khopde, S.M., and Biswas, S.B. (2003). Mechanism and stoichiometry of interaction of DnaG primase with DnaB helicase of Escherichia coli in RNA primer synthesis. J Biol Chem *278*, 52253-52261.

Miwa, Y., Horiguchi, T., and Shigesada, K. (1995). Structural and functional dissections of transcription termination factor rho by random mutagenesis. J Mol Biol *254*, 815-837.

Moffitt, J.R., Chemla, Y.R., Aathavan, K., Grimes, S., Jardine, P.J., Anderson, D.L., and Bustamante, C. (2009). Intersubunit coordination in a homomeric ring ATPase. Nature *457*, 446-450.

Mok, M., and Marians, K.J. (1987). The Escherichia coli preprimosome and DNA B helicase can form replication forks that move at the same rate. J Biol Chem *262*, 16644-16654.

Moreau, M.J., McGeoch, A.T., Lowe, A.R., Itzhaki, L.S., and Bell, S.D. (2007). ATPase site architecture and helicase mechanism of an archaeal MCM. Mol Cell *28*, 304-314.

Nadanaciva, S., Weber, J., Wilke-Mounts, S., and Senior, A.E. (1999). Importance of F1-ATPase residue alpha-Arg-376 for catalytic transition state stabilization. Biochemistry *38*, 15493-15499.

Nakayama, N., Arai, N., Kaziro, Y., and Arai, K. (1984). Structural and functional studies of the dnaB protein using limited proteolysis. Characterization of domains for DNA-dependent ATP hydrolysis and for protein association in the primosome. J Biol Chem *259*, 88-96.

Neuwald, A.F., Aravind, L., Spouge, J.L., and Koonin, E.V. (1999). AAA+: A class of chaperone-like ATPases associated with the assembly, operation, and disassembly of protein complexes. Genome Res *9*, 27-43.

Nitharwal, R.G., Verma, V., Subbarao, N., Dasgupta, S., Choudhury, N.R., and Dhar, S.K. (2012). DNA binding activity of Helicobacter pylori DnaB helicase: the

role of the N-terminal domain in modulating DNA binding activities. FEBS J *279*, 234-250.

Nunez-Ramirez, R., Robledo, Y., Mesa, P., Ayora, S., Alonso, J.C., Carazo, J.M., and Donate, L.E. (2006). Quaternary polymorphism of replicative helicase G40P: structural mapping and domain rearrangement. J Mol Biol *357*, 1063-1076.

Oakley, A.J., Loscha, K.V., Schaeffer, P.M., Liepinsh, E., Pintacuda, G., Wilce, M.C., Otting, G., and Dixon, N.E. (2005). Crystal and solution structures of the helicase-binding domain of Escherichia coli primase. J Biol Chem *280*, 11495-11504.

Panne, D., Muller, S.A., Wirtz, S., Engel, A., and Bickle, T.A. (2001). The McrBC restriction endonuclease assembles into a ring structure in the presence of G nucleotides. EMBO J *20*, 3210-3217.

Panne, D., Raleigh, E.A., and Bickle, T.A. (1998). McrBs, a modulator peptide for McrBC activity. EMBO J *17*, 5477-5483.

Panne, D., Raleigh, E.A., and Bickle, T.A. (1999). The McrBC endonuclease translocates DNA in a reaction dependent on GTP hydrolysis. J Mol Biol *290*, 49-60.

Pape, T., Meka, H., Chen, S., Vicentini, G., van Heel, M., and Onesti, S. (2003). Hexameric ring structure of the full-length archaeal MCM protein complex. EMBO Rep *4*, 1079-1083.

Pettersen, E.F., Goddard, T.D., Huang, C.C., Couch, G.S., Greenblatt, D.M., Meng, E.C., and Ferrin, T.E. (2004). UCSF Chimera--a visualization system for exploratory research and analysis. J Comput Chem *25*, 1605-1612.

Pieper, U., Brinkmann, T., Kruger, T., Noyer-Weidner, M., and Pingoud, A. (1997). Characterization of the interaction between the restriction endonuclease McrBC from E. coli and its cofactor GTP. J Mol Biol *272*, 190-199.

Pieper, U., Groll, D.H., Wunsch, S., Gast, F.U., Speck, C., Mucke, N., and Pingoud, A. (2002). The GTP-dependent restriction enzyme McrBC from Escherichia coli forms high-molecular mass complexes with DNA and produces a cleavage pattern with a characteristic 10-base pair repeat. Biochemistry *41*, 5245-5254.

Pieper, U., and Pingoud, A. (2002). A mutational analysis of the PD...D/EXK motif suggests that McrC harbors the catalytic center for DNA cleavage by the GTP-dependent restriction enzyme McrBC from Escherichia coli. Biochemistry *41*, 5236-5244.

Pieper, U., Schweitzer, T., Groll, D.H., Gast, F.U., and Pingoud, A. (1999a). The GTP-binding domain of McrB: more than just a variation on a common theme? J Mol Biol *292*, 547-556.

Pieper, U., Schweitzer, T., Groll, D.H., and Pingoud, A. (1999b). Defining the location and function of domains of McrB by deletion mutagenesis. Biol Chem *380*, 1225-1230.

Pomerantz, R.T., and O'Donnell, M. (2007). Replisome mechanics: insights into a twin DNA polymerase machine. Trends Microbiol *15*, 156-164.

Remus, D., and Diffley, J.F. (2009). Eukaryotic DNA replication control: lock and load, then fire. Curr Opin Cell Biol *21*, 771-777.

Ribeck, N., Kaplan, D.L., Bruck, I., and Saleh, O.A. (2010). DnaB helicase activity is modulated by DNA geometry and force. Biophys J *99*, 2170-2179.

Ross, T.K., Achberger, E.C., and Braymer, H.D. (1989). Nucleotide sequence of the McrB region of Escherichia coli K-12 and evidence for two independent translational initiation sites at the mcrB locus. J Bacteriol *171*, 1974-1981.

Rothenberg, E., Trakselis, M.A., Bell, S.D., and Ha, T. (2007). MCM forked substrate specificity involves dynamic interaction with the 5'-tail. J Biol Chem *282*, 34229-34234.

Sanders, C.M., Kovalevskiy, O.V., Sizov, D., Lebedev, A.A., Isupov, M.N., and Antson, A.A. (2007). Papillomavirus E1 helicase assembly maintains an asymmetric state in the absence of DNA and nucleotide cofactors. Nucleic Acids Res *35*, 6451-6457.

San Martin, C., Radermacher, M., Wolpensinger, B., Engel, A., Miles, C.S., Dixon, N.E., and Carazo, J.M. (1998). Three-dimensional reconstructions from cryoelectron microscopy images reveal an intimate complex between helicase DnaB and its loading partner DnaC. Structure *6*, 501-509.

San Martin, M.C., Stamford, N.P., Dammerova, N., Dixon, N.E., and Carazo, J.M. (1995). A structural model for the Escherichia coli DnaB helicase based on electron microscopy data. J Struct Biol *114*, 167-176.

Sawaya, M.R., Guo, S., Tabor, S., Richardson, C.C., and Ellenberger, T. (1999). Crystal structure of the helicase domain from the replicative helicase-primase of bacteriophage T7. Cell *99*, 167-177.

Scheres, S.H., Nunez-Ramirez, R., Sorzano, C.O., Carazo, J.M., and Marabini, R. (2008). Image processing for electron microscopy single-particle analysis using XMIPP. Nat Protoc *3*, 977-990.

Scheres, S.H., Valle, M., Nunez, R., Sorzano, C.O., Marabini, R., Herman, G.T., and Carazo, J.M. (2005). Maximum-likelihood multi-reference refinement for electron microscopy images. J Mol Biol *348*, 139-149.

Schneidman-Duhovny, D., Hammel, M., and Sali, A. (2010). FoXS: a web server for rapid computation and fitting of SAXS profiles. Nucleic Acids Research *38*, W540-W544.

Schwartz, A., Rabhi, M., Jacquinot, F., Margeat, E., Rahmouni, A.R., and Boudvillain, M. (2009). A stepwise 2'-hydroxyl activation mechanism for the bacterial transcription termination factor Rho helicase. Nat Struct Mol Biol *16*, 1309-1316.

Seitz, H., Weigel, C., and Messer, W. (2000). The interaction domains of the DnaA and DnaB replication proteins of Escherichia coli. Mol Microbiol *37*, 1270-1279.

Seo, Y.S., Muller, F., Lusky, M., and Hurwitz, J. (1993). Bovine papilloma virus (BPV)-encoded E1 protein contains multiple activities required for BPV DNA replication. Proc Natl Acad Sci U S A *90*, 702-706.

Shaikh, T.R., Gao, H., Baxter, W.T., Asturias, F.J., Boisset, N., Leith, A., and Frank, J. (2008). SPIDER image processing for single-particle reconstruction of biological macromolecules from electron micrographs. Nat Protoc *3*, 1941-1974.

Singleton, M.R., Dillingham, M.S., and Wigley, D.B. (2007). Structure and mechanism of helicases and nucleic acid translocases. Annu Rev Biochem *76*, 23-50.

Singleton, M.R., Sawaya, M.R., Ellenberger, T., and Wigley, D.B. (2000). Crystal structure of T7 gene 4 ring helicase indicates a mechanism for sequential hydrolysis of nucleotides. Cell *101*, 589-600.

Stelter, M., Gutsche, I., Kapp, U., Bazin, A., Bajic, G., Goret, G., Jamin, M., Timmins, J., and Terradot, L. (2012). Architecture of a dodecameric bacterial replicative helicase. Structure *20*, 554-564.

Stewart, F.J., Panne, D., Bickle, T.A., and Raleigh, E.A. (2000). Methyl-specific DNA binding by McrBC, a modification-dependent restriction enzyme. J Mol Biol *298*, 611-622.

Stewart, F.J., and Raleigh, E.A. (1998). Dependence of McrBC cleavage on distance between recognition elements. Biol Chem *379*, 611-616.
Sutherland, E., Coe, L., and Raleigh, E.A. (1992). McrBC: a multisubunit GTP-dependent restriction endonuclease. J Mol Biol *225*, 327-348.

Story, R.M., and Steitz, T.A. (1992). Structure of the recA protein-ADP complex. Nature *355*, 374-376.

Story, R.M., Weber, I.T., and Steitz, T.A. (1992). The structure of the E. coli recA protein monomer and polymer. Nature *355*, 318-325.

Subramanya, H.S., Bird, L.E., Brannigan, J.A., and Wigley, D.B. (1996). Crystal structure of a DExx box DNA helicase. Nature *384*, 379-383.

Suloway, C., Pulokas, J., Fellmann, D., Cheng, A., Guerra, F., Quispe, J., Stagg, S., Potter, C.S., and Carragher, B. (2005). Automated molecular microscopy: the new Leginon system. J Struct Biol *151*, 41-60.

Sutton, M.D., Carr, K.M., Vicente, M., and Kaguni, J.M. (1998). Escherichia coli DnaA protein. The N-terminal domain and loading of DnaB helicase at the E. coli chromosomal origin. J Biol Chem *273*, 34255-34262.

Syson, K., Thirlway, J., Hounslow, A.M., Soultanas, P., and Waltho, J.P. (2005). Solution structure of the helicase-interaction domain of the primase DnaG: a model for helicase activation. Structure *13*, 609-616.

Tamura, J.K., and Gellert, M. (1990). Characterization of the Atp Binding-Site on Escherichia-Coli DNA Gyrase - Affinity Labeling of Lys-103 and Lys-110 of the B-Subunit by Pyridoxal 5'-Diphospho-5'-Adenosine. Journal of Biological Chemistry *265*, 21342-21349.

Tanner, N.A., Hamdan, S.M., Jergic, S., Loscha, K.V., Schaeffer, P.M., Dixon, N.E., and van Oijen, A.M. (2008). Single-molecule studies of fork dynamics in Escherichia coli DNA replication. Nat Struct Mol Biol *15*, 998.

Thomsen, N.D., and Berger, J.M. (2008). Structural frameworks for considering microbial protein- and nucleic acid-dependent motor ATPases. Mol Microbiol *69*, 1071-1090.

Thomsen, N.D., and Berger, J.M. (2009). Running in reverse: the structural basis for translocation polarity in hexameric helicases. Cell *139*, 523-534.

Thirlway, J., and Soultanas, P. (2006). In the Bacillus stearothermophilus DnaB-DnaG complex, the activities of the two proteins are modulated by distinct but overlapping networks of residues. J Bacteriol *188*, 1534-1539.

Thirlway, J., Turner, I.J., Gibson, C.T., Gardiner, L., Brady, K., Allen, S., Roberts, C.J., and Soultanas, P. (2004). DnaG interacts with a linker region that joins the N- and C-domains of DnaB and induces the formation of 3-fold symmetric rings. Nucleic Acids Res *32*, 2977-2986.

Toth, E.A., Li, Y., Sawaya, M.R., Cheng, Y., and Ellenberger, T. (2003). The crystal structure of the bifunctional primase-helicase of bacteriophage T7. Mol Cell *12*, 1113-1123.

Tougu, K., and Marians, K.J. (1996). The interaction between helicase and primase sets the replication fork clock. J Biol Chem *271*, 21398-21405.

Tougu, K., Peng, H., and Marians, K.J. (1994). Identification of a domain of Escherichia coli primase required for functional interaction with the DnaB helicase at the replication fork. J Biol Chem *269*, 4675-4682.

Voss, N.R., Yoshioka, C.K., Radermacher, M., Potter, C.S., and Carragher, B. (2009). DoG Picker and TiltPicker: software tools to facilitate particle selection in single particle electron microscopy. J Struct Biol *166*, 205-213.

Wahle, E., Lasken, R.S., and Kornberg, A. (1989). The dnaB-dnaC replication protein complex of Escherichia coli. II. Role of the complex in mobilizing dnaB functions. J Biol Chem *264*, 2469-2475.

Walker, J.E., Saraste, M., Runswick, M.J., and Gay, N.J. (1982). Distantly related sequences in the alpha- and beta-subunits of ATP synthase, myosin, kinases and other ATP-requiring enzymes and a common nucleotide binding fold. EMBO J *1*, 945-951.

Wang, J. (2004). Nucleotide-dependent domain motions within rings of the RecA/AAA(+) superfamily. J Struct Biol *148*, 259-267.

Wang, J., Song, J.J., Seong, I.S., Franklin, M.C., Kamtekar, S., Eom, S.H., and Chung, C.H. (2001). Nucleotide-dependent conformational changes in a protease-associated ATPase HsIU. Structure *9*, 1107-1116.

Wang, G., Klein, M.G., Tokonzaba, E., Zhang, Y., Holden, L.G., and Chen, X.S. (2008). The structure of a DnaB-family replicative helicase and its interactions with primase. Nat Struct Mol Biol *15*, 94-100.

Waterhouse, A.M., Procter, J.B., Martin, D.M., Clamp, M., and Barton, G.J. (2009). Jalview Version 2--a multiple sequence alignment editor and analysis workbench. Bioinformatics *25*, 1189-1191.

Webb, M.R. (1992). A continuous spectrophotometric assay for inorganic phosphate and for measuring phosphate release kinetics in biological systems. Proc Natl Acad Sci U S A *89*, 4884-4887.

Wei, R.R., and Richardson, J.P. (2001). Mutational changes of conserved residues in the Q-loop region of transcription factor Rho greatly reduce secondary site RNA-binding. J Mol Biol *314*, 1007-1015.

Weigelt, J., Brown, S.E., Miles, C.S., Dixon, N.E., and Otting, G. (1999). NMR structure of the N-terminal domain of E. coli DnaB helicase: implications for structure rearrangements in the helicase hexamer. Structure *7*, 681-690.

Wickner, S., and Hurwitz, J. (1975). Interaction of Escherichia coli dnaB and dnaC(D) gene products in vitro. Proc Natl Acad Sci U S A *72*, 921-925.

Wu, C.A., Zechner, E.L., Hughes, A.J., Jr., Franden, M.A., McHenry, C.S., and Marians, K.J. (1992a). Coordinated leading- and lagging-strand synthesis at the Escherichia coli DNA replication fork. IV. Reconstitution of an asymmetric, dimeric DNA polymerase III holoenzyme. J Biol Chem *267*, 4064-4073.

Wu, C.A., Zechner, E.L., and Marians, K.J. (1992b). Coordinated leading- and lagging-strand synthesis at the Escherichia coli DNA replication fork. I. Multiple effectors act to modulate Okazaki fragment size. J Biol Chem *267*, 4030-4044.

Wu, C.A., Zechner, E.L., Reems, J.A., McHenry, C.S., and Marians, K.J. (1992c). Coordinated leading- and lagging-strand synthesis at the Escherichia coli DNA replication fork. V. Primase action regulates the cycle of Okazaki fragment synthesis. J Biol Chem *267*, 4074-4083.

Xie, Y., and He, Z.G. (2009). Characterization of physical interaction between replication initiator protein DnaA and replicative helicase from Mycobacterium tuberculosis H37Rv. Biochemistry (Mosc) *74*, 1320-1327.

Xu, Y., Kohn, H., and Widger, W.R. (2002). Mutations in the rho transcription termination factor that affect RNA tracking. J Biol Chem *277*, 30023-30030.

Yakamavich, J.A., Baker, T.A., and Sauer, R.T. (2008). Asymmetric nucleotide transactions of the HslUV protease. J Mol Biol *380*, 946-957.

Yang, S., Yu, X., VanLoock, M.S., Jezewska, M.J., Bujalowski, W., and Egelman, E.H. (2002). Flexibility of the rings: structural asymmetry in the DnaB hexameric helicase. J Mol Biol *321*, 839-849.

Yoshimoto, K., Arora, K., and Brooks, C.L., 3rd (2010). Hexameric helicase deconstructed: interplay of conformational changes and substrate coupling. Biophys J *98*, 1449-1457.

Yu, X., Jezewska, M.J., Bujalowski, W., and Egelman, E.H. (1996). The hexameric E. coli DnaB helicase can exist in different Quaternary states. J Mol Biol *259*, 7-14.

Yu, X., VanLoock, M.S., Poplawski, A., Kelman, Z., Xiang, T., Tye, B.K., and Egelman, E.H. (2002). The Methanobacterium thermoautotrophicum MCM protein can form heptameric rings. EMBO Rep *3*, 792-797.

Yuzhakov, A., Kelman, Z., and O'Donnell, M. (1999). Trading places on DNA--a three-point switch underlies primer handoff from primase to the replicative DNA polymerase. Cell *96*, 153-163.

Zechner, E.L., Wu, C.A., and Marians, K.J. (1992a). Coordinated leading- and lagging-strand synthesis at the Escherichia coli DNA replication fork. II. Frequency of primer synthesis and efficiency of primer utilization control Okazaki fragment size. J Biol Chem *267*, 4045-4053.

Zechner, E.L., Wu, C.A., and Marians, K.J. (1992b). Coordinated leading- and lagging-strand synthesis at the Escherichia coli DNA replication fork. III. A polymerase-primase interaction governs primer size. J Biol Chem *267*, 4054-4063.

# Appendix – protocols

## *Aa*DnaB PURIFICATION PROTOCOL
## (adapted from Jan Erzberger and Melissa Mott)

Expression

BL21 Codon+ RIL cells, grown O/N on Kan plates (old *Aa*DnaB plasmid from Jan Erzberger and Melissa Mott has 3 mutations, new wild type *Aa*DnaB was cloned into an $Amp^R$ plasmid)

Pick a single colony and grow a small O/N (20mL per 1L) in 2xYT.

Grow 1L cultures at 37°C to $OD_{600}$ of 0.3
Induce with 0.25 – 0.5mM IPTG
Express for 3-5hours

Harvesting

Resuspend cells in DnaB **Resuspension Buffer**:

50 mM HEPES-KOH pH 7.5
1 M KCl
10% Glycerol
5mM $MgCl_2$
1 mM ATP
protease inhibitors (1:1000)

*you can freeze cell pellets or drop resuspended pellets into liquid nitrogen

Purification

1) Thaw cells, sonicate (4 x 15sec at 40Watts) and spin at 15,000rpm for 20min

2) Place lysate in a 65C water bath for 15min

3) Place lysate on ice for 30min

4) Spin (15K for 30min), *Aa*DnaB will stay in the supernatant, dilute the salt down to 200mM KCl with **No Salt Q Buffer**:

   20mM Hepes pH 7.5
   10% Glycerol
   5mM $MgCl_2$
   0.1mM ATP
   protease inhibitors (7uL per 100mL)

(do not use reducing reagents, *Aa*DnaB has a cysteine disulfide bond in the N-terminal domain)

5) Flow resuspension over Q column equilibrated in **200mM KCl Q Buffer**. Wash with **200mM KCl Q Buffer**, check for completion by Bradford.

6) Wash column with **300mM and 400mM KCl Q Buffer**:
   300mM KCl
   20mM Hepes pH 7.5
   10% Glycerol
   5mM $MgCl_2$
   0.1mM ATP
   protease inhibitors

7) Elute with **500mM KCl Q Buffer** (and then again with 600mM KCl):
   500mM KCl / 600mM KCl
   20mM Hepes pH 7.5
   10% Glycerol
   5mM $MgCl_2$
   0.1mM ATP
   protease inhibitors

8) Concentrate to 1-2mL using 10K Amicon

9) Run an S300 sizing column twice equilibrated in:
   20mM Tris pH 8.5
   800mM KCl
   10% Glycerol
   5mM $MgCl_2$
   0.1-1mM ATP
   protease inhibitors

- for crystallography/EM purposes pool and concentrate peak from the first S300 column and run a second sizing column for complete separation of aggregates and contaminating DNA
- for crystallography do not flash freeze the protein before setting trays

## *Ec*DnaB PURIFICATION PROTOCOL

Expression

C41 cells, grown O/N on Amp plates
Pick a single colony and grow small O/N (20mL per 1L) in 2xYT with 1% glucose

Grow 1L cultures at 37°C to $OD_{600}$ of 0.3 (between 0.3 and 0.5 should work)
Induce with 1mM IPTG
Express for 2-3hours

Harvesting

Resuspend cells in DnaB **Resuspension Buffer**:

500mM NaCl
20mM Hepes pH 7.5
10% Glycerol
10mM $MgCl_2$
protease inhibitors (1:1000)

*you can freeze cell pellets or drop resuspended pellets into liquid nitrogen

Purification

1) Thaw cells, sonicate (4 x 15sec at 40Watts) and spin at 15,000rpm for 20min

2) Add saturated liquid ammonium sulfate to lysate:
- Pre cut w/10% AmSulf (save supernatant, many contaminating proteins should be crushed out at this step). Then add AmSulf to a final 30% concentration. (You also might want to back extract from the pellet with 25%/30% 2-3 times).

3) Spin (15K for 30min), decant supernatant and resuspend pellet in **100mM NaCl Q Buffer**:

100mM NaCl
20mM Hepes pH 7.5
10% Glycerol
10mM $MgCl_2$
0.01mM ATP
1mM β-mercaptoethanol (7ul per 100mL)
protease inhibitors (100uL per 100mL)

4) Flow resuspension over Q column equilibrated in **100mM NaCl Q Buffer**. Wash with **100mM NaCl Q Buffer**, check for completion by Bradford.

5) Wash column with **300mM NaCl Q Buffer**:
    300mM NaCl
    20mM Hepes pH 7.5
    10% Glycerol
    10mM $MgCl_2$
    0.01mM ATP
    1mM β-mercaptoethanol
    protease inhibitors

6) Elute with **400mM NaCl Q Buffer** (and then again with 500mM NaCl):
    400mM NaCl / 500mM NaCl
    20mM Hepes pH 7.5
    10% Glycerol
    10mM $MgCl_2$
    0.01mM ATP
    1mM β-mercaptoethanol
    protease inhibitors

    (Store elution at 4°C until ready to concentrate)

7) Concentrate to 1-2mL using 10K Amicon (when volume decreases – add ATP so that it is at 0.1mM)

8) Run an S300 sizing column equilibrated in:
    20mM Tris pH 8.5
    800mM NaCl
    10% Glycerol
    5mM $MgCl_2$
    1mM DTT
    0.1mM ATP
    protease inhibitors

9) Concentrate, aliquot and flash freeze (use for biochemistry)

- for crystallography/EM purposes pool and concentrate peak from the first S300 column and run a second sizing column for complete separation of aggregates and contaminating DNA

## PERIPLASMIC *EC*DNAB ($H_6$MBP TAG) PURIFICATION PROTOCOL (adapted from Valerie O'Shea)

Expression (glucose is crucial during cloning and expression!!!)

C41 cells, grown O/N on Amp plates with 2% glucose
Pick a single colony and grow a small O/N culture (20mL per 1L) in 2xYT supplemented with at least 2% glucose.

Grow 1L cultures at 37°C to $OD_{600}$ of 0.3 – 0.6 (0.6 for constricted SRIR mutant)
Induce with 0.5mM – 1mM IPTG (1mM IPTG for constricted SRIR mutant)
Express for 16 – 22 hours at 16°C

Harvesting

*Use pellets from at most 3L of culture, if you want to purify more protein – run two preps separately over two Ni-columns. You can combine fractions following the TEV protease digest.

Resuspend cells in PPL DnaB **Resuspension Buffer**:

20mM HEPES-KOH pH 7.5
500mM NaCl
10% Glycerol
10mM $MgCl_2$
30mM Imidazole
0.1mM ATP
1mM β-mercaptoethanol
protease inhibitors (1:1000)

*you can freeze cell pellets or drop resuspended pellets into liquid nitrogen

Purification

1) Thaw cells, sonicate (4 x 2-5sec at 40Watts or few 1sec pulses) and spin at 15,000rpm for 20min (you can also try enzymatic lysis and periplastiing to further reduce heat damage to the sample)

2) Flow lysate over a Ni-column (use separate column for each mutant) pre-equilibrated in **Resuspension Buffer**

3) Wash the column with **High Salt Buffer** (verify by Bradford):

20mM HEPES pH 7.5
1M NaCl
10% Glycerol
10mM $MgCl_2$
30mM Imidazole
0.1mM ATP

1mM β-mercaptoethanol
protease inhibitors (1:1000)

4) Wash with 1-2 column-volumes of **Low Salt Buffer** (same as above but with 100mM NaCl).

5) Elute from the Ni-column on the Q column pre-equilibrated in **Ni Elution Buffer:**
   20mM Hepes pH 7.5
   100mM NaCl
   10% Glycerol
   10mM $MgCl_2$
   300mM Imidazole
   0.1mM ATP
   1mM β-mercaptoethanol
   protease inhibitors

6) Run gradient from 100mM – 1M NaCl over the Q-column (each constricted and dilated mutant elutes at different salt concentration from 400-800mM NaCl):
   20mM Hepes pH 7.5
   XmM NaCl
   10% Glycerol
   10mM $MgCl_2$
   0.1mM ATP
   1mM β-mercaptoethanol
   protease inhibitors

7) Concentrate to ~5mL using 30K Amicon (do not concentrate to more than 5mg/ml or protein will crash out during TEV digest, add 1mg TEV per 20mg of DnaB). At this step you will know whether the prep worked, if the total yield is <10mg of protein it is not worth going through with the rest of the protocol. Expression levels vary and pumping protein into periplasmic space will occasionally result in aggregated or unfolded protein that will not bind Ni-resin.

8) Digest with TEV protease overnight at 4°C

9) Adjust imidazole to 30mM and run over Ni-column equilibrated in **Ortho-Nickel Equilibration Buffer** (wash until no more protein is coming off as verified by Bradford):
   20mM Hepes pH 7.5
   300mM NaCl
   10% Glycerol
   10mM $MgCl_2$
   30mM Imidazole
   0.1mM ATP

1mM β-mercaptoethanol
protease inhibitors

10) Elute TEV protease with **Ortho-Nickel Elution Buffer**:
    20mM Hepes pH 7.5
    300mM NaCl
    10% Glycerol
    10mM $MgCl_2$
    300mM Imidazole
    0.1mM ATP
    1mM β-mercaptoethanol
    protease inhibitors

11) Concentrate to ~1mL and run an S300 sizing column in **PPL S300 Buffer**:
    20mM Tris pH 8.5
    800mM NaCl
    10% Glycerol
    10mM $MgCl_2$
    0.1mM ATP
    1mM β-mercaptoethanol
    protease inhibitors

- for crystallography/EM purposes pool and concentrate peak from the first S300 column and run a second sizing column in 100mM NaCl

- if you are doing biochemistry the protein will be less active after the second sizing column so dialysis into a buffer with 100mM NaCl, 20mM HEPES pH 7.5, 10% Glycerol, 10mM $MgCl_2$ and 0.1mM ATP (protein aliquots can be flash-frozen and stored at -80°C in this buffer).

## *Ec*DnaC ($H_6$MBP tag) purification protocol (adapted from Valerie O'Shea)

Expression

C41 cells, grown O/N on Amp plates
Pick a single colony and grow 50mL starter in 2xYT.

Grow 1L 2xYT cultures to $OD_{600}$ of 0.4 – 0.5 at 37°C
Induce with 1mM IPTG
Express for 2-2.5 hours at 37 °C

Harvesting

Resuspend pellet in 30 mL buffer:
50mM HEPES pH 7.5
1M KCl
10% glycerol
30mM imidazole
10mM $MgCl_2$
10mM ATP
1mM β-mercaptoethanol
protease inhibitors

* flash freeze, or flash freeze pellet and resuspend frozen cells, or resuspend and lyse right away.

Purification

* You will need to pour a 30mL Amylose column to run either in the cold room by gravity or on the FPLC. The buffer volumes are for doing the first Nickel and Amylose columns in-line on the FPLC

**Cell Resuspension / Lysis / Ni Loading Buffer** – 500mL
50mM HEPES pH 7.5
1M KCl
10% glycerol
30mM imidazole
10mM $MgCl_2$
10mM ATP
1mM β-mercaptoethanol
protease inhibitors

After cell lysis, add 5 μg/mL DNase I.

**Ni Low Salt Low Imidazole wash** – 500mL
Same as above except 500mM KCl

**Ni Elution / Amylose Load and Wash Buffer** – 250mL
Same as above, with 500mM KCl and 500mM imidazole

**Amylose Elution Buffer** – 250 mL
Same as above except NO imidazole and 10mM Maltose

Add ATP to 0.1mM and concentrate, TEV digest overnight at 4°C (concentrating without raising the ATP will lead to aggregation. TEV digestion will not work without concentrating)

Run ortho-Ni column with 30mM imidazole, elute with 500mM imidazole to check for complete TEV digestion by gel. (Can run the column in 0.01mM ATP but raise it to 0.1mM before concentrating all the way)

Concentrate the flowthrough to < 1mL. Run sizing column.

**S200 (or S300) Buffer** – 500 mL
50mM HEPES pH 7.5
500mM KCl
10% glycerol
10mM $MgCl_2$
0.1mM ATP
1mM β-mercaptoethanol
protease inhibitors

## *Ec*McrB PURIFICATION PROTOCOL

Expression

BL21 Codon+ RIL cells, grown O/N on Kan plates

Pick a single colony and grow 60mL of an overnight culture (start early ~2pm because it takes a long time to grow).

Grow 1L cultures at 37°C to $OD_{600}$ of 0.6
Induce with 0.5mM IPTG
Express for 3hours

Harvesting

Resuspend cells in DnaB **A1 Buffer**:

20 mM HEPES-KOH pH 7.5
0.5M NaCl
10% Glycerol
5mM $MgCl_2$
10mM Imidazole
0.1 mM GTP
5mM β-mercaptoethanol
protease inhibitors (1:1000)

*you can freeze cell pellets or drop resuspended pellets into liquid nitrogen

Purification

1) Thaw cells, sonicate (4 x 15sec at 40Watts) and spin at 15,000rpm for 20min

2) Repack, strip and recharge a large Nickel column (~15mL of resin)

3) Load lysate onto the Nickel column and wash with one loop volume of **A1 Buffer**. Wash with one loop volume of **A2 Buffer**:

   20mM HEPES-KOH pH 7.5
   1M NaCl
   10% Glycerol
   5mM $MgCl_2$
   10mM Imidazole
   0.1 mM GTP
   5mM β-mercaptoethanol
   protease inhibitors (1:1000)

4) Return to **A1 Buffer** until conductivity levels off and elute with a gradient of **B1 Buffer** (100% over 100mL):

20mM Hepes pH 7.5
0.5M NaCl
10% Glycerol
5mM $MgCl_2$
0.5M Imidazole
0.1mM GTP
5mM β-mercaptoethanol
protease inhibitors

5) Pool peak, concentrate to 1mL and add 14mL of **A1 Buffer supplemented with 1mM GTP**. Add TEV protease (1mg of TEV per 20mg of protein) and **digest for 3hours at room temperature** (it will crash out if you try to cleave the tags overnight in the cold room).

6) Concentrate to 1-2mL and run over fresh Ni-column (HisTrap 5mL column pre-equilibrated in A1 Buffer with 1mM GTP). Pool flow through and concentrate to 1mL

7) Run an S300 sizing column equilibrated in:
20mM Hepes pH 7.5
0.5M NaCl
10% Glycerol
5mM $MgCl_2$
1mM GTP
5mM β-mercaptoethanol
protease inhibitors

- aliquots of protein can be flash frozen and stored for biochemistry experiments at -80°C, however best results are obtained when protein is dialyzed into freshly made buffer with nucleotide the night before (or 4hours before) it is used in ATPase or translocation assays,
- for crystallography do not flash freeze the pellets (or protein) before setting trays

## PERIPLASTING PROTOCOL

Reagents:

1. Peripreps periplasting buffer: 200mM Tris-HCl (pH 7.5), 20% sucrose, 1mM EDTA, and 30U/uL Ready-Lyse Lysozyme.
2. Peripres Lysis Buffer: 10mM Tris-HCl (pH 7.5), 50mM KCl, 1mM EDTA, and 0.1% deoxycholate

Procedure:

*amount of reagents determined based on wet cell pellet

1. Grow the bacterial cell culture and induce expression. The cells should be in log-phase or early stationary phase
2. Pellet cells by centrifugation at a minimum of 1,000g for 10min at room temperature.
   - the cells must be fresh, not frozen, determine the weight of the cell pellet
3. To degrade contaminating nucleic acids, dilute 2uL of OmniCleave Endonuclease and 10μL of 1M MgCl2 up to 1mL with Peripreps Lysis buffer for each ml of Lysis buffer needed in Step 10.
4. Thoroughly resuspend the cells in a minimum of 2mL of peripreps periplasting buffer for each gram of cells either by vortex mixing or by pipeting until the cell suspension is homogenous.
5. Incubate for 5min at room temperature.
6. Add 3mL of purified water at 4°C for each gram of original cell pellet weight and mix by inversion
7. Incubate for 10min on ice
8. Pellet the lyzed cells by centrifugation at a minimum 4000g for 15min at room temperature
9. Transfer the supernatant containing the periplasmic fraction to a clean tube.
10. Resuspend the pellet in 5mL of Peripreps lysis buffer for each gram of original cell pellet weight
11. Incubate at RT for 10min (Endonuclease will decrease viscosity to consistency of water)
12. Pellet cellular debris by centrifugation at a minimum of 4000g for 15min at 4°C
13. Transfer the supernatant containing spheroplast fraction to a clean tube.
14. If Endonuclease was added, add 20μL of 500mM EDTA for each mL of the resultant spheroplasmic fraction, to chelate the magnesium (the final concentration in lysate is 10mM).

## ENZYMATIC LYSIS OF GRAM-NEGATIVE BACTERIA (*E. COLI*)

Reagents:

1. Tris-sucrose buffer: 50mM Tris-HCl (pH 7.5), 10% sucrose
2. Lysis solution: 0.3M spermidine-HCl, 2M NaCl, 10% sucrose, adjust to pH 7.5

Lysis procedure:

1. To the frozen *E. coli* cells, add prewarmed (at 37C) Tris-sucrose buffer (2.5 times of packed cell weight) and lysis solution (0.25 times of packed cell weight).
2. Once a thawed homogenous mixture is achieved, add lysozyme (1mg/g of packed cell). Incubate on ice for 1h. Fresh solution of lysozyme should be used each time.
3. Incubate the homogenate at 37C water bath for about 4min with gentle agitation.
4. Place the homogenate immediately on ice for a few minutes.
5. Centrifuge at 23,000g for 1h at 4C. Decant and save the supernatant. (If cells are not lysed completely, a more vigorous lysis is performed by adding EDTA [5-10mM final concentration] to the Tris-sucrose buffer or by extending the lysis reacting up to 15min).

## CROSSLINKING OF PROTEINS

1. When incubating with the crosslinking reagent, use temperature at which you run your standard reactions (30-37°C).
2. To find the best concentration to use for your protein, titrate glutaraldehyde or another crosslinking reagent over the range of 0 – 10mM.
3. Pre-incubate proteins at the reaction temperature for 10min before crosslinking.
4. Add 1/10 volume of a 10X glutaraldehyde dilution to the reaction and continue the incubation for another 10min.
5. Quench the crosslinking by adding a stopmix of glycine, to at least 2X the final concentration of glutaraldehyde, in 10mM Hepes pH 7.6. (Nancy Crisona used 1/10 volume of 200mM glycine in 10mM Hepes pH 7.6).

- Do not use Tris buffer when crosslinking with glutaraldehyde, switch to triethanolamine or Hepes to avoid inhibition.
- Use only highest grade glutaraldehyde, the ampules come at 8% concentration. Dilute them in water and keep on ice covered in parafilm until ready to use. Discard unused glutaraldehyde in organic waste at the end of the day.

- Run crosslinked protein samples on Phosphate Gels (recipe in the Appendix)

## PHOSPHATE/SDS POLYACRYLAMIDE GELS (adapted from Nancy Crisona)

1. 4X PO4/SDS buffer, pH 7.2 = 0.4M Sodium Phosphate/0.4% SDS

| | 1liter | 500mL |
|---|---|---|
| $NaH_2PO_4 \cdot H_20$ | 15.6g | 7.8g |
| $Na_2HPO_4$ | 40.88g | 20.44g |
| SDS | 4g | 2g |

Do not adjust pH, store at 4°C for up to one month.

2. 30% acrylamide, 80:1 acrylamide:bis

| | 20mL | 50mL |
|---|---|---|
| acrylamide | 6g | 14.82g |
| bis | 0.075g | 0.18g |

Filter through 0.45μM filter, store in foil-wrapped bottle at 4°C

3. 4X sample loading buffer

| | final 4X concentration |
|---|---|
| 300μL 4X PO4/SDS buffer | ~42mM NaPO4 |
| 450μL 25% ultrapure SDS | 4% |
| 50μL 2% bromophenol blue | 0.035% |
| 1mL 1M DTT | 0.4M |
| 1mL 80% Glycerol | 28% |

Store at -20°C in aliquotes

- when running crosslinking gels of DnaB mutants crosslinked through disulfide bonds – do not use DTT in the loading buffer!

4. Gel recipe: 10mL for one minigel

| | 4.5% | 5% |
|---|---|---|
| 30% acrylamide | 1.5mL | 1.66mL |
| 4X buffer | 2.5mL | 2.5mL |
| water | 6mL | 5.84mL |

Degas for 10min
Add 100μL of 10% ammonium persulfate and 8μL TEMED. Mix well and pour the gel.

Run gels slowly (30Volts) for 4-6hours.

## NUCLEOTIDE HYDROLYSIS ASSAY (COUPLED ENZYME ASSAY)

Use **Costar 3695** plates – 96 clear, round, flat bottom wells

In a total reaction volume of 100µL combine 10µL of 10X protein with 10µL of 10X nucleotide dilutions and 80µL of buffer with NADH (nicotinamide adenine dinucleotide), PEP (Phosphoenolpyruvate) and PK/LDH (Pyruvate kinase/Lactic dehydrogenase) mixture.

For DnaB

Reaction buffer:

20mM HEPES-KOH pH 7.5,
5mM Magnesium Acetate,
50mM Potassium Glutamate,
5 % Glycerol,
4 mM DTT (can add DTT when working with wild type *Ec*DnaB or mutants based on electrostatic and steric clashes but do not add reducing reagent when working with cross-linked DnaB or *Aa*DnaB),
0.2mg/mL BSA (bovine serum albumin)

**600µM NADH**
**0.8% v.v PK/LDH**
**2mM PEP**

Coupled hydrolysis activity:

- serial dilute nucleotide into reaction buffer lacking NADH, PEP and PK/LDH (measure concentration of the nucleotide after dilution),
- you can do two-fold or three-fold dilutions to span a wider range ,
- in a crystal block (2mL wells) mix nucleotide with reaction buffer (10µL of 10X nucleotide with 80µL of reaction buffer per every reaction – I usually prepare enough for 10 reactions at each nucleotide concentration), let it sit on ice for 10min and at RT for 30sec so that any contaminating ADP/GDP gets converted before you add the protein,
- for reactions with DNA add DNA to the reaction buffer at the desired concentration and then mix with nucleotide dilutions,
- use multichannel pipette to dispense 10µL of protein at 10X concentration (DnaB assays are usually done at 10-50nM hexamer) into wells of a Costar 3695 plate (keep plate on ice until ready to measure)
- add 90µL of nucleotide/buffer mix to each well (adding 90µL to 10µL usually takes care of mixing but you can gently pipette up and down 2-3 times to mix the reactions more thoroughly, be careful not to introduce bubbles),
- measure assay on the plate reader at RT – 37°C (lowering temperature will slow the assay down)

Controls:
Buffer alone with nucleotide, no protein
Protein with no nucleotide
Protein with nucleotide but no DNA

Calculate rate by determining the slope of the curve (change in OD/time). The extinction coefficient can be calculated by titrating NADH in your reaction buffer (without PEP and PK/LDH or nucleotide) and reading it in the plate reader.

Make stocks:
5X reaction buffer (no BSA, no DTT)
50mM PEP
5mM NADH
10mg/mL BSA
100mM nucleotide (in water or your reaction buffer if you want to perform hydrolysis assay at high nucleotide concentrations)

## TRIPLEX DISPLACEMENT ASSAYS

### McrB experiments

Reagents:

1) A derivative of a 3kB pBS-SK(+) plasmid with a DNA triplex promoting site (TBS) – AGGGAAGAAAAGAAAGAAGAAAGAAA - cloned in between EcoRV and PstI sites was obtained from Jerod Ptacin from the Bustamante Laboratory.
2) A DNA triplex forming oligonucleotide (TFO) – TTCTTTTCTTTCTTCTTTCTTT – labeled with Fluorescein (6FAM) was purchased from Integrated DNA Technologies.
3) 1X Triplex Forming Buffer: 25mM MES pH 5.5, 10mM $MgCl_2$
4) Quenching Buffer: 250mM MES pH 5.5, 3% (wt/vol) SDS, 15% glucose

Protocol:

Triplex assembly reactions contained TFO at 100-500nM and a 2fold excess of either linear or plasmid DNA with a TBS site to drive the triplex forming reactions to completion. The reactions were heated to 57°C and allowed to cool overnight, formed triplexes were stored in aliquots at -20°C until use.

Assembled triplexes were diluted down ~10fold into the protein reaction buffer (*keep concentration of the fluorescent triplex at least at 10-15nM and higher if possible to see accumulation of TFO over background on the gel). Translocation assays were performed at 37°C and at pH between 7 and 8.5 so that displaced TFO could not re-anneal and its accumulation could be monitored on a gel.

Translocation reactions were quenched by the addition of an equal volume of the quenching buffer and run on a gel at 10V/cm at 4°C. Gels were scanned using Typhoon and Imagequant software.

*** NOTE – never use EDTA when working with triplexes!

### Agarose Gel (for McrB):

1.5% agarose
40mM Tris Acetate
5mM Sodium Acetate (prevents short pieces of ssDNA from running of the gel)
1mM $MgCl_2$
pH 5.5 (prevents not-unwound triplexes from falling apart in the gel)

Run gel at 10V/cm at 4°C.

Loading buffer/quenching buffer:
250mM MES, pH 5.5, 3% (w.v) SDS, 15% (w.v) Glucose, 0.4mg/mL bromophenol blue (don't use the dye with fluorescent labeled DNA) – add equal volume of buffer to each reaction

**Adapting gel-based assay for DnaB:**

Reagents:

1) A DNA duplex with a 5' 25(T) flap for loading and a 16bp dsDNA region followed by the TBS site was annealed from pieces of DNA purchased from Integrated DNA Technologies,

2) A DNA triplex forming oligonucleotide (TFO) – TTCTTTTCTTTCTTCTTTCTTT – labeled with Fluorescein (6FAM) was purchased from Integrated DNA Technologies.

3) 1X Triplex Forming Buffer: 25mM MES pH 5.5, 10mM $MgCl_2$
4) 5X Quenching Buffer: 12.5% Ficoll, 10% LDS

**Polyacrylamide Gel (for DnaB):**

12 - 15% polyacrylamide (19:1 or 29:1)
0.5-1X Tris Borate Magnesium (TBM) or Tris Taurine Magnesium (TTM) buffer
0.1% SDS (protein will not migrate into the gel without SDS)
pH 5.5

| 1X TTM | 1X TBM |
|---|---|
| 89mM Tris | 89mM Tris |
| 29mM Taurine | 89mM Boric Acid |
| 10mM $MgCl_2$ | 10mM $MgCl_2$ |
| pH to 5.5 in the cold room | pH to 5.5 in the cold room |

- degas the gel for at least 30min
- pre-run the gel at the voltage you will run it for 0.5-1hour (I run large gels at 100-200Volts for 2-4hours)

Loading buffer/quenching buffer:
2.5% Ficoll, 2% LDS (does not crash out in the cold), pH 5.5 – final concentrations in each reaction

**Plate reader version of the triplex displacement assay for DnaB**

Protocol:

1) Mix equimolar concentrations of DnaB and DnaC and incubate on ice for 10 minutes,

2) Add triplex DNA substrate (at 2 $Dna(BC)_6$ : 1 DNA triplex ratio) and incubate for additional 10 minutes,

3) Add ATP (to 1mM concentration) – no capture strand necessary at pH 7.5

4) Immediately transfer the plate to the plate reader at 37 °C and start monitoring for fluorescence increase at 37 °C for 15-20 minutes on a Victor V3 plate reader (Perkin Elmer).

*Make ~60-75µL for each condition and use multichannel pipettes to aliquot 20µL reactions for each triplicate point, then mix another 60µL for a second triplicate set. Use 200nM DnaB hexamer (with or without 1.2µM DnaC monomer) and 100nM triplex substrate. I usually mix equal volume (~35µL) of protein and DNA (data is less noisy if both protein and DNA are diluted in 1X reaction buffer as opposed to keeping DNA in water and protein in 2X reaction buffer) and add small amount of ATP (5µL) and mix before transferring into the plate for measurement. Analyze data in Excel (Microsoft) and plot using PRISM (GraphPad).

**** DnaB unwinds triplex DNA substrates in an ATP-independent manner, longer dsDNA reagion might be necessary to make the triplex displacement reaction work.**

## dsDNA translocation assay for DnaB

Reagents:

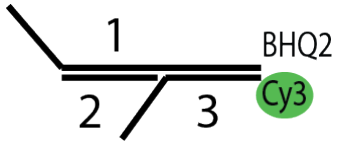


1) Oligonucleotides 1 (5'25(T)GCAGGCTCGTTACGTAGGACAGTGTAGTATTA) labeled at 3' end with the Black Hole Quencher; 2 (5' TACGTAACGAGCCTGC ) and 3 (5'Cy3-TAATACTACACTGTCC 25(T)) were purchased from Integrated DNA Technologies,

2) 4X Reaction Buffer:
   20mM Magnesium Acetate
   80mM HEPES-KOX pH 7.5
   200mM Potassium Glutamate
   20% Glycerol
   0.8mg/mL BSA
   (NO DTT when testing cross-linked mutants)

Protocol:

1) DNA substrate was formed by annealing 10μM Cy3-labeled oligonucleotide 3 with a 2-fold excess of oligo 1 and 3-fold excess of oligo 2 to ensure full quenching of the fluorescent DNA. Substrates were run on a gradient TBE gel to verify formation of the product,

2) Additionally, we annealed a substrate where the oligonucleotide 2 carried a 3' Cy5 label to ensure that our annealing protocol resulted in formation of a desired substrate where every piece of DNA with Cy3 label would also have the initial double-stranded DNA region,

3) Mix equimolar concentrations of DnaB and DnaC and incubate on ice for 10 minutes,

4) Add DNA substrate (at 2 $Dna(BC)_6$ : 1 DNA substrate ratio) and incubate for additional 10 minutes,

5) Add ATP (to 1mM concentration) and a capture strand of DNA (complementary to the base-paired region of the Cy3-labeled oligo (5'-GGACAGTGTAGTATTA-3'),

6) Immediately transfer the plate to the plate reader at 37 °C and start monitoring for fluorescence increase at 37 °C for 15-20 minutes on a Victor V3 plate reader (Perkin Elmer).

* 20µl reactions contain 200nM DnaB hexamer and equimolar concentration of DnaC (1.2µM DnaC monomer), 100nM DNA substrate, 200nM capture strand and 1mM ATP. Each reaction is measured six separate times to generate robust statistics. Data were first processed in Excel (Microsoft) and plotted using PRISM (GraphPad). As a control we tested DnaB for unwinding of a blunt fork lacking the 3' flap region that mimicked the first half of our dsDNA translocation substrate, and observed minimal activity even in the presence of DnaC loader. We also measured duplex DNA translocation on the doubly-labeled substrate that contained Cy5 label on 3' end of the oligo 2 and 5' Cy3 label on the oligo 3; the observed trends were similar to the duplex DNA translocation measured on a substrate without the additional Cy5 label, but DnaB was significantly less efficient on the doubly-labeled substrate.

**dsDNA translocation reactions were also loaded onto a gradient TBE gel (or a 12% large gel). The substrates designed for the plate reader assay would however fall apart when run on a polyacrylamide gel containing SDS; if SDS was omitted the DNA substrates would remain intact but once DnaB was added to the reactions it would bind DNA so strongly that nothing could migrate into the gel and reactions could not be monitored. It is possible that with a longer dsDNA region and higher GC content the substrates would be more robust and could be visualized on an SDS gel but we have not tested this hypothesis.

## HELICASE FORK UNWINDING ASSAY

Reagents:

1) HPLC-purified DNA oligonucleotides (purchased from Integrated DNA Technologies labeled with Cy3 or Black Hole Quencher 2):
- the basic forked DNA substrate was formed by annealing 20μM 5'-Cy3-TACGTAACGAGCCTGC$(dT)_{25}$-3' with a 1.2 molar excess of a 5'-$(dT)_{25}$-GCAGGCTCGTTACGTA-BHQ2-3' in annealing buffer (10 mM Tris-HCl, 1 mM EDTA, and 100 mM NaCl, pH 7.5).

2) 4X Reaction Buffer:
   20mM Magnesium Acetate
   80mM HEPES-KOX pH 7.5
   200mM Potassium Glutamate
   20% Glycerol
   0.8mg/mL BSA
   (NO DTT when testing cross-linked mutants)

Protocol:

1) Mix equimolar concentrations of DnaB and DnaC and incubate on ice for 10 minutes,

2) Add forked DNA substrate (at 2 $Dna(BC)_6$ : 1 DNA fork ratio) and incubate for additional 10 minutes,

3) Add ATP (to 1mM concentration) and a capture strand of DNA (complementary to the base-paired region of the Cy3-labeled oligo (5'-GCAGGCTCGTTACGTA-3'),

4) Immediately transfer the plate to the plate reader at 37 °C and start monitoring for fluorescence increase at 37 °C for 15-20 minutes on a Victor V3 plate reader (Perkin Elmer).

*Make ~60-75μL for each condition and use multichannel pipettes to aliquot 20μL reactions for each triplicate point, then mix another 60μL for a second triplicate set. When comparing mutants I use 200nM DnaB hexamer (with or without 1.2μM DnaC monomer) and 100nM fork substrate with 200nM capture strand. I usually mix equal volume (~35μL) of protein and fork (data is less noisy if both protein and DNA are diluted in 1X reaction buffer as opposed to keeping DNA in water and protein in 2X reaction buffer) and add small amount of ATP mixed with capture strand (5μL). For reactions that are not testing cross-linked mutants add 4mM DTT to the reaction buffer (DnaC is more active in the presence of DTT). Analyze data in Excel (Microsoft) and plot using PRISM (GraphPad).

## DnaB-dependent primer synthesis assay

Reagents:

1) Individual solutions of ATP, UTP, CTP and GTP at 100 mM concentration (certified as RNase free, New England Biolabs)
2) RNase free Potassium Glutamate and HEPES-KOH were purchased from Teknova at 1M concentration and pH 7.5
3) RNase free stocks of powdered Magnesium Acetate and BSA were purchased from Sigma and dissolved in RNase free water

5X Reaction Buffer:
500mM Potassium Glutamate
100mM HEPES pH 7.5
50mM Magnesium Acetate
1mg/mL BSA
(NO DTT when working with cross-linked mutants or comparing cross-linked mutant activity to the wild type DnaB protein under identical conditions)

Protocol:

1) Dilute DnaB, DnaC and DnaG into 1X reaction buffer containing 100mM potassium glutamate, 20mM HEPES-KOH pH 7.5, 10mM magnesium acetate and 0.2 mg/ml BSA,
2) Mix DnaB and DnaC at equimolar concentration and pre-incubate on ice for 10 min,
3) Mix 10µl of pre-incubated $Dna(BC)_6$ with 10µl of DnaG and incubate for 1 min at 37° C,
4) Combine 4 nucleotides with single stranded M13 DNA in the 1X reaction buffer and add 10µl of the obtained mixture to initiate priming,
5) Incubate for 5 min at 37° C and quench with 30µl of 1:100 Pico Green stock solution (Invitrogen) in 20mM Tris-HCl, 50mM EDTA (pH 7.5),
6) Incubate stopped reactions in the dark for 5 min and measure raw fluorescence in a Victor $^3$V plate reader (Perking Elmer)

*All reactions were carried out in triplicate, fluorescent data was background corrected by subtracting raw fluorescence of reactions that lacked DnaG and $Dna(BC)_6$ proteins. Obtained data was plotted using PRISM (GraphPad).

**Proteins, nucleotide mix and quenching solution were all aliquoted into a PCR plate and all mixing was done using multi-channel pipettes.